TECHNICKÁ UNIVERZITA V LIBERCI

FAKULTA TEXTILNÍ

DOKTORSKÁ PRÁCE

2014 **Guocheng Zhu**

TECHNICKÁ UNIVERZITA V LIBERCI

FAKULTA TEXTILNÍ

DOKTORSKÁ PRÁCE

STUDY ON THE THERMAL PROPERTY OF TEXTILE EXPERIMENTALLY AND NUMBERICALLY

MSc. Guocheng Zhu

Liberec

2014

Název disertační práce:	Study on the thermal property of textile experimentally and numerically
Autor:	MSc. Guocheng Zhu
Obor doktorského studia:	Textilní technika
Forma studia:	Full-time
Školící pracoviště	Department of material engineering
Školitel:	doc. Dr. Ing. Dana Křemenáková
Počet stránek textu:	106
Počet obrázků:	44
Počet tabulek:	12

DECLARATION BY THE AUTHOR

"I hereby declare that this submission is my own work and that, to the best of my knowledge and belief, it contains no material previously published or written by another person nor material which has been accepted for the award of any other degree or diploma of the university or other institute of higher learning, except where due acknowledgment has been made in the text.

Liberec
29.09.2014 ***MSc. Guocheng ZHU***

CERTIFICATE FROM SUPERVISOR

*This is to certify that the thesis entitled "**Study on the thermal property of textile experimentally and numerically**" submitted by **Guocheng Zhu** to Technical university of Liberec for the award of the degree of Doctor of Philosophy is a bona fide record of the research work carried out by him under my supervision and guidance. The content of the thesis, in full or parts have not been submitted to any other Institute or University for the award of any other degree or diploma.*

Liberec
29.09.2014 ***doc. Dr. Ing. Dana Křemenáková***

ACKNOWLEDGEMENTS

I have been most fortunate to have had associate professor Dana Kremenakova as my advisor. I am deeply grateful to her for her invaluable support and encouragement throughout my Ph.D. study. She always provided the right level of guidance in my research, giving me the freedom to think independently and pursue my own ideas. Working with her has been a great learning experience and I thank her for sharing her vision of science, world and life in general. I will always regard her as a mentor and role model.

I want to thank all the outstanding scientists with whom I had the privilege to work with. I am especially indebted to Yan Wang and Juan Huang, my main collaborators and co-authors in many of my publications: thanks for all the helpful discussions, your advice and most important, your friendship. I like to thank all the group members in our department that I had a chance to interact with over the years. This includes Prof. Jiri Militky, Prof. Sayed Ibrahim, Dr. Rajesh Mishra, Dr. Mohammed, Dr. Kausik Bal…… They made my graduate life very enjoyable. I would also like to thank my committee members, for all their advice and help.

I also very thank for the support from SGS which I would like to thank all my innumerable friends in Technical University of Liberec, who made my stay here a memorable experience.

Finally, I thank my parents for their belief in me and provided all the help and support throughout my life. I am forever indebted to them.

ABSTRAKT

Tepelné vlastnosti netkaných textilií a jiných textilních materiálů jsou jedněmi z nejdůležitějších vlastností pro jejich použití jako ochranné oděvy, spací pytle a další podobné technické textilie. Tepelné vlastnosti textilií mohou být ovlivněny mnoha faktory jako např. tepelné vlastnosti samotného materiálu, struktury vlákna textilie, příze a látky, okolní podmínky jako teplota, vlhkost a pohyb vzduchu. Různé okolní podmínky mohou vést k různým mechanismům přenosu tepla (vedením, sáláním a zářením) a přenosu vlhkosti. Práce byla zpracována v mnoha oblastech (1) návrh a vylepšení testovacího zařízení pro hodnocení tepelných vlastností textilií za různých podmínek; (2) hlubší porozumění přenosu tepla v textiliích; (3) přesnější predikovaní tepelných vlastností textilií na základě analytického modelu; (4) návrh a použití textilních produktů v souvislosti s jejich použitím včetně ekonomicky výhodného využití zdrojů. Ačkoliv je na trhu mnoho měřících a testovacích zařízení pro zjišťování tepelných vlastností textilií, není v nabídce žádný, který by nabízel měření textilií během každodenního přenosu tepla sáláním. Je také dobře známo, že každý materiál se za různých podmínek chová jinak. Navíc absence testovacího zařízení a komplexnost textilní struktury stěžovala hlouběji porozumět přenosu tepla v textiliích. Na druhou stranu velice málo prací se zmiňovalo o vlhkých textiliích uvolňující teplo, což by mohl být jeden z ovlivňujících faktorů. V teoretickém výzkumu existuje několik analytickým modelů pro odhad tepelných vlastností textilií, ale všechny tyto modely jsou zjednodušené pro struktury příze, látka/netkaná textilie ignorující přenos tepla sáláním a závislost tepelné vodivosti na teplotě. Na základě výše uvedených problémů nemůže být správně odhadnuto chování textilií z hlediska tepelných vlastností a je zapotřebí ještě dalšího výzkumu v optimalizaci produktů v souvislosti s jejich použitím.

Proto byly v této práci výše zmíněné problémy studovány pro lepší porozumění tepelných vlastností textilií. Tato dizertační práce obsahuje sedm kapitol. První kapitola uvádí čtenáře

do problematiky přenosu tepla v textiliích (vedením, sáláním a zářením), předkládá měření teplotní vodivosti/odporu textiliích ve formě vlákna a textilie. Je v ní uveden provedený experimentální a teoretický výzkum disertační práce, což byl hlavní cíl. Druhá kapitola se zabývá vlivy na některé parametry, jako je tvar a velikost pórů, distribuce pórů, délka hlavní osy póru a kontaktní plocha pro tepelnou vodivost porézního materiálu/textilie pomocí numerických simulací zatížené náročným hledáním vhodných vzorků a spolehlivých výsledků numerických metod. Také je v této kapitole porovnána tepelná vodivost textilií z již existujících analytických modelů a jiných numerických simulací ke zjištění rozdílů mezi nimi. Třetí kapitola hodnotí tepelnou vodivost netkaných textilií s vysokou pórovitostí (nad 95%) pod vlivem sálajícího tepla. Je zkoumán vliv porozity, velikost a tloušťka pórů na tepelnou vodivost a také je stanoven poměr přenosu tepla vedením, sáláním a zářením. Čtvrtá kapitola studuje prodyšnost a tepelný odpor textilií během přenosu tepla sáláním, pro které bylo sestrojeno samostatné měřící zařízení. Pátá kapitola se zabývá numericky vlivem struktury na tepelný odpor textilie během sálání tepla. Dále je zde řešena distribuce lokální teploty, lokálního tepelného proudu, lokálního/průměrného koeficientu přenosu teplat a lokálních Nusseltových čísel textilie a porézního materiálu za působení přenosu tepla vedením a sáláním. Šestá a sedmá kapitola shrnuje výsledky práce do závěru a dalšího bádání.

ABSTRACT

Thermal property of non-woven and other textile fabrics is one of most important aspects for their applications in protective clothing, sleeping bags and related technical textiles. The thermal property of textiles can be influenced by many factors, such as thermal property of materials, structure of textiles in forms of fiber, yarn, and fabric, surrounding conditions including temperature, humidity, and air movement. And the different surrounding conditions would result in different heat transfer mechanisms (heat conduction, heat convection, and heat radiation) and moisture transfer. Therefore, a lot of work has been doing in thermal property of textile in the following aspects: (1) design and improve testing devices for evaluating the thermal property of textiles under various conditions; (2) deeply understand the heat transfer process in textiles; (3) predict the thermal property of textile more accurately by analytical model; (4) design and apply the textile products to meet various applications, and utilize the resources in an economically efficient way. Even though a lot of the testing instruments which are available to evaluate the thermal property of textiles under conductive heat transfer. There still has no any commercial instrument for measuring the thermal property of textile under convective heat transfer, which happens almost everywhere in daily life. And it is well known that the performances of one material would be quite different when it is under different conditions. Besides, the lack of testing instrument and the complexity of textile structure increase the difficulty to deeply understand the heat transfer process in textiles. On the other hand, very few work reported in heat release when the textile absorbs liquid/moisture, which could be also one important factor influencing the thermal property of textiles. In theoretical research, there are several analytical models for predicting the effective thermal conductivity of textiles, but all of the models simplified the structures of yarn and fabric/non-woven fabric, ignored the convective transfer heat in textiles, and

ignored the temperature dependent thermal conductivity. Based on the above problems, the performances of textiles in thermal property still cannot be precisely predicted, and plenty of experimental work is still needed for optimizing the products or for meeting various applications.

Therefore, some of the above problems were studied in this work in order to understand more about thermal property of textiles. This dissertation consists of seven chapters. Chapter one introduced the three heat transfer mechanisms (conduction, convection, and radiation) in textile, presented the measurements of thermal conductivity/resistance of textile in forms of fiber and fabric, introduced the experimental and theoretical research work has done in thermal property of textile, and the aim of this work. Chapter two studied the effect of some parameters which are pore shape, pore size, distribution of pores, major-axis length of pore, and the contact area on thermal conductivity of porous materials/textiles by numerical simulation owing to the difficulty in finding suitable samples and the reliable results from numerical method; and also compared the thermal conductivity of textiles from some existing analytical models and from numerical simulation to know about the difference among them. Chapter three evaluated the thermal conductivity of nonwoven fabrics with very high porosity (>95%) under heat conduction, investigated the effect of porosity, pore size and thickness on thermal conductivity, and also determined the ratio of heat transfer causing by conductive, convective, and radiative. Chapter four studied the air permeability and thermal resistance of textile under convective heat transfer, for which one self-designed device was constructed; investigated the effect of porosity, pore size and pore's area ratio to total sample's area on air permeability and thermal resistance. Chapter five studied the impact of structure on the thermal resistance of fabric under heat convection numerically. The local temperature distributions, local heat flux distributions, local/average heat transfer coefficients, and local

Nusselt numbers of fabrics taken as plate and porous material under conductive and convective heat transfer were investigated.

Chapter six and chapter seven gave the conclusions and the future work.

CONTENT

LIST OF SYMBOLS

Symbols	Long name	Units
A	the heat transfer area normal to the direction of heat transfer	m^2
	fraction of fibers which is parallel to the heat flow	-
A_f	cross-sectional area of fiber	m^2
A_r	cross-sectional area of resin	m^2
a	thermal diffusivity	$m^2 \cdot s^{-1}$
B	fraction of fibers which is series to the heat flow	-
C	constant depends on geometry and flow,	-
c	specific heat capacity	$J \cdot kg^{-1} \cdot K^{-1}$
c_e	effective specific heat capacity	$J \cdot kg^{-1} \cdot K^{-1}$
c_w	specific heat capacity of water	$J \cdot kg^{-1} \cdot K^{-1}$
c_f	specific heat capacity of fiber	$J \cdot kg^{-1} \cdot K^{-1}$
D	effective pore diameter	m
d	mean fiber diameter	m
D_e	deviation	-
$dT, \Delta T$	temperature difference	K or °C
Dx	thickness difference	m
dT/dx	temperature gradient	$K \cdot m^{-1}$
e_1, e_2	effusivity of sensor and sample, $= \sqrt{k\rho c}$	$J \cdot m^{-2} \cdot K^{-1} \cdot s^{-1/2}$
G	power flux supplied to sensor	W
g	gravitational acceleration	$m \cdot s^{-2}$
H	Enthalpy	$J \cdot kg^{-1}$
h	heat transfer coefficient by convection	$W \cdot m^{-2} \cdot K^{-1}$
	thickness of sample	m
h_{rad}	heat transfer coefficient by radiation	$W \cdot m^{-2} \cdot K^{-1}$
h_e	effective heat transfer coefficient	$W \cdot m^{-2} \cdot K^{-1}$

h_x	Local heat transfer coefficient	$W \cdot m^{-2} \cdot K^{-1}$
H_w	integral heat of sorption	J/g
k	thermal conductivity	$W \cdot m^{-1} \cdot K^{-1}$
	Heat capacity ratio	-
k_e	effective thermal conductivity	$W \cdot m^{-1} \cdot K^{-1}$
k_f	thermal conductivity of fiber	$W \cdot m^{-1} \cdot K^{-1}$
k_a	thermal conductivity of air	$W \cdot m^{-1} \cdot K^{-1}$
k_F	thermal conductivity of the fluid	$W \cdot m^{-1} \cdot K^{-1}$
k_r	thermal conductivity of resin	$W \cdot m^{-1} \cdot K^{-1}$
k_{sf}	thermal conductivity of fiber in series arrangement	$W \cdot m^{-1} \cdot K^{-1}$
k_{pf}	thermal conductivity of fiber in parallel arrangement	$W \cdot m^{-1} \cdot K^{-1}$
k_p	flow permeability coefficient	m^2
L_c	characteristic length	m
L	distance	m
m	constant exponent	-
	mass	kg
m_t	total mass	kg
m_w	mass of water	kg
m_f	mass of fiber	kg
Ma	Mach number	-
n	constant exponent	-
Nu	Nusselt number	-
Nu_x	Local Nusselt number	-
p	Pressure	Pa
p_t	Total pressure	Pa
p_b	Back pressure	Pa
Δp	Pressure drop	Pa
Pr	Prandtl number	-

Q	heat flow	J
	air flow volume flowing in time	m^3
Q_t	total heat flow	J
Q_{cond}	heat flow by conduction	J
Q_{conv}	heat flow by convection	J
Q_{rad}	heat flow by radiation	J
Q_l	the heat energy when liquid water become absorbed water	J/g
Q_d	differential heat of sorption	J/g
q_{rad}	heat flux by radiation	W
q	rate of flow	$m \cdot s^{-1}$
q_x	Heat flux	$W \cdot m^{-2}$
Q_f	heat flow through fiber	J
Q_r	heat flow through resin	J
R_{fabric}	thermal resistance of the fabric	$K \cdot W^{-1}$
R_c	contact thermal resistance	$K \cdot W^{-1}$
R	Gas constant	$J \cdot kg^{-1} \cdot K^{-1}$
Re	Reynolds number	-
Re_x	Local Reynolds number	-
r	radius of fiber	m
T_0	Air temperature at inlet	K
T_s	Temperature of solid	K
T_f	Temperature of fluid	K
T_{skin}	Temperature of skin	K
T_{air}	Air temperature	K
ΔT	Temperature difference, (K)	K or °C
T_s	the surface temperature	K or °C
T_∞	the temperature of the fluid sufficiently far from the surface	K or °C

	ambient temperature	K or °C
T_w	wall temperature	K or °C
T_1 , T_2	surface temperatures of body one and body two	K or °C
T_m	mean temperature	K or °C
T_{in} , T_{out}	temperature on both sides of one body	K or °C
t	time	s
μ	the filling coefficient of the fabric	-
	dynamic viscosity	Pa·s or $kg \cdot m^{-1} \cdot s^{-1}$
v	idealized portion of fibers oriented vertically to the isotherms in the fabric	-
	speed	$m \cdot s^{-1}$
V	volume	m^3
V_a	volume fraction of air	-
V_f	volume fraction of fiber	-
V_r	volume fraction of resin	-
w	moisture regain value	-
ws	saturated moisture regain value	-
x	Thickness or Distance	m
Z	yarn twist coefficient	-
ε	emissivity of the body surface	-
ε_1 , ε_2	emissivity of the body one and body two	-
σ	the Stefan-Boltzmann constant, =5.67 x 10^{-8}	$W \cdot m^{-2} \cdot K^{-4}$
ρ_n , ρ_h	density of nonwoven fabric and hollow fiber	$kg \cdot m^{-3}$
ϕ	porosity	-
ϕ_n	mean porosity of the nonwoven fabric	-
β	is coefficient of volume expansion	-
β_R	Rosseland average extinction coefficient	-
υ	kinematic viscosity, $= \mu / \rho$	$m^2 \cdot s^{-1}$

u_0	Inlet velocity	$m \cdot s^{-1}$
U	Velocity vector	$m \cdot s^{-1}$
ρ	Density	$kg \cdot m^{-3}$
μ	Dynamic viscosity	$Pa \cdot s$ or $kg \cdot m^{-1} \cdot s^{-1}$
v	Kinematic viscosity	$m^2 \cdot s$
α	Thermal diffusivity	$m^2 \cdot s$

LIST OF FIGURES

Temperature distribution of simulation 3 in xz-plane at y=2; (D) Temperature distributions of simulations in xz-plane at x=15mm and y=2mm

Fig. 5.3. Temperature and heat flux distributions on the fabric surface (A) Temperature distribution of simulation 1 on the upper surface of fabric; (B) Heat flux distribution of simulation 1 through fabric; (C) Temperature distribution of simulation 2 on the upper surface of fabric; (D) Heat flux distribution of simulation 2 through fabric; (E) Temperature distribution of simulation 3 on the upper surface of fabric; (F) Heat flux distribution of simulation 3 through fabric

Fig. 5.4. Velocity profile of simulation 3

Fig. 5.5. Comparison of temperature and heat flux distributions (A) Temperature distributions of simulations in xy-plane at y=2mm and z=0 (upper surface of fabric); (B) Heat flux distributions of simulations through fabric

Fig.5.6. Comparison of local heat transfer coefficients and Nusselt numbers (A) comparison of local heat transfer coefficient of model and simulation 1 and 2; (B) comparison of local heat transfer coefficient of model and simulation 3 at y=2 and y=3; (C) comparison of local Nusselt number of model and simulation 1 and 2; (D) comparison of local Nusselt number of model and simulation 3 at y=2 and y=3

LIST OF TABLES

1 INTRODUCTION

Textiles have been being one part of people's daily life, are widely used for clothing, protection, fashion statement, and technical applications [1, 2]. In order to apply textiles properly, a lot of properties of textile are needed to be evaluated. Among them, thermal property of non-woven and other textile fabrics is one of most important aspects. For instance, the clothing as 'the second skin' of human body needs to provide a pleasant state for human body in both hot and harsh conditions since the temperature of human body has a big influence in physiological response (as shown in table 1.1). Under the conditions of comfort, the mind is alert and the body operates at maximum efficiency. In contrast, serious physiological disorders or even death may occur if the temperature rises or falls to extreme levels. Besides, textiles are used for the thermal protection and insulation applications in order to conserve the thermal energy due to their excellent thermal insulation property. Therefore, the effective thermal conductivity/resistance of textiles has been studying in order to deeply understand the heat transfer process in fibrous structure materials, in order to predict, design and apply the textile products to meet various applications, and utilize the resources in an economically efficient way.

Table 1.1 Physiological responses at different body temperatures[3]

Body temperature (°C)	Physiological response
43.3	Brian damage, fainting, nausea
37.8	Sweating
37	Normal
<37	Shivering and goose bumps
<32.2	Speechless
26.5	Stiff and deformed body
<26.5	Irreversible body cooling

1.1 THE THERMAL CONDUCTIVITY OF TEXTILES

Physical property of a material related to application of heat energy is defined as a thermal property. The absorbed heat energy by a material may be transported to cooler regions if temperature gradients exist, and ultimately, the material may melt. Heat capacity, thermal expansion and thermal conductivities are few very important properties that are often critical in the practical and engineering applications of materials[4].

The thermal conductivity of a material is a measure of the ability of the material to conduct heat, can be defined as the rate of heat transfer through a unit thickness of the material per unit area per unit temperature difference[5]. A high value for thermal conductivity indicates that the material is a good heat conductor, and a low value indicates that the material is a poor heat conductor or insulator. From micro point of view, the thermal conductivity of solid electrically insulating materials is affected by the scattering of phonons. The phonon scattering is considered to be introduced by imperfections in the material. For example, crystal or amorphous boundary, defects, chemical bridge points, and the ends and entanglements of the molecular chains can scatter phonons and interfere with the thermal transmittance in polymer materials[5]. In the case of polymer fibers, the thermal conductivity in fiber direction depends on the crystallinity, orientation, crystal size, length of molecular chains, chemical bridge points, and morphologies composed of crystal and amorphous[6]. From the macro point of view, the thermal conductivity is affected by the components of material like composite[7-9], by the structure of material like porous material[10-12], by the heat transfer mechanisms such as conduction, convection, and radiation[13-16], by the surrounding conditions such as temperature and humidity[17, 18].

Generally, heat can be transferred in three different modes: conduction, convection, and radiation[5]. All modes of heat transfer require the existence of a temperature difference, and all modes are from the high-temperature medium to a lower-temperature one.

1.1.1 HEAT CONDUCTION

Heat conduction is the transfer of energy from the more energetic particles of a substance to the adjacent less energetic particles of a substance as a result of interactions between the particles. In gases and liquids, conduction is due to the collisions and diffusion of the molecules during their random motion. In solids, it is due to the combination of vibrations of the molecules in a lattice and the energy transport by free electrons. And heat transfer in conduction states that the rate of heat conduction through a plane layer is proportional to the temperature difference across the layer and the heat transfer area, but is inversely proportional to the thickness of the layer, which can be mathematically expressed by Fourier's law[5],

$$Q_{cond} = -kA\frac{dT}{dx} \tag{1.1}$$

Where Q_{cond} is heat flow by conduction (J), k is thermal conductivity ($W \cdot m^{-1} \cdot K^{-1}$), A is the heat transfer area normal to the direction of heat transfer (m^2), dT/dx is the temperature gradient (K/m), which is the slope of the temperature curve on a T-x diagram. Heat is conducted in the direction of decreasing temperature, and the temperature gradient becomes negative when temperature decreases with increasing x. The negative sign in Eq. 1.1 ensures that heat transfer in the positive x direction is a positive quantity.

1.1.1.1 Effective thermal conductivity of yarn

The effective thermal conductivity of yarn is always taken as the combination of thermal conductivities of yarn material and air. Kavlany[19] took the yarn as fiber-air matrix and assumed that the yarn complies with the system of series arrangement (figure 1.2). According to Kavlany's theory, the effective thermal conductivity of yarn can be given by,

$$\frac{k_e}{k_a} = \frac{k_f / k_a}{\phi k_f / k_a + 1 - \phi} \tag{1.2}$$

Where k_e is effective thermal conductivity ($W \cdot m^{-1} \cdot K^{-1}$), k_f is the thermal conductivity of fiber, k_a is the thermal conductivity of air, and ϕ is the porosity of the yarn.

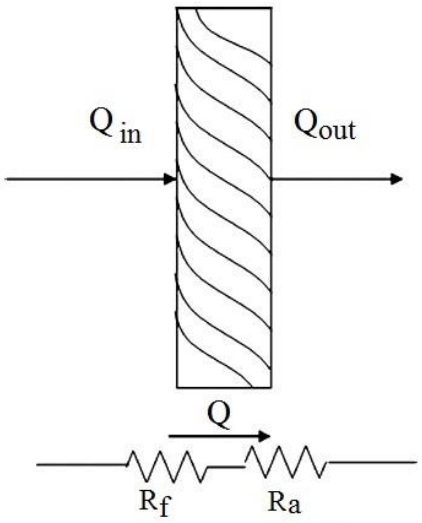

Figure 1.1. Fiber-Air matrix of a twisted yarn as a system of resistances[20]

Militky[21] introduced yarn twist coefficient to predict the effective thermal conductivity of yarn since Neckar[22] found that the mean packing density/porosity of yarn is a function of yarn twist. And the effective thermal conductivity is given by[21],

$$k_e = k_f + \frac{k_a - k_f}{1 + \frac{1-\phi}{\phi}\left[1 + Z\frac{k_a - k_f}{k_a + k_f}\right]} \tag{1.3}$$

Where k_e is effective conductivity ($W \cdot m^{-1} \cdot K^{-1}$), k_f is the thermal conductivity of fiber, k_a is the thermal conductivity of air, and ϕ is the porosity of the yarn, Z is yarn twist coefficient. Z=1 indicates all fibers are perpendicular to the direction of heat flow, Z=2/3 for random fiber orientation and Z =5/6 for half of fibers being random and the other half being normal to the direction of heat flow.

1.1.1.2 Effective thermal conductivity of fabric

Bogaty[23] firstly described the thermal conductivity of a textile material as a fiber-air mixture. And the thermal conductivity is given by,

$$k_e = A\left(V_f k_f + V_a k_a\right) + B\left(\frac{k_f k_a}{V_a k_f + V_f k_a}\right) \tag{1.4}$$

Where the effective thermal conductivity k_e of a textile material is described by the volume fractions V_f and V_a and the thermal conductivities k_f and k_a, of the solid fiber and air, respectively. The first term of the right side of this equation describes an ideal model of a fabric construction whose fibers are totally parallel to the flow of heat, while the second term describes an ideal model of a fabric construction whose fibers are totally in series to the flow of heat (A and B are the parallel and series fractions).

1.1.2 HEAT CONVECTION

Convection is the mode of energy transfer between a solid surface and the adjacent liquid or gas that is in motion, and it involves the combined effects of conduction and fluid motion[5]. The faster the fluid motion, the greater the convection heats transfer. The rate of convection heat transfer is observed to be proportional to the temperature difference, and is conveniently expressed by Newton's law of cooling as[5],

$$Q_{conv} = hA_s\left(T_s - T_\infty\right) \tag{1.5}$$

Where h is the convection heat transfer coefficient ($W/(m^2 \cdot K)$), A_s is the surface area through which convection heat transfer takes place (m^2), T_s is the surface temperature (K), and T_∞ is the temperature of the fluid sufficiently far from the surface (K). The convection heat transfer coefficient h is the most important parameter for evaluating the rate of heat convection,

which is not a property of the fluid. It is an experimentally determined parameter whose value depends on all the variables influencing convection such as the surface geometry, the nature of fluid motion, the properties of the fluid, and the bulk fluid velocity. And the heat transfer coefficient *h* also can be expressed by,

$$h = Nu \cdot \frac{k_F}{L_c} \tag{1.6}$$

Where *Nu* is Nusselt number, k_F is the thermal conductivity of the fluid ($W \cdot m^{-1} \cdot K^{-1}$), L_c is the characteristic length (m). And the overall heat transfer in terms of Nusselt number around a circular cylinder is typically correlated by a power law relationship,

$$Nu = C \cdot Re^m \cdot Pr^n \tag{1.7}$$

Where *m* and *n* are constant exponents, and the value of the constant *C* depends on geometry and flow, *Re* and *Pr* are Reynold number and Prandtl number, respectively. Several empirical correlations of the overall heat transfer under heat convection are given in table 1.2.

Table 1.2 Empirical correlations for the average Nusselt number for force convection [24-28]

Cross section of cylinder	Correlation	fluid	Range of Re
Circle	$Nu = 0.989\,Re^{0.330}\,Pr^{1/3}$	Gas or liquid	$0.4 < Re_L < 4$
	$Nu = 0.911\,Re^{0.385}\,Pr^{1/3}$		$4 < Re_L < 40$
	$Nu = 0.683\,Re^{0.466}\,Pr^{1/3}$		$40 < Re_L < 4000$
	$Nu = 0.193\,Re^{0.618}\,Pr^{1/3}$		$4\times10^3 < Re_L < 4\times10^4$
	$Nu = 0.027\,Re^{0.805}\,Pr^{1/3}$		$4\times10^4 < Re_L < 4\times10^5$
	$Nu = 0.3 + \frac{0.62\,Re^{0.5}\,Pr^{1/3}}{\left[1+\left(0.4/Pr\right)^{2/3}\right]^{1/4}} \times\left[1+\left(Re/282000\right)\right]^{4/5}$		$10^2 < Re_L < 10^7$
Square	$Nu = 0.102\,Re^{0.675}\,Pr^{1/3}$	Gas	$5 < Re_L < 10^5$
Square (tilted 45°)	$Nu = 0.246\,Re^{0.588}\,Pr^{1/3}$	Gas	$5 < Re_L < 10^5$
Hexagon	$Nu = 0.153\,Re^{0.638}\,Pr^{1/3}$	Gas	$5 < Re_L < 10^5$
Hexagon (tilted 45°)	$Nu = 0.160\,Re^{0.638}\,Pr^{1/3}$	Gas	$5 < Re_L < 19500$
	$Nu = 0.0385\,Re^{0.782}\,Pr^{1/3}$		$19500 < Re_L < 10^5$
Vertical plate	$Nu = 0.228\,Re^{0.731}\,Pr^{1/3}$	Gas	$4\times10^3 \le Re_L \le 15000$
Ellipse	$Nu = 0.248\,Re^{0.612}\,Pr^{1/3}$	Gas	$2500 \le Re_L \le 15000$

1.2.3 HEAT RADIATION

Radiation is the energy emitted by matter in the form of electromagnetic waves (or photons) as a result of the changes in the electronic configurations of the atoms or molecules. Unlike conduction and convection, the transfer of energy by radiation does not require the presence of an intervening medium[5].

Stefan–Boltzmann law states that the total energy radiated per unit surface area of a body in unit time is directly proportional to the fourth power of the black body's thermodynamic temperature T (also called absolute temperature),

$$Q_{rad} = \varepsilon A \sigma \left(T_w^4 - T_\infty^4 \right) \tag{1.8}$$

Where Q_{rad} is the heat flow by radiation (J), ε is the emissivity of the body surface, σ is the Stefan-Boltzmann constant, 5.67 x 10^{-8} W/($m^{2\cdot}K^4$), A is the surface area of the radiating object (m^2), T_w is the wall temperature and T_∞ is the ambient temperature (K).

When the radiation happens between two objects, the generally known equation characterized by the fourth power of temperature[29, 30],

$$q_{rad} = \sigma \left(T_1^4 - T_2^4 \right) \Big/ \left(\varepsilon_1^{-1} + \varepsilon_2^{-1} - 1 \right) \tag{1.9}$$

Where q_{rad} is the heat flux by radiation (W), ε_1 and ε_2 are the emissivities of the body one and body two, T_1 and T_2 are the surface temperatures of body one and body two (K). Equation (1.9) can be approximated by a linear one with the use of the mean temperature $T_m=(T_1+T_2)/2$,

$$q_{rad} = 4\sigma T_m^3 \left(\varepsilon_1^{-1} + \varepsilon_2^{-1} - 1 \right) \left(T_1 - T_2 \right) \tag{1.10}$$

Therefore, the radiation heat transfer coefficient h_{rad} can be defined by[31],

$$h_{rad} = 4\sigma T_m^3 \left(\varepsilon_1^{-1} + \varepsilon_2^{-1} - 1 \right) \tag{1.11}$$

Hes Lubos[32] proposed one formula to determine the radiation heat transfer coefficient through textiles, which is given by,

$$h_{rad} = \frac{4h\sigma T_m^3}{2/\varepsilon - 1} exp \frac{0.188h\left(v-1\right)\mu}{r\sqrt{\pi}} \tag{1.12}$$

Where μ represents the filling coefficient of the fabric, and v is the (idealized) portion of fibers oriented vertically to the isotherms in the fabric. The terms h and σ present the thickness and the radiation constant, and ε and r are the mean emissivity and radius of fibers.

Kaemmerlen[33] reported that radiation heat transfer coefficient can be obtained by,

$$h_{rad} = \frac{16\sigma T_m^3}{3\beta_R} \tag{1.13}$$

Where β_R is the Rosseland average extinction coefficient.

1.2 MEASUREMENT OF THERMAL CONDUCTIVITY OF TEXTIELS

Strictly speaking, the real property of materials can never be obtained since there is no instrument or testing device which can get rid of error. Besides, the property of materials will be different when they are evaluated in various instruments, different standard and under different conditions.

1.2.1 MEASUREMENT OF THERMAL CONDUCTIVITY OF SINGLE FIBER

The interest in measuring the thermal conductivity of fibers is twofold. From the fundamental point of view, the measurement of the temperature variation of the thermal conductivity of a crystalline solid allows the investigation of structure defects, phonon-phonon interactions and eventually, in good electrical conductors, electron-phonon interactions[34]. The advantage of the thermal conductivity method as regards structural defects is that it complements the information obtained on a microscopic basis by other techniques since gives an overall view over the entire sample[35, 36]. The second point of interest is that thermal conductivity measurements permit determination of the value of this parameter, which is important to know in a practical device in order to be able to account for heat transfer. However, it is not an easy work to measure the thermal conductivity of fiber due to its particular geometry and very fine diameter. Specifically, there are three difficulties for measuring the thermal conductivity of single fiber. The first one is the contact problem between heater and fiber; the second one is the contact between thermal sensor and fiber, and the last is the heat loss from heater due to conduction and radiation, and heat loss along the fiber.

1.2.1.1Thermal potentiometer method

The thermal potentiometer is a steady-state apparatus for measuring thermal conductivity. And the schematic diagram of the thermal potentiometer testing device is showing in figure 1.2, which was elaborated by Piraux [37]. In this system three guards are needed. The first

guard, G_0, shields the sample heater, H_s, in order to reduce both heat losses arising from conduction through the current leads and radiation from the heater itself. Two other guards, G_1 and G_2, reduce heat losses via the thermometer wires from the two points, C_1 and C_2, on the sample where the temperature sensors are connected. A compensating heater, H_0, is wound around guard G_0. A differential thermocouple senses the temperature difference between the sample heater, H_s, and the guard, G_0. All the leads in contact with the sample heater, including those of the differential thermocouple, ΔT_0, are thermally anchored to the heater guard, G_0. Two more compensating heaters, H_1 and H_2, are wound around G_1 and G_2, respectively. Two differential thermocouples, ΔT_1 and ΔT_2, whose output leads are thermally anchored to G_1 and G_2 respectively, sense the temperature differences between C_1 and G_1 and C_2 and G_2, respectively. An additional differential thermocouple, ΔT_{diff}, measures the temperature difference between G_1 and G_2. When the sample heater, H_s, is energized, temperature gradients are induced along the sample and supports. As a result, the heat generated in H_s flows, not only through the sample, but also through the heater and guard supports, S_0 , S_0', S_1 , S_1', S_2 , and S_2'. In order to minimize heat losses through the leads and structure members, heaters H_0 , H_1 and H_2 are adjusted until the temperature differences between H_s and G_0 , G_1 and C_1 , G_2 and C_2 are zeroed[37].

The experimental procedure is as follows. Firstly, the sample heater, H_s, is energized in order to establish a temperature difference between the heater, H_s, and the heat sink. Then the currents in the three guard heaters (H_0, H_1 and H_2) are adjusted to minimize the temperature differences (ΔT_0, ΔT_1 and ΔT_2). At this point, the signal from thermocouple ΔT_{diff} is recorded, yielding a precise value for the temperature difference along the sample between the points C_1 and C_2. This temperature difference is then used, together with the cross-sectional area of the sample and the distance between the points C_1 and C_2, to calculate the thermal conductivity of the fibers[38].

This apparatus measures a fiber sample's thermal response to a controlled thermal gradient. It is capable of measuring the temperature dependence of the thermal conductivity with a high degree of accuracy[39]. However, this method is more suitable for the particular case of carbon fibers, whose thermal conductivity is high at high temperatures and low at low temperatures, than for other types of fibers (polymers, glass, etc) whose thermal conductivity is usually very poor at all temperature. As a result of the low thermal conductivity of fibers, the main problem in the entire temperature range is relative to the connecting wires. That is those wires feeding the sample heater with current and those measuring the corresponding

voltage, those of the temperature sensors on fiber and the leads for thermopower measurements. Indeed, since the sample has a very small diameter, it is technically difficult to find metallic wires of reasonable length and small enough diameter yielding a thermal conductance which is negligible with respect to that of the fibers. The problem is even more pronounced for the heater leads, which should have good electrical conductivity. Besides, since the fibers are small, it is practically impossible to hang the temperature sensors and the heater on them and insure good thermal contact. Therefore, the thermometers sensing the temperature on fiber, and the heater must be supported mechanically by some other means. This will introduce new heat losses by conduction through solids. Moreover, when increasing the temperature of heater the heat loss by radiation from the heater and fiber become increasingly important and should be accounted for.

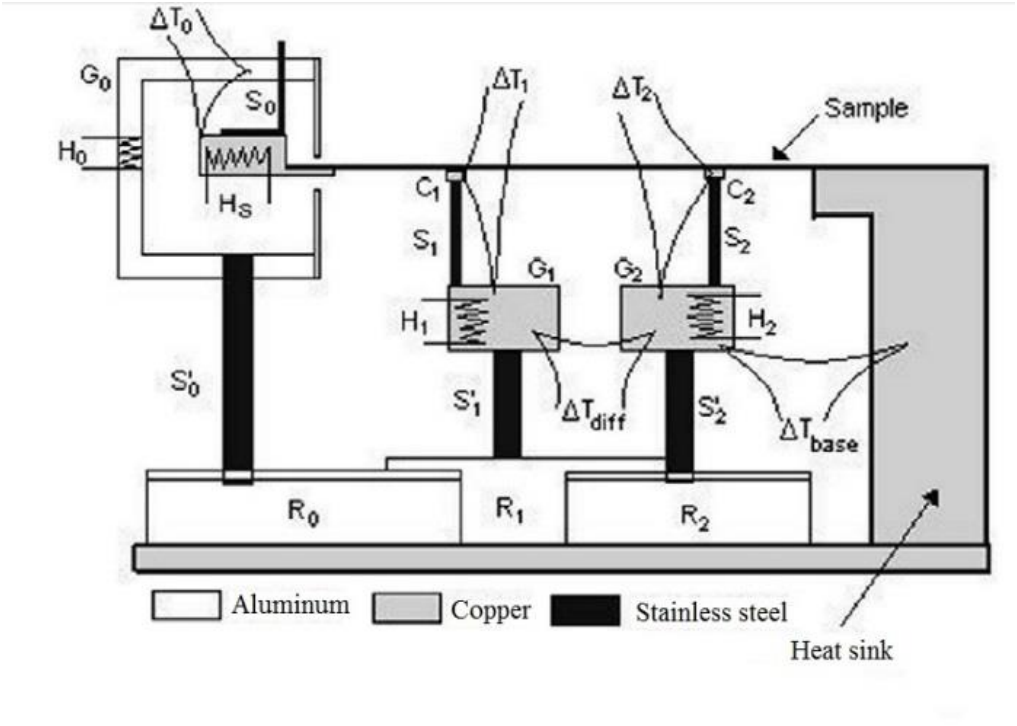

Figure 1.2. Schematic diagram of the thermal potentiometer testing device[12, 37]

1.2.1.2 Short-hot-wire method

This method reported by Zhung[40-42] was used to measure the thermal conductivity of single fine fiber. The schematic diagram of testing device and physical model are shown in figure 1.3.

The principle of this method is to attach one end of the test fiber to one hot wire which was fixed and supplied with a constant direct current to generate a uniform heat flux; another end of the test fiber is to connect a heat sink which is maintained at the initial temperature during

the entire measurement. Therefore, the thermal conductivity of test fiber can be calculated from a series of equations after determining the heat generation rate and average temperature of the hot wire since the temperature at the junction point of the hot wire and test fiber depends on the values of the thermal conductivity of the hot wire and the test fiber, the heat generation rate of the hot wire, and the heat transfer coefficients around the hot wire and test fiber. But this method asks a vacuum condition and small Biot number. On the other hand, the results have a higher uncertainty based on theoretical analysis even for very high thermal conductivity carbon fiber.

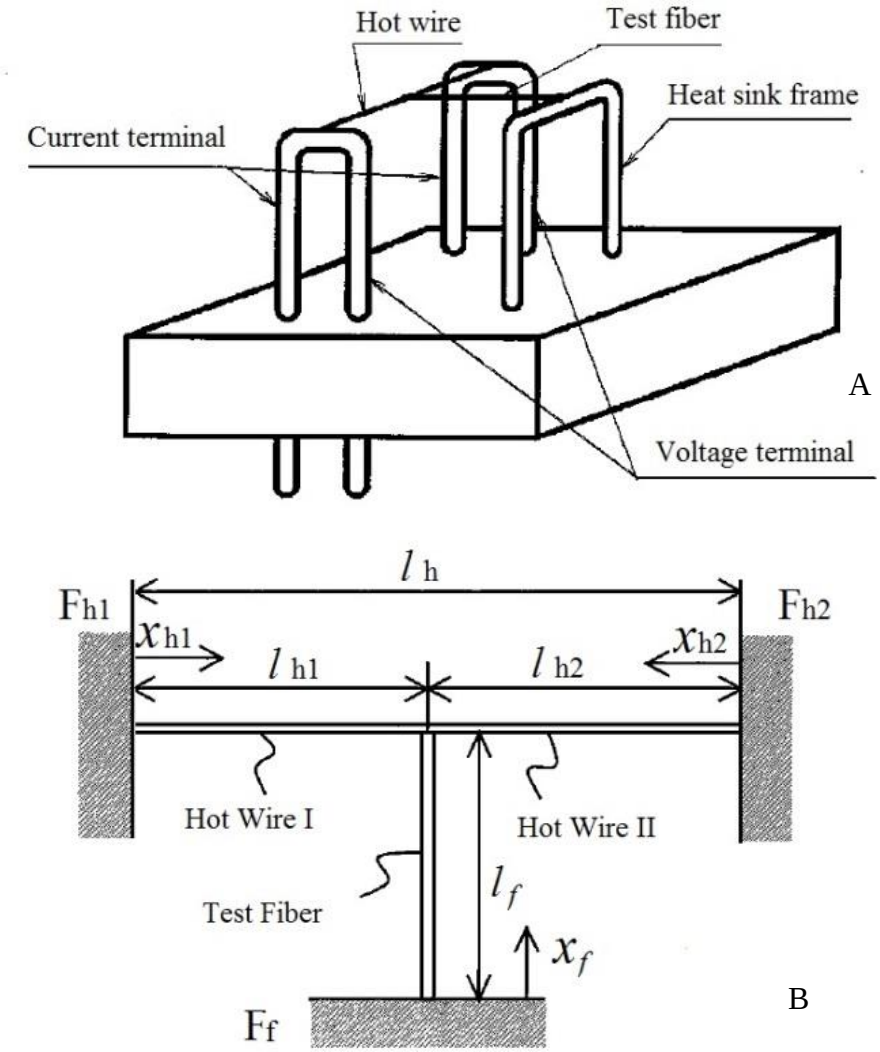

Figure 1.3. Schematic diagram of testing device (A) and the physical model (B) [40]

1.2.1.3 Angstrom's apparatus

The schematic of Angstrom's set-up is given in figure 1.4, which consisted of a computer, a multimeter, an interface, and a testing unit surrounded by a water-cooled evacuated test

chamber. A periodic thermal wave was applied to the sample by a synthesized function/sweep generator. Moreover, in order to minimize gas conduction and convection heat losses, an absolute pressure lower than 10^{-4} mbar was provided[12]. This method is based on the fact that, if one end of a sample is periodically heated, the temperature along the sample varies with the same period but with diminishing amplitude. Therefore, the thermal diffusivity can be determined by measuring the amplitude decrement and the phase difference[43]. Although the temperature wave travels along the sample with finite velocity, the phase varies. Measurement of the amplitude decrement and the phase difference enables the thermal diffusivity to be determined according to the following expression,

$$a = \frac{L^2}{2 \cdot \Delta t \cdot \ln\left(\Delta T_1 / \Delta T_2\right)} \tag{1.14}$$

Where L is the distance between temperature sensors; Δt is the time delay (the time taken by the thermal wave to travel from one sensor to the other), and ΔT_1 and ΔT_2 are the amplitudes of the thermal wave measured by the sensors nearest to the heat source and far away from the heat source, respectively. Thermal diffusivity is related to the thermal conductivity by the following expression,

$$k = a \cdot \rho \cdot c \tag{1.15}$$

Where a is thermal diffusivity, ρ is density, and c is heat capacity.

The principle and the apparatus are compendious, but the accuracy of experiment was easily influenced by the surrounding conditions, in addition, this method is measuring thermal diffusivity.

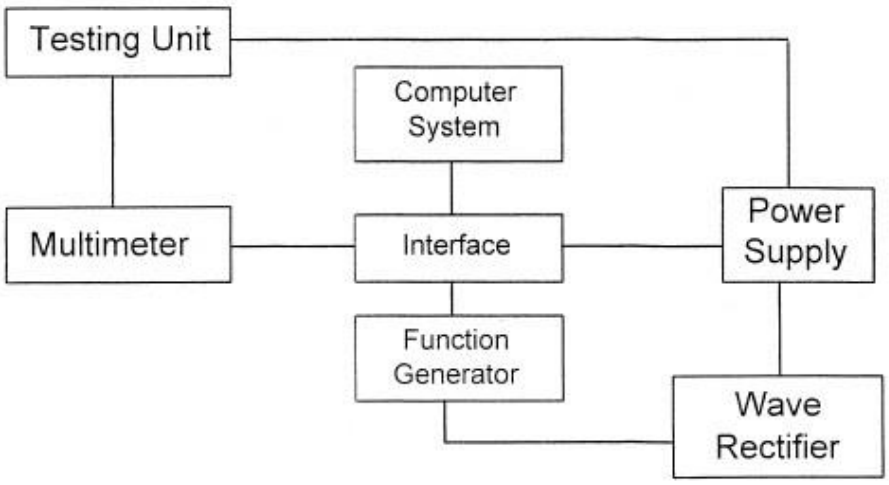

Figure 1.4. Schematic view of Angstrom's apparatus set-up

1.2.1.4 Composite including fibers

Measurement of thermal conductivity of fibers is practically difficult since most of the measurement techniques require solid materials. However, the thermal conductivity of fiber-reinforced composite laminates and the resin are easily measured. Thus, the ability of accurately predicting the thermal conductivity of fibers through the composite and resin properties is highly desirable.

The principle of this method is to measure the effective thermal conductivity of composite by conventional method (hot guarded plate method)[44-46], and then to calculate the thermal conductivity of each composition according their volume fraction. In addition, the arrangement of fiber's orientations should be taken into consideration due to the anisotropy (axial and radial) of fiber in heat conduction [47, 48]. The simplified arrangements of fibers in composite are given in figure 1.5.

For the parallel structure, the physical problem and the equivalent thermal circuit for parallel thermal resistance can be described through the heat conduction equation (1.1),

Simplifies to,

$$\begin{aligned} Q_t &= k_e A_t \left(T_{out} - T_{in}\right)/L \\ &= Q_f + Q_r \\ &= \left(k_f \times A_f + k_r \times A_r\right) \times \left(T_{out} - T_{in}\right)/L \end{aligned} \tag{1.16}$$

Therefore,

$$k_e = k_f V_f + k_r V_r \tag{1.17}$$

And

$$\frac{k_{pf}}{k_r} = \frac{k_e/k_r - V_r}{V_f} \tag{1.18}$$

Where Q_t is the total heat flow through composite, Q_f and Q_r are the heat flow through fiber and resin, respectively, k_e, k_{pf}, and k_r are the thermal conductivities of composite, fiber in parallel stucture and resin, T_{out} and T_{in} are the temperatures of both sides of composite, L is the thickness of composite, A_t, A_f, and A_r are the areas of composite, fiber and resin, V_f and V_r are the volume fraction of fiber and resin.

Similarly, the fiber thermal conductivity of fiber for the series structure can be expressed by,

$$k_{sf} = \frac{k_e}{k_r}\left(k_r V_f + k_f V_r\right) \tag{1.19}$$

Where k_{sf} is the thermal conductivity of fiber in series structure.

This hot guarded plate method is simple and easy to operate, and the results are reliable. The thermal conductivity of fibers can be easily obtained after determining the volume fraction of each component. But the accuracy of thermal conductivity of fibers would be influenced by the fiber orientation, size, shape, and the void fraction in composite [49-52].

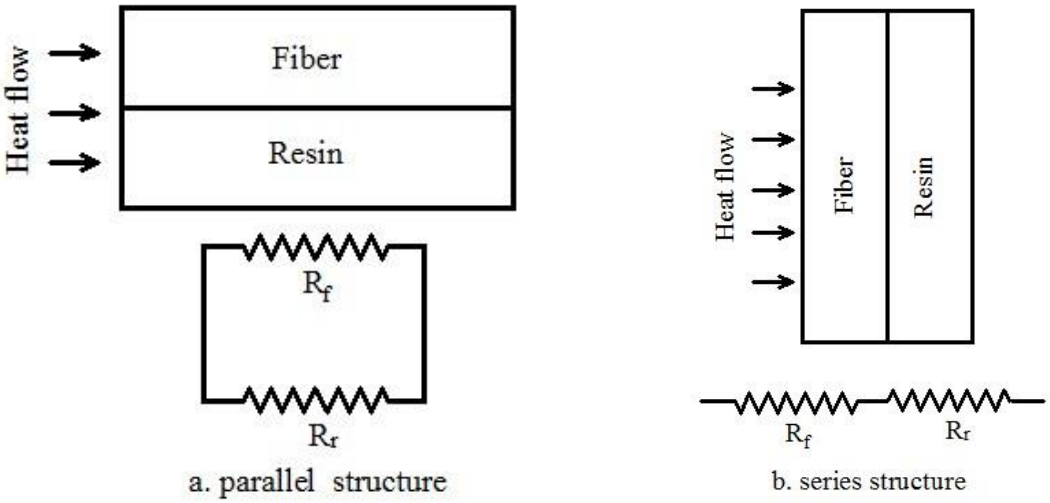

Figure 1.5. Parallel and series structures of fibers in composite

In addition, some researchers have used laser flash analysis of a unidirectional composite sample to measure the thermal diffusivity of fibers, but this method is considered less reliable than steady-state methods[12, 53]. In the laser flash method, the fiber component of the thermal diffusivity must be estimated using the rule of mixtures. Thus, fiber volume fraction and fiber alignment must be accurately measured. Additionally, values of density and heat capacity of the sample are needed in order to estimate the thermal conductivity. The uncertainty associated with the heat capacity and density measurements adds to the uncertainty of the thermal conductivity measurement.

1.2.2 MEASUREMENT OF THERMAL CONDUCTIVITY OF TEXTIELS

Two principles, which are guarded hot plate principle[54, 55] and photopyroelectric technique [56-58], are widely applied for determining the thermal conductivity/resistance of textiles even though various instruments come out in market.

1.2.2.1 Alambeta

The principle of Alambeta instrument is based on guarded hot plate principle which is simplified described in figure 1.6. Alambeta instrument enables the quick measurement of both steady-state and transient-state thermal properties (thermal insulation and thermal contact properties). The instrument consists of two measuring heads between which the test specimen is placed. Both measuring heads are equipped with thermocouples and so-called heat flow sensors. The lower measuring heads is adjusted to the ambient temperature by suitable cooling means; the upper, heated measuring head is adjusted to a controlled constant differential temperature (the temperature difference on sample's both sides can be 40°C or 20°C). The heat flow sensors act up at the contact faces of both measuring heads under a 200Pa or 1000Pa contact pressure. When upper measuring head is lowered on the measuring specimen the heat flow at the upper surface and the underside of the test specimen can be measured[54]. The fundamental measuring principal implies the measuring and processing of the heat flows in dependence of time. At last, the values of thermal conductivity, thermal diffusion, thermal absorption, thermal resistance, the ratio of maximal to stationary heat flow density, and stationary heat flow density at the contact point. The instrument also determines the fabric thickness.

This method is widely accepted in measuring thermal conductivity/resistance of textiles [31, 56, 59-61]. Especially, it can give thermal resistance directly since the thickness of samples can be obtained during the measuring process. As the fabric thickness can depend on the locally applied pressure, the resulting precision of the calculated thermal resistance might be affected by this thickness measurement precision. However, the precision of measurement could be affected by sample's thickness since the edges of sample cannot be insulated and the heat loss will happen at the edges.

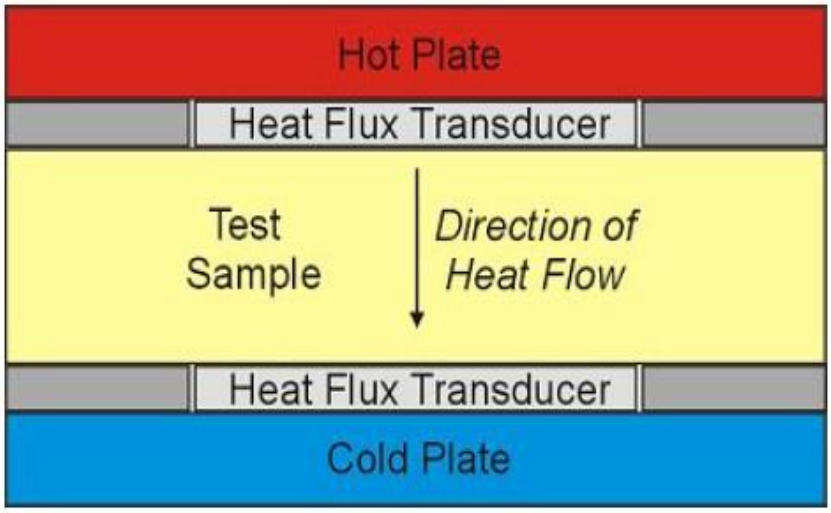

Figure 1.6. Schematic diagram of guarded hot plate method

1.2.2.2 TCi-Thermal property analyzer

The principle of TCi analyzer (standard numbers are EN61326 and EN61010) is based on PhotoPyro-Electric principle, whose schematic diagram of is shown in figure 1.7. TCi analyzer is comprised of a sensor, which has a central heater/sensor element in the shape of a spiral surrounded by a guard ring. The guard ring generates heat in addition to the spiral heater, thus, approximating a one-dimensional heat flow from the sensor into the material under test in contact with the sensor. The voltage drop on the spiral heater is measured before and during the transient. The voltage data is then translated into the effusivity value of the tested material.

The TCI analyzer is firstly to measures the voltage output of the sensor, and then to convert the temperature change into equivalent voltage signal change by assuming that there is a perfect linearity correlation between the sensor's resistance and its temperature. After that two equations are applied to get the thermal conductivity,

$$\Delta T = \left(1.1284 G\sqrt{t}\right) \Big/ \left(e_1 + e_2\right) \tag{1.20}$$

Where ΔT is the change in sensor surface temperature, G is power flux supplied to sensor, t is time, e_1 and e_2 are equivalent effusivity of sensor and sample, respectively.

$$e_2 = \sqrt{k \rho c_p} \tag{1.21}$$

Where k is thermal conductivity of sample, ρ and c_p are density and specific heat of sample. Therefore, the precision of TCI analyzer mostly depends on the sensor's calibration in temperature, conductivity and effusivity, and different calibrations are required for materials

with dissimilar thermo properties. For instance, it is necessary to calibrate solids and liquids separately. Measuring a liquid with a calibration made for solids, or vice versa, will generate an invalid result. In addition, the density and the specific heat of material are needed since this method for determining the thermal conductivity of the material is based on the effusivity measurement.

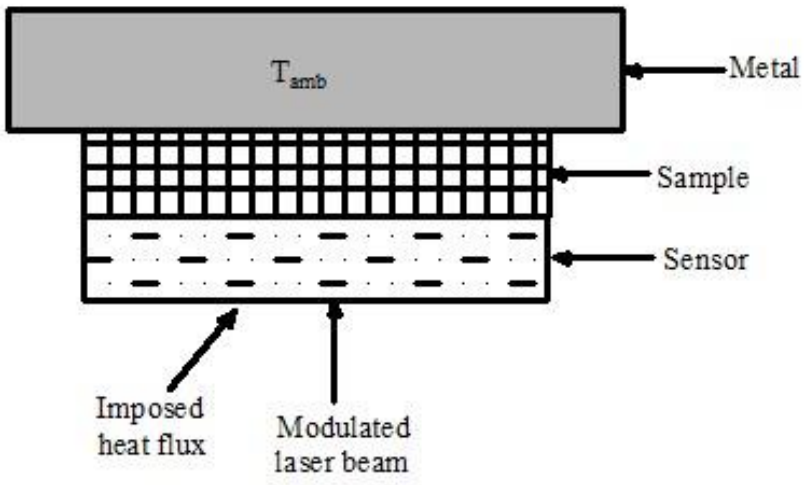

Figure 1.7. Schematic diagram of PhotoPyro-Electric method

1.2.2.3 ASTM standard testing method

This method is based on guarded hot plate principle to measure the steady state heat transfer properties of textile materials in convective and non-convective modes, and the detail information of testing set-up of ASTM standard D1518 is shown in figure 1.8[55].

The unidirectional flow conditions are obtained by the guarded hot plate surrounding the test plate. The test area comprises a square copper plate, being surrounded by a guard ring of the same metal and same thickness. The width of the guard ring is the same on all sides. The guard ring minimizes the lateral heat losses. The test plate and the guard ring are heated separately. The temperatures of the test plate and the guard plate are sensed by resistive temperature detectors. Insulation has been provided to prevent bottom heat losses with the help of reflective insulation. A wind tunnel is attached to the instrument with a suction fan by which airflow at various speeds can be obtained over the fabric surface. Heat flow rate can be measured by noting the current and voltage input to the test plate heater. Therefore, the thermal resistance of the fabric in a natural and forced convective mode can be obtained by the following formula,

$$R_{fabric} = \frac{(T_t - T_a) A_t}{Q_t} - R_c \tag{1.22}$$

Where T_t is the temperature of the test plate; T_a is the temperature of the air; A_t is the area of the test plate; Q_t is the watt given to the test plate; R_{fabric} is the thermal resistance of the fabric and R_c is the contact thermal resistance which builds up due to the thin still air film over the test plate when no fabric is placed on the top[62].

But there is no commercial instruments produced according to this standard. Besides, the sample is covered by plates, and the air flow can't go through sample or even can't contact the surface of sample. Therefore, this method didn't simulate some real conditions when the wind moves facing textiles and penetrates the textiles.

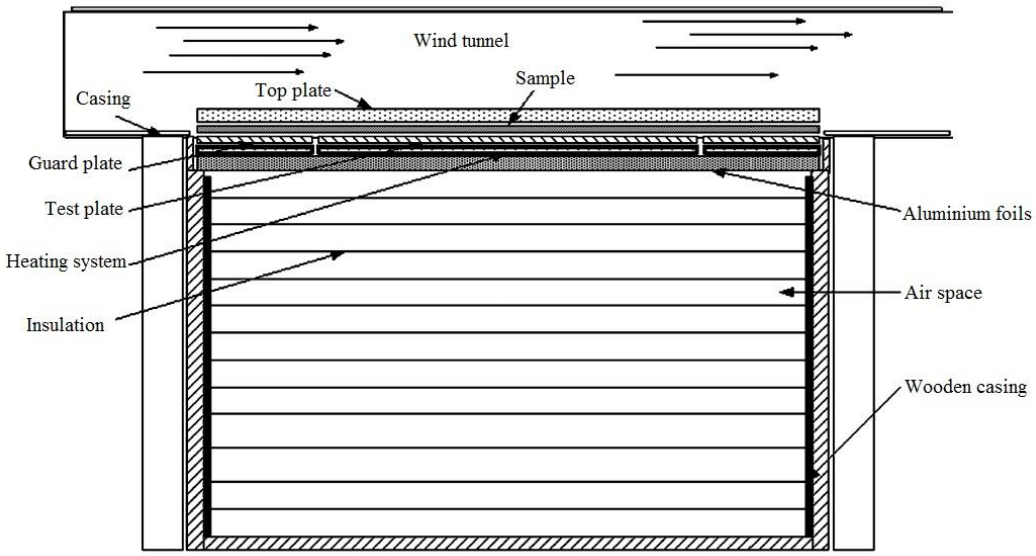

Figure 1.8. ASTM D1518: Standard Test Method for Thermal Transmittance of Textile Materials

1.3 RESEARCH IN THERMAL CONDUCTIVITY OF TEXTILES

As mentioned previously, owing to the importance of thermal conductivity of material in their application, a lot of work has done in evaluating the thermal conductivity of textiles. However, almost all of the thermal conductivity of textiles is evaluated under heat conduction[2, 31, 32, 59, 60, 63, 64] due to the limitation of existing testing instruments and the difficulties of producing one instrument to meet various real conditions in human's daily life (temperature range, convection conditions, and humidity, etc.). Theoretically, if only consider the conduction mechanism in textiles or porous materials, thermal conductivity should decrease continually with decreasing bulk density, finally approaching the conductivity of the gas filling the void spaces. However, nonwoven fabrics typically show

first a decrease and then an increase in the apparent thermal conductivity with decreasing bulk density. This suggests that other heat transfer mechanisms must contribute appreciably to the apparent thermal conductivity of these materials[5]. Esra[59] reported that the thermal conductivity of fabrics made of hollow fiber and solid fiber from the experiment didn't demonstrate significant difference because the porosity of fabric played a more important role than the porosity of fibers. Lizak[60] stated that the thermal conductivity of fabric from hollow fibers got lower thermal conductivity than the fabric from solid fibers, but the difference was not significant. Stuart and Holcombe[65] have published data for polyester and polypropylene nonwovens showing an increased role in fiber conduction at high solidities. Heather[66] investigated the thermal insulation of three type of fibers (solid fiber, hollow fiber and grooved fiber) in terms of various denier, interstitial void fractions, interstitial void media, and orientations to the applied temperature gradient to evaluate their applicability. And their results indicated that the best conductive insulation is achieved for a high-void-fraction configuration with a grooved fiber cross section, aerogel void medium, and the fibers oriented normal to the heat flux vector. The experiments of Hager and Steere[67] show that fiber conduction accounts for only 0.3% of the total heat transfer in high porosity fibrous structure. Strong[68] studied glass fiber systems, found that solid conduction could account for 6-7% of the total, but they obtained these results with highly compressed samples (solidities 10-19%), and so a large degree of fiber-fiber contact might be expected. Monika Baczek investigated the thermal conductivity of nonwoven fabrics; found that the ratio of thermal conductivity by radiation to conduction was about 15%[31]. Therefore, there appears to be a consensus that heat flux passing through textile or a porous medium may in general be represented by several mechanisms: conduction through solid fibers, conduction through air in the interfiber spaces, free and forced convection, and radiation[69]. However, there is no instrument for evaluating the thermal conductivity/resistance of textiles under heat conduction, heat convection and heat radiation simultaneously. Fortunately, some kinds of heat transfer mechanisms can be ignored in some cases, for instance, the convective heat transfer can be ignored when the speed of air flow is very small, and the convective and the radiative heat transfer can be ignored when the temperature difference is small. Based on heat transfer in conduction, some analytical models were proposed to predict the thermal conductivity of textiles.

The first analytical model for predicting the thermal conductivity of textiles was reported by Bogaty[23], whose mathematical expression is described in equation (1.4). In his model, the

volume fraction of air and textile material, the orientations (the heat flow is parallel and perpendicular to the fiber) of fibers, and also the percentage of fibers in parallel and series arrangement are taken considerations. For simplified cases, this model can be applied if all the fibers are parallel to the heat flow or perpendicular to the heat flow. But for real structures of textiles or nonwovens, it is very difficult to determine the orientations of fibers as well as the percentages of fibers in parallel and series arrangement. Therefore, this model cannot be widely used. Since the difficulties from Bogaty's model, Militky[21] simplified the model by assuming that the parallel and series arrangements of fibers have the same quantity in textiles, therefore, the average value of the parallel and the series models can be used for the thermal conductivity of textile. Faleh [48] stated one polynomial predicting model which needs to get the coefficient from every practical experiment for evaluated the thermal conductivity of fiber in composites. Maxwell-Eucken model [70, 71] was used for materials with continuous phase and dispersed phase. It assumes a dispersion of small spheres within a continuous matrix of a different component, with the spheres being far enough apart so that the local distortions to the temperature distributions around each of the spheres do not interfere with their neighbors' temperature distributions. Wang [72] deduced a mathematical expression for co-continuous structural materials based on Maxwell-Eucken model, but his model also can be expressed by the series and parallel models. Levy's [73] gave a model based on the Maxwell-Eucken model, but levy's model was derived solely by algebraic manipulation, with no stated physical basis. Ismail[74] developed a mathematical model for predicting the effective thermal conductivity of plain woven fabric containing circular warp yarns and elliptic weft yarns. In this model, the fractional concept is adopted, which means the thermal resistances of solid parts and gas parts are calculated separated first, and then the total thermal resistance according to the combinations of solid and gas parts can be obtained. But this model is only convenient for simple structures. Even these analytical models are available, all of them assumed that the air in textiles is stagnant, no heat loss/thermal resistance happens in contact area, the pore size and pore shape don't have influence in thermal resistance. And according to the literature research, there lacks of analytical model for thermal conductivity of textiles under convective heat transfer and radiative heat transfer. Kothari[11] proposed a model for prediction of thermal resistance of woven fabrics by using thermal electrical analogy technique. Yoshihiro[64] developed structural models of yarns, plain weave fabrics and plain weave fabric/resin composites and theoretical formulas for the effective thermal conductivity which were derived from these models. Zhu[10] developed a fractal effective thermal conductivity model for woven fabrics with multiple layers. Das[9] developed a mathematical

model for prediction of thermal resistance of multilayer clothing in non-convective media. Matusiak[75] developed a model of thermal resistance of woven fabrics and considered cross-section of yarn as square shape. But the prediction models for special-shaped fibers and yarns are missing.

On the other hand, moisture transmission through a textile material is not only associated with the mass transfer processes, but also related to heat transfer. During the transmission of water molecules through textile materials, they are absorbed by fiber molecules due to their chemical nature and structure. With an increase in humidity, the heat transfer efficiency of the material increases. And the adsorption of moisture/liquid of textiles is inevitably accompanied by exchange of heat or energy, which will cause temperature changes of textiles at the same time[76-78]. It makes the small environment between human body and cloth system more complicated. The increased temperature due to the production of heat on the surface of the material led to the decrease of the rate of moisture vapor transmission [79-81]. King and Cassie[77] observed that in a textile material, immersed in a humid atmosphere, the time required for the fibers to come to equilibrium with the atmosphere is negligible compared with the time required for the dissipation of heat generated and absorbed by the fibers when regain changes. On the other hand, this kind of heat would be helpful for moisture evaporation and would provide a much warmer condition for human body in a period of time. In other cases, the heat of liquid absorption could result in the deterioration of textile's qualities when the textiles packed and the heat cannot dissipate quickly. And this kind of heat also could be one reason for spontaneous combustion of warehouse where stored a lot of textiles. Therefore, it is very important to investigate the temperature change of textiles when they are absorbing moisture/liquid.

1.4 NUMERICAL SIMULATION

Although the most reliable information about a physical process is often given by actual measurement, however, it would take plenty of time and labor force to carry out measurements for evaluating, designing and optimizing a product. In addition, there are serious difficulties of measurement in many situations, and the measuring instruments are not free from errors. In contrast, a theoretical prediction works out the consequences of mathematical models rather than those of an actual physical process. In a theoretical calculation, both the realistic conditions and ideal conditions can be simulated in a very short time comparing with practical experiments. Besides, more detail information can be provided by computer. And numerical method has been widely used in every area due to its reliable

accuracy, flexibility for both realistic conditions and ideal conditions, and more detailed information.

The use of numerical simulations to study effective thermal is very common and several different numerical methods have been employed, including boundary element methods, finite difference methods, and finite element methods. Boundary element methods may be thought of as a special class of finite element methods. Finite difference methods have the potential for simplicity and lower computing requirements than finite element methods, while finite element methods have the advantage that the discretization process is not constrained by regular node positioning, and they are therefore more suitable for irregular geometries and spatially variable properties and conditions. Carson[82] and Dasgupta [83] stated that the numerical simulation for heat transfer had good agreements with the experimental results.

1.5 AIM OF THIS WORK

The aim of this work includes:

(1) Investigate the factors which would influence the thermal conductivity of textiles under conductive heat transfer by numerical method;

(2) Study the effect of structure on the effective thermal conductivity of high porosity textiles;

(3) Study the factors of thermal resistance of textiles under convective heat transfer;

(4) Investigate the temperature changes of textile during the adsorption process.

2 STUDY ON THE EFFCTIVE THERMAL CONDUCTIVITY OF TEXTILES BY NUMERICAL METHOD

In this chapter, several widely used analytical models and the numerical method for prediction the thermal conductivity of textiles are compared, and also the factors which would influence the thermal conductivity are investigated by numerical method due to the difficulties in experiments.

2.1 METHODOLOGY

In order to compare the accuracy and difference of analytical models and numerical simulation, textiles with variables in terms of pore shapes, volume fractions, pore size, pore distribution, cross section of pores, and contact area were adopted. For simplification, two kinds of materials which have thermal conductivity of k_1 (=0.4 $W \cdot m^{-1} \cdot K^{-1}$) and k_2 (= 1 $W \cdot m^{-1} \cdot K^{-1}$), which can be any kinds of materials for the aim is to compare the accuracy and difference of analytical models and numerical simulation.

2.2.1 FOURIER'S LAW OF HEAT CONDUCTION

2.2.1.1 Thermal resistance networks

Thermal resistance network is one effective method to analyze thermal conductivity of porous materials, but it's only suitable for simple structure porous materials. And this method is based on Fourier's law. One simple example is given in figure 2.1.

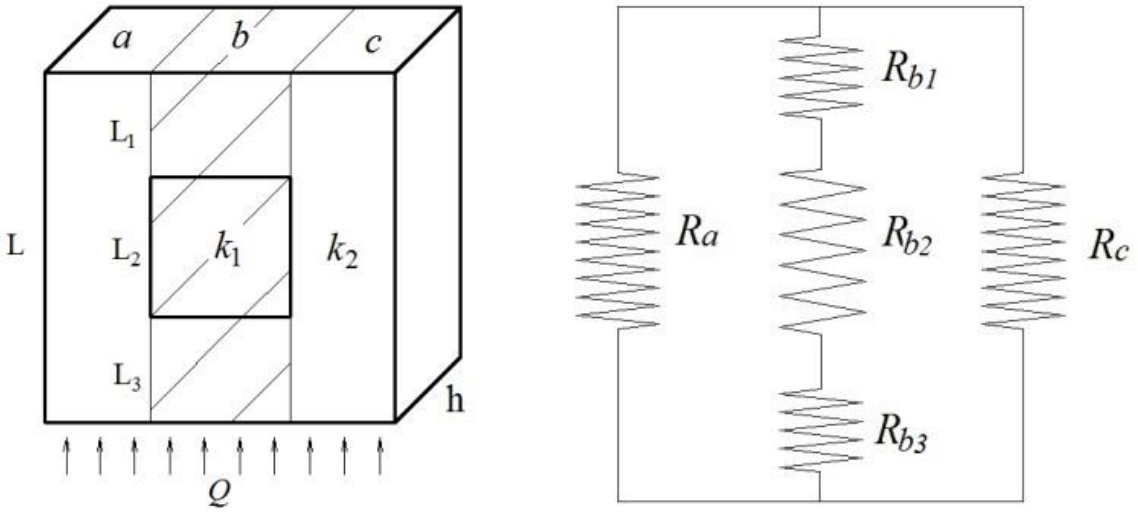

Figure 2.1. left: structure of one porous material; right: The corresponding thermal resistance networks

The following equations are used for calculating the effective thermal conductivity of porous material with square and rectangular inclusions.

$$R_a = \frac{L}{a \cdot h \cdot k_2} \tag{2.1}$$

$$R_b = R_{b1} + R_{b2} + R_{b3};\ R_{b1} = \frac{L_1}{b \cdot h \cdot k_2},\ R_{b2} = \frac{L_2}{b \cdot h \cdot k_1},\ R_{b3} = \frac{L_3}{b \cdot h \cdot k_2} \tag{2.2}$$

$$R_c = \frac{L}{c \cdot h \cdot k_2} \tag{2.3}$$

$$R_{tot} = \frac{R_a R_b R_c}{R_a R_b + R_a R_c + R_b R_c} \tag{2.4}$$

$$k_e = \frac{L}{A \cdot R_{tot}} \tag{2.5}$$

Where k_1 and k_2 are thermal conductivities of material 1 and material 2, k_e represents effective thermal conductivity of porous material ($W \cdot m^{-1} \cdot K^{-1}$), R_a, R_b, R_c, and R_{tot} represent thermal resistance of zone *a*, *b*, *c* and total thermal resistance (K/W), *A* is area where heat flow goes through (m^2), and other symbols represent the dimensions as shown in figure 2.1.

Heat flow by infinitesimal method. Unfortunately, it's not easy to distinguish the sub-regions of a porous material including circular and elliptic inclusions; therefore, the differential concept was adopted. The geometrical model is divided into infinitesimal area (figure 2.2), and accumulated the heat flow from each infinitesimal area, then calculated the effective thermal conductivity by Fourier's equation. Owing to the symmetry of the geometrical model, only half part was taken into consideration. The heat flow and effective thermal conductivity can be obtained from following equations,

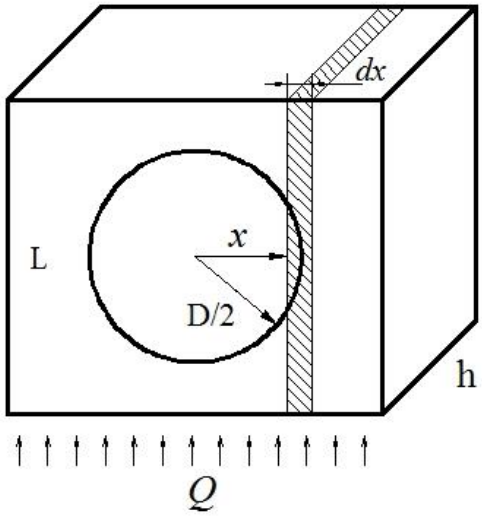

Figure 2.2. The geometrical model of porous material including circular pore

The heat flow goes through material can be divided into two parts, Q1, heat flow goes through both inclusion and covering material (J); Q2, heat flow only goes through covering material (J).

$$\frac{Q_1}{2} = \int_0^{\frac{D}{2}} \frac{\Delta T \cdot h \cdot dx}{\frac{L - 2\sqrt{(D/2)^2 - x^2}}{k_2} + \frac{2\sqrt{(D/2)^2 - x^2}}{k_1}} \tag{2.6}$$

$$\frac{Q_2}{2} = \int_{D/2}^{L/2} \frac{\Delta T \cdot h \cdot dx}{L/k_2} \tag{2.7}$$

$$k_e = \frac{Q \cdot L}{A \cdot \Delta T}, (Q = Q_1 + Q_2) \tag{2.8}$$

Where L and A are distance (m) and area (m^2) of heat flow goes through, D is diameter of circular inclusion (m), h is thickness of porous material (m), ΔT is temperature difference (K).

Similarity, the expressions for effective thermal conductivity of porous material including elliptic inclusion are,

$$\frac{Q_1}{2} = \int_0^{a} \frac{\Delta T \cdot h \cdot dx}{\frac{L - 2\sqrt{b^2 - b^2x^2/a^2}}{k_2} + \frac{2\sqrt{b^2 - b^2x^2/a^2}}{k_1}} \tag{2.9}$$

$$\frac{Q_2}{2} = \int_a^{L/2} \frac{\Delta T \cdot h \cdot dx}{L/k_2} \tag{2.10}$$

$$k_e = \frac{Q \cdot L}{A \cdot \Delta T} \tag{2.11}$$

Where *a* is the length of major semi-axis in *x* direction (m), *b* is the length of minor semi-axis in *y* direction (m).

2.2.2 SOME ANALYTICAL MODELS

Some models for predicting effective thermal conductivity of porous materials are shown in table 2.1.

Table 2.1. Some effective thermal conductivity models of porous materials

Models	Effective thermal conductivity equation	References
Series-parallel 1	$k_P = \phi k_1 + (1-\phi)\, k_2$, $k_s = \frac{k_1 k_2}{\phi k_2 + (1-\phi)\, k_1}$, $k_e = (k_P + k_S)/2$	[21]
Series-parallel 2	$k_e = k_s/2\left(\sqrt{1+8k_p/k_s}-1\right)$, $k_s = 1\Big/\sum_{i=1}^{N}\frac{v_i}{k_i}$, $k_p = \sum_{i=1}^{N} k_i v_i$	[72]
Maxwell–Eucken	$k_e = k_1 \frac{2k_1 + k_2 - 2(k_1 - k_2)v_2}{2k_1 + k_2 + (k_1 - k_2)v_2}$	[70, 71]
Levy's	$k_e = k_1 \frac{2k_1 + k_2 - 2(k_1 - k_2)F}{2k_1 + k_2 + (k_1 - k_2)F}$, $F = \frac{2/G - 1 + 2v_2 - \sqrt{(2/G - 1 + 2v_2)^2 - 8v_2/G}}{2}$, $G = \frac{(k_1 - k_2)^2}{(k_1 + k_2)^2 + k_1 k_2/2}$	[73]

Note: ϕ is volume fraction of material 1, k_p and k_s are TC of materials with parallel structure and series structure, k_i and v_i are the thermal conductivity and volume fraction of ith material, k_e is effective thermal conductivity of porous material.

2.3 NUMERICAL SIMULATION

Numerical methods include finite difference methods, boundary element methods, and finite element methods which have the advantage that the discretization process is not constrained by regular node positioning, and they are therefore more suitable for irregular geometries and for spatially variable properties and conditions.

Therefore, the finite element models were set up to simulate a three-dimensional steady-state thermal conductivity measurement apparatus. One of geometrical models and grid topologies of simulations are given in figure 2.3. The boundary conditions imposed on the model faces were: one side was kept at constant temperature while its opposite side was subjected to heat flow; the other two sides were kept thermally insulated. Hence, after getting temperature distribution of porous material, the effective thermal conductivity can be calculated from equation (8).

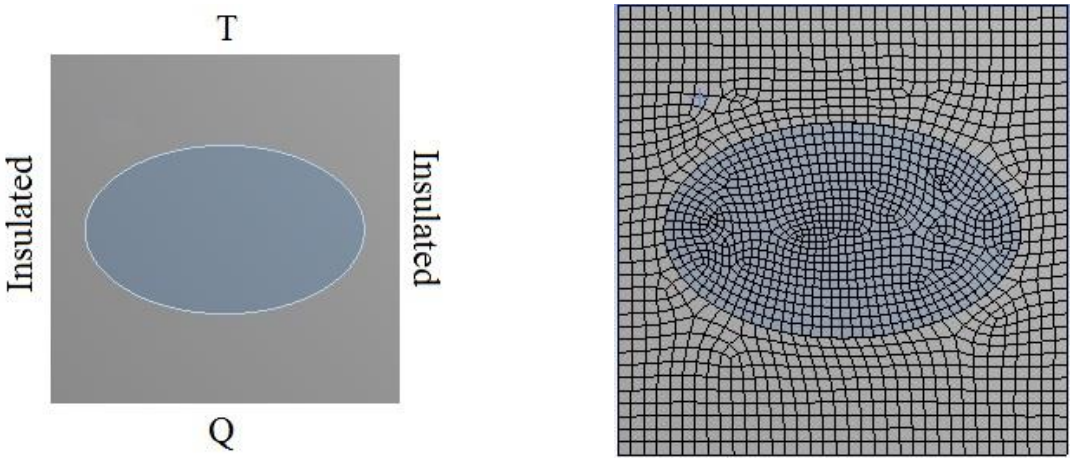

Figure 2.3. Geometrical model and grid topology

And the governing equations used in numerical simulation are,

$$[C(T)]\{\dot{T}\}+[K(T)]\{T\}=[Q(T)] \tag{2.12}$$

Where $\{T\}$ represents temperature matrix, $[C]$ represents specific heat matrix, $[K]$ represents thermal conduction matrix, $[Q]$ represents heat flux vector matrix, $\{\dot{T}\}$ is the derivative of the temperature with respect to time.

Therefore, the equation for steady- state thermal analysis is

$$[K]\{T\}=\{Q\} \tag{2.13}$$

Where $\{Q\}$ is the heat flux vector at nodes.

Simulation 1. Four types of inclusion shapes which were square (SI), rectangle (RI), circle (CI), and ellipse (EI) were investigated; and the volume fractions of inclusions were from 10% to 70%.

Simulation 2. The inclusion sizes were from 0.12% to 30% of total size of porous material, and the inclusion volume fraction was kept constant.

Simulation 3. Six distributions of inclusions were investigated, and the inclusion volume fraction was kept constant. The circles represent fibers, and the rest represents another material.

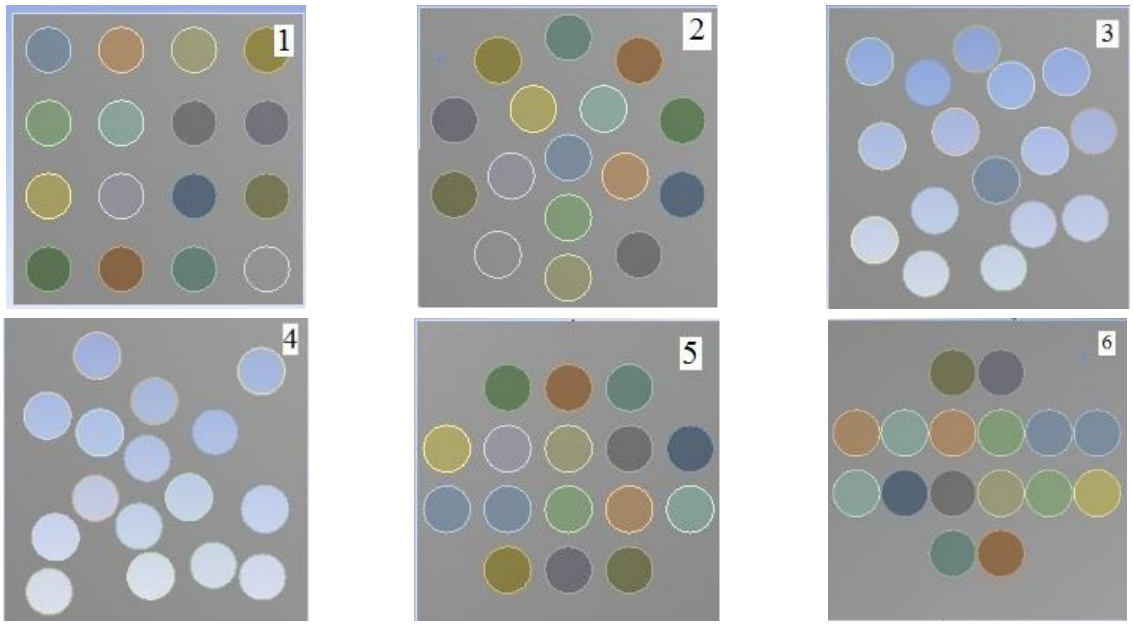

Figure 2.4. Different distributions of pores

Simulation 4. The major semi-axes of elliptic inclusions were from 41.52% to 95.49% of the total cross section length of porous materials, and the inclusion volume fraction was kept constant.

Simulation 5. The contact length/area between inclusions was from 0% to 63% of inclusion length, and the inclusion volume fraction was kept constant.

2.4 RESULTS AND DISCUSSION

Some of the simulated results from Ansys are given in figure 2.5.

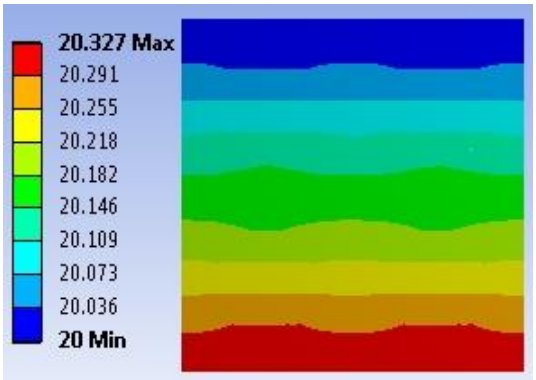

(a) temperature distribution of sample with 4 pores

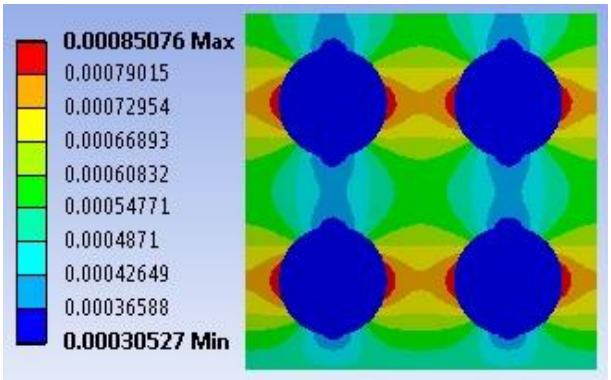

(b) heat flux distribution of sample with 4 pores

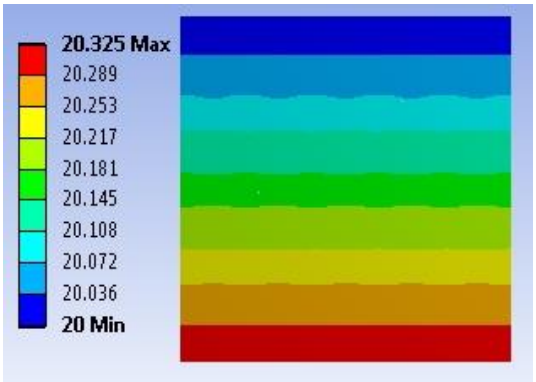

(c) temperature distribution of sample with 25 pores

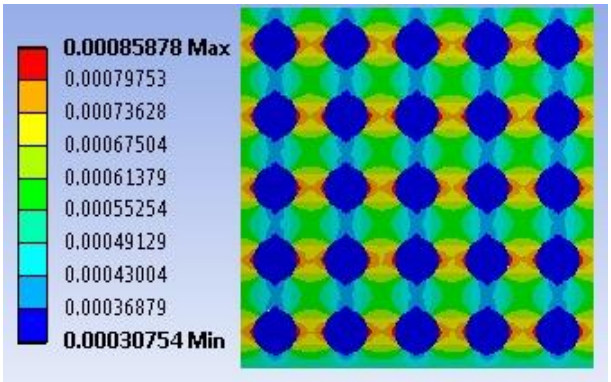

(d) heat flux distribution of sample with 25 pores

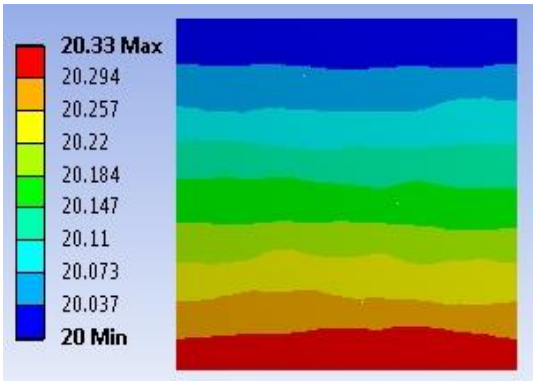

(e) temperature distribution of sample with random distribution 4 of pores

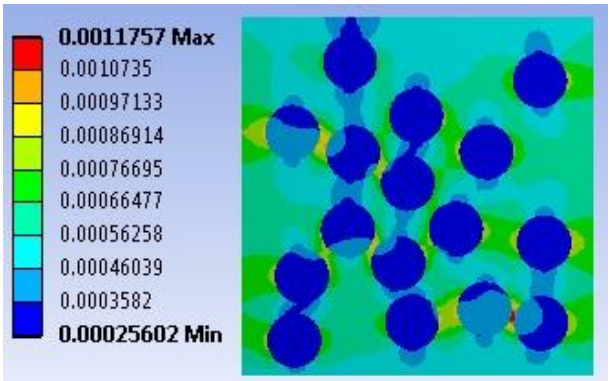

(f) heat flux distribution of sample with random distribution 4 of pores

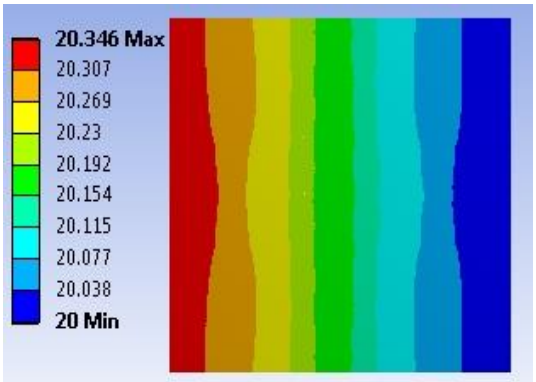

(g) temperature distribution of sample with random distribution 6 of pores

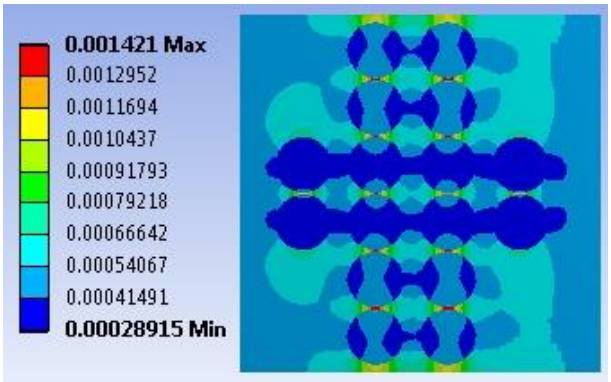

(h) heat flux distribution of sample with random distribution 6 of pores

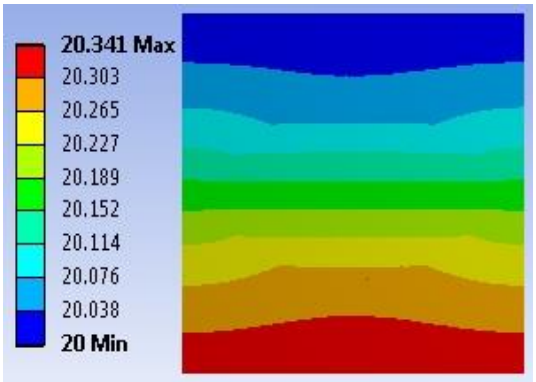

(i) temperature distribution of sample with larger major axis length

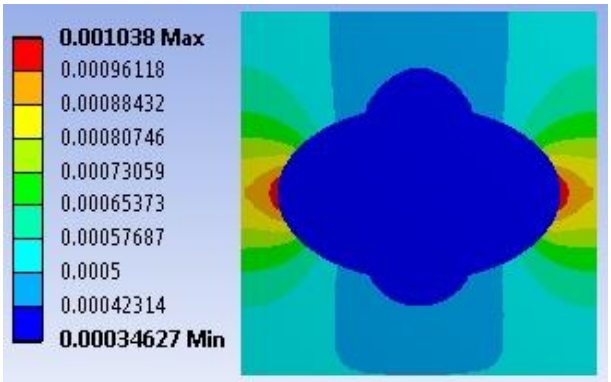

(j) heat flux distribution of sample with larger major axis length

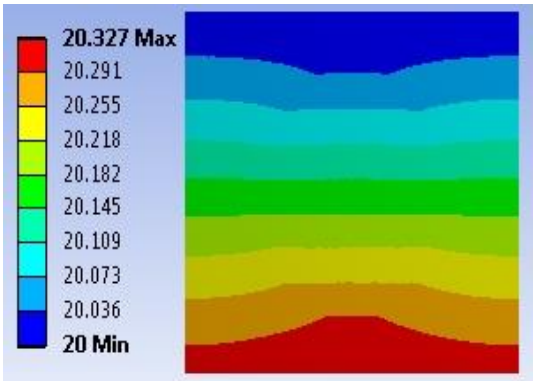

(k) temperature distribution of sample with smaller major axis length

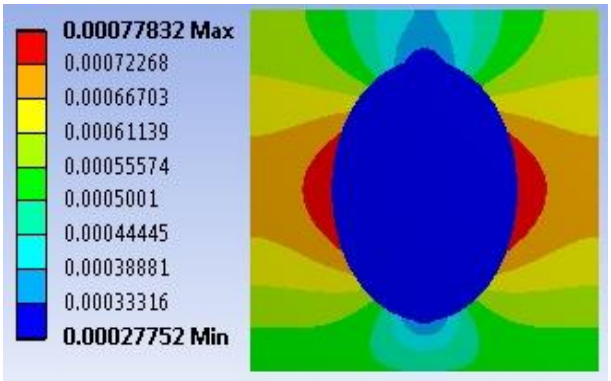

(m) heat flux distribution of sample with smaller major axis length

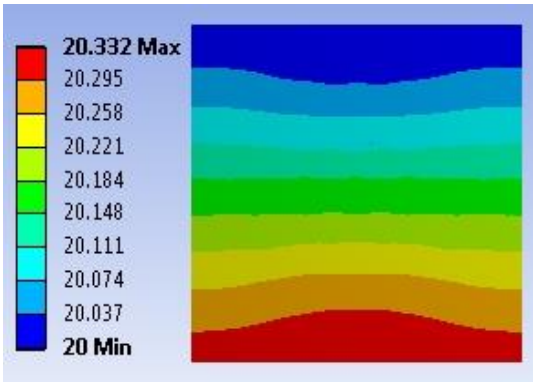

(n) temperature distribution of sample with smaller contact area

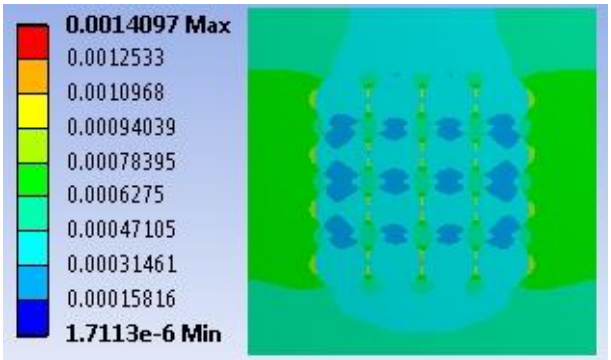

(l) heat flux distribution of sample with smaller contact area

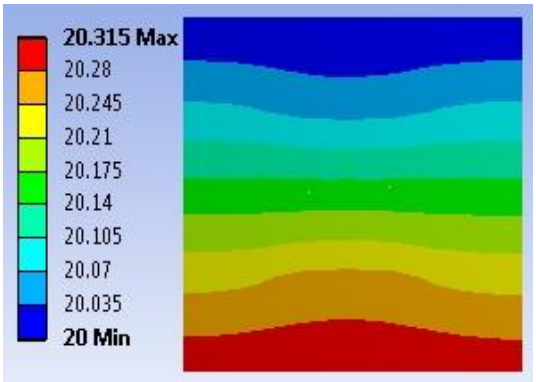

(o) temperature distribution of sample with larger contact area

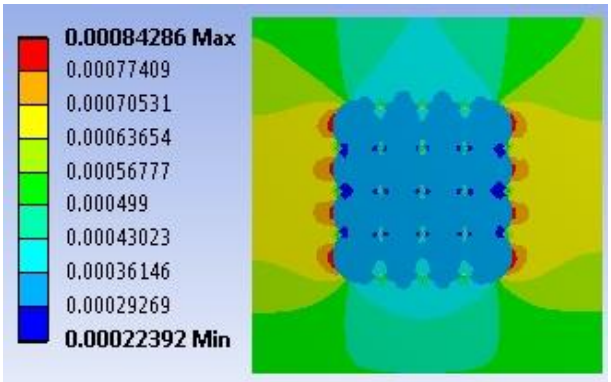

(p) heat flux distribution of sample with larger contact area

Figure 2.5 Temperature distrubtion and heat flux distribution of samples from numerical simulation

By using Fourier's law and equation (1.1), the thermal conductivity from simulation can be easily obtained, and the thermal conductivity from analytical models can be obtained by Matlab, which are given in table 2.2 and table 2.3.

Table 2.2 Thermal conductivity of samples including different porosity and pore shape from analytical models and simulation

Pore shape	Thermal conductivity ($W \cdot m^{-1} \cdot K^{-1}$)						
	Porosity (%)	Fourier's law	From simulation	PSM1	ME model	Levy's model	PSM2
square	10	0.8984	0.9091	0.9048	0.9143	0.9212	0.9157
	20	0.8205	0.8278	0.8246	0.8364	0.8473	0.8408
	30	0.753	0.753	0.7548	0.7652	0.7784	0.7731
	40	0.6924	0.6868	0.6925	0.7	0.7138	0.711
	50	0.6361	0.6265	0.6357	0.64	0.6533	0.6532
	60	0.5837	0.5721	0.5831	0.5846	0.5964	0.5988
	70	0.5344	0.523	0.5339	0.5333	0.5429	0.5469
Rectangule	10	0.9318	0.916	0.9048	0.9143	0.9212	0.9157
	20	0.8636	0.8361	0.8246	0.8364	0.8473	0.8408
	30	0.7955	0.7622	0.7548	0.7652	0.7784	0.7731
	40	0.7273	0.6964	0.6925	0.7	0.7138	0.711
	50	0.6591	0.6345	0.6357	0.64	0.6533	0.6532
	60	0.5905	0.5747	0.5831	0.5846	0.5964	0.5988
	70	0.5227	0.5176	0.5339	0.5333	0.5429	0.5469
circle	10	0.8964	0.9124	0.9048	0.9143	0.9212	0.9157
	20	0.816	0.8305	0.8246	0.8364	0.8473	0.8408
	30	0.7458	0.7553	0.7548	0.7652	0.7784	0.7731
	40	0.6822	0.6868	0.6925	0.7	0.7138	0.711
	50	0.6232	0.6234	0.6357	0.64	0.6533	0.6532
	60	0.568	0.5643	0.5831	0.5846	0.5964	0.5988
	70	0.516	0.5081	0.5339	0.5333	0.5429	0.5469
ellipse	10	0.8752	0.8803	0.9048	0.9143	0.9212	0.9157
	20	0.7858	0.7987	0.8246	0.8364	0.8473	0.8408
	30	0.7182	0.7331	0.7548	0.7652	0.7784	0.7731
	40	0.6654	0.6757	0.6925	0.7	0.7138	0.711
	50	0.6228	0.6234	0.6357	0.64	0.6533	0.6532
	60	0.5876	0.5695	0.5831	0.5846	0.5964	0.5988

Table 2.3 Thermal conductivities of samples with variables in terms of pore size, pore distribution, major axis length and contact depth

Pore number	TC	Distribution	TC	Major axis length (mm)	TC	Contact Depth (mm)	TC
1	0.7553	1	0.768	0.23873	0.7102	0	0.753
4	0.7645	2	0.74627	0.2	0.7331	0.02	0.7576
9	0.7669	3	0.753	0.15915	0.753	0.04	0.7692
16	0.768	4	0.7576	0.1545	0.7553	0.08	0.7937
25	0.7692	5	0.7508	0.13263	0.7645		
		6	0.7225	0.11937	0.7669		
				0.1038	0.77		

Remark: the samples including circular pores with 30% porosity, the unit of TC is $W{\cdot}m^{-1}{\cdot}K^{-1}$, and the distribution types are given in figure 2.4.

2.4.1 COMPARISON OF RESULTS FROM SOME MODELS AND RESULTS BASED ON FOURIER'S LAW

Comparing with the results based on Fourier's law, analytical models would be less accurate since these models were either based on some assumptions or based on experimental results. During the experimental process, there are serious difficulties of measurement in many situations, and the measuring instruments are not free from errors. Therefore, the results based on Fourier's law were taken as reference values and the accuracy of analytical models was checked by comparing with the reference values. In order to evaluate the accuracy of analytical models easier, the deviation was adopted (table 2.4). The deviation, D_e, can be obtained from the following equation,

$$D_e = \left| \frac{k' - k_F}{k_F} \right| \tag{2.14}$$

Where k' represents the TC from models or numerical simulation, k_F represents the TC based on Fourier's law.

The effective thermal conductivity from analytical models and based on Fourier's law had slight difference at each volume fraction, and the effective thermal conductivity decreased as the increase of volume fraction of inclusions owing to the lower TC of inclusion (figure 2.6). The deviations of effective thermal conductivity from analytical models are shown in table 2.4. Every analytical model has its advantages and limitations due to assumptions. Based on

this work, PSM1 has better predicting accuracy than the other models. The results from PSM1 provided the smallest deviation when the inclusion shapes were square, circle, and ellipse comparing with the results from other models, especially when the inclusion shape was square. The reason could be that the geometrical model is regular and easy to be divided into bulk sub-regions, which is more close to the thermal resistance networks analysis method. ME model is usually derived from a specific assumed physical structure as mentioned above, but it also can provide results which have good agreement with the results based on Fourier's law. PSM2 extended the application of ME model to co-continuous structure porous materials, but it did not improve the accuracy of ME model since all assumptions were based on ME model. Levy's model added one coefficient to ME model, which in some conditions can improve the accuracy of predicting results. Moreover, the accuracy of effective thermal conductivity from analytical models was influenced by inclusion shapes. For PSM1 and ME, they have better predicting results for square and circular inclusions than rectangular and elliptic inclusions; for PSM2 and LM, the better predicting results were for square and rectangular inclusions. Some researchers stated that the prediction of the TC of porous materials has proven to be a difficult task. Part of the difficulty may be due to an over-simplification of the structure[49].

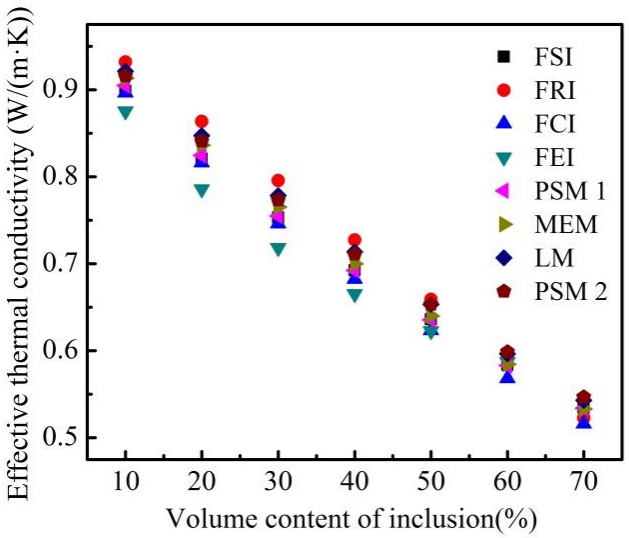

Figure 2.6. Comparison of results from some models and results based on Fourier's law
FSI: results of square inclusions based on Fourier's law; FRI: results of rectangular inclusions based on Fourier's law; FCI: results of circular inclusions based on Fourier's law; FEI: results of elliptic inclusions based on Fourier's law; PSM1: parallel-series model 1; MEM: Maxwell- Eucken model; LM: levy's model; PSM2: parallel-series model 2

Table 2.4. Deviation of effective thermal conductivity from analytical models

Pore shape	Parallel-series model 1		Parallel-series model 2		ME model		Levy's model	
	Max. deviation (%)	Mean deviation (%)	Max. deviation (%)	Mean deviation (%)	Max. deviation (%)	Mean deviation (%)	Max. deviation (%)	Mean deviation (%)
Square	0.9	0.24	2.69	2.48	1.94	1.05	3.37	2.68
Rectangle	4.24	3.46	4.63	2.34	3.81	2.65	3.86	1.83
Circle	3.47	1.83	5.99	4.19	3.35	2.67	5.21	4.38
Ellipse	3.08	3.39	7.64	5.49	6.54	4.32	8.38	5.86

2.4.2 COMPARISON OF RESULTS FROM NUMERICAL SIMULATION AND RESULTS BASED ON FOURIER'S LAW

The ETC of porous materials from numerical simulation and results based on Fourier's law were given in figure 2.7. As mentioned above, the results based on Fourier's law were taken as reference values. And then, the accuracy of numerical simulation was checked by comparing with the reference values. The maximum deviation and mean deviation of effective thermal conductivity from numerical simulation were given in table 3. Porous material including rectangular inclusions gave the biggest deviation, and the circular inclusions provided the smallest deviation. Generally, the deviations from numerical simulations were less than 3%, which provided enough accurate results. On the other hand, comparing with the analytical models, the numerical simulation is suitable for any types of inclusion shapes.

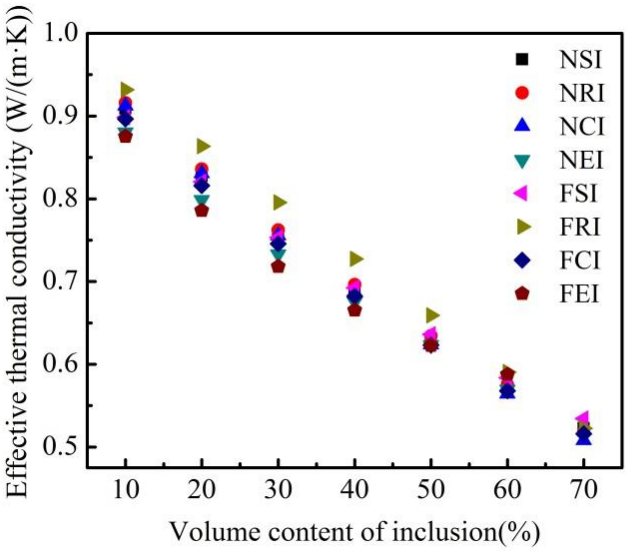

Figure 2.7. Comparison of effective thermal conductivity from numerical simulation and results based on Fourier's law

NSI: results of square inclusions from numerical simulation; NRI: results of rectangular inclusion from numerical simulation; NCI: results of circular inclusions from numerical simulation; NEI: results of elliptic inclusions from numerical simulation

Table 2.5. Deviation of effective thermal conductivity from numerical simulation

Inclusion shape	Square	Rectangle	Circle	Ellipse
Maximum deviation (%)	2.13	4.24	1.78	3.08
Mean deviation (%)	1.22	2.95	1.09	1.5

2.4.3 EFFECT OF PORE SHAPE ON EFFECTIVE THERMAL CONDUCTIVITY

It has been discussing that the inclusion shape has the potential to influence the effective thermal conductivity of porous materials [49, 84]. In this work, four types of inclusion shapes which were square, rectangle, circle, and ellipse at different volume fraction were investigated based on Fourier's law of heat conduction. For rectangular and elliptic inclusions, the dimensions are also related to the inclusion shapes even though the volume fractions could be the same. Therefore, one side length of rectangular inclusion and the major semi-axis of elliptic inclusion were kept as a constant which was 80% of porous material's side length. The porous material including elliptic inclusions gave smallest effective thermal conductivity. Square and circular inclusions in porous materials showed very similar results, which has the same result with Carson's work[82]. Rectangular inclusions showed the biggest effective thermal conductivity, which does not have an agreement with Carson's

result[82], because in his work, the dimension of rectangular inclusions were set as 2:1, and these inclusions were distributed randomly. These different results indicated that the dimensions of inclusion also could be one factor which would influence effective thermal conductivity of porous materials. Comparing with the effective thermal conductivity of porous materials including different inclusion shapes with the same volume fraction, the biggest difference can reach to 10.67% (figure 2.8), which revealed that the inclusion shape is a significant factor.

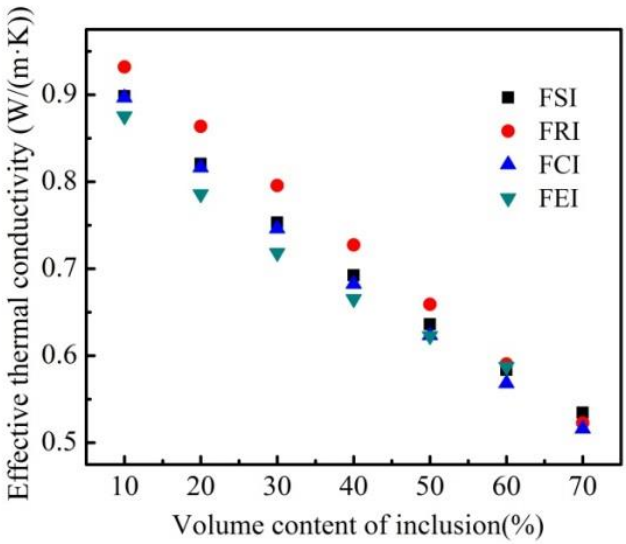

Figure 2.8. effective thermal conductivity of porous material including different pore shapes

2.4.4 EFFECT OF PORE SIZE ON EFFECTIVE THERMAL CONDUCTIVITY

Some researchers[49, 82] stated that the effect of porosity on thermal conductivity cannot be described solely by volume fraction. And Carson[82] reported that the effective thermal conductivity of porous materials with different inclusion sizes were similar over the range of volume fractions. In this work, the effective thermal conductivity decreased obviously as the increase of inclusion size (figure 2.9). The possible reason is that the small inclusions increased the interface area, which is helpful for dissipating heat when they contacted with better conductor.

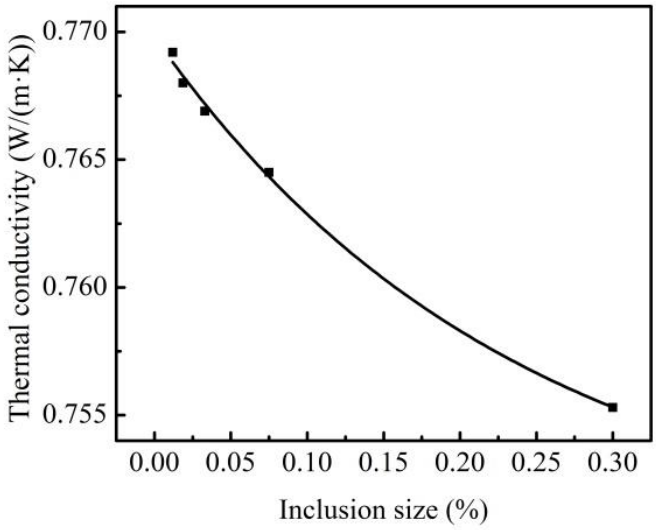

Figure 2.9. Effect of pore size on effective thermal conductivity of porous material

2.4.5 EFFECT OF DISTRIBUTION OF PORE ON EFFECTIVE THERMAL CONDUCTIVITY

Generally, the distribution of inclusions has the same effect with the inclusion shape since different combination of small inclusions can form different structure of a larger inclusion. The difference between the largest and smallest effective thermal conductivity was 6.3%. Comparing with these results corresponding to the distribution, the smallest effective thermal conductivity happened when more inclusions are at cross section (distribution 6), and the opposite case is distribution 1. In order to confirm the conclusion that the inclusion length ratio in cross section would influence effective thermal conductivity, one more simulation focusing on the cross section length of inclusion was carried out subsequently.

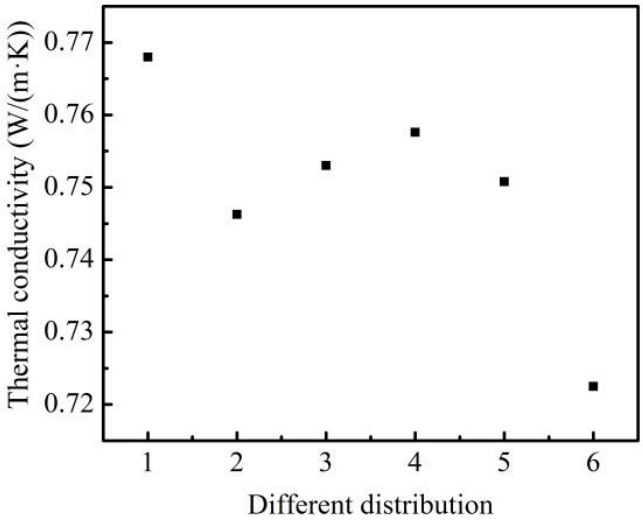

Figure 2.10. Effect of pore's distribution on effective thermal conductivity of porous material

2.4.6 EFFECT OF MAJOR-AXIS LENGTH OF PORE ON EFFECTIVE THERMAL CONDUCTIVITY

Based on the conception of parallel and series structures, the cross section length of inclusions should have effect on effective thermal conductivity of porous material. Therefore, elliptic inclusions with different dimensions at the same volume content were investigated. The results showed that effective thermal conductivity was inversely proportional to the cross section length of inclusions, and the biggest difference reached to 8.45%.

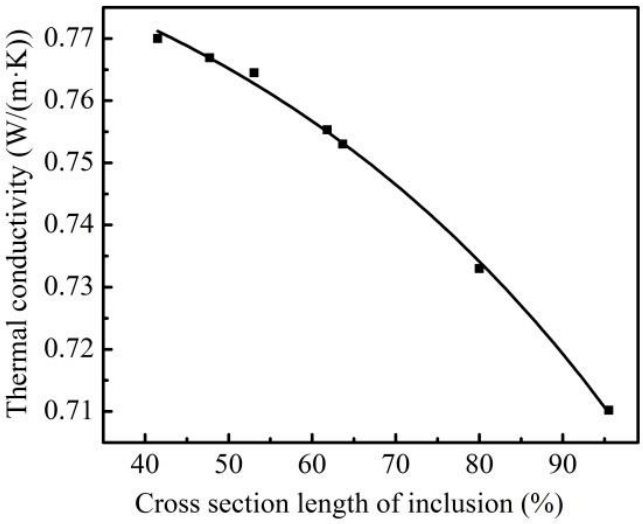

Figure 2.11. Effect of major-axis length of pore on effective thermal conductivity of porous material

2.4.7 EFFECT OF CONTACT LENGTH/AREA AMONG INCLUSIONS ON EFFECTIVE THERMAL CONDUCTIVITY

Heat conduction happens only when materials contact with each other, and the larger the contact area is, the faster the heat conduction will be. The results suggested that the contact had a significant effect on effective thermal conductivity, and the biggest deviation was 5.41% which was not very large difference due to the small different of thermal conductivity of these two materials. This simulation also can be used to analyze the effective thermal conductivity of yarns with different packing density.

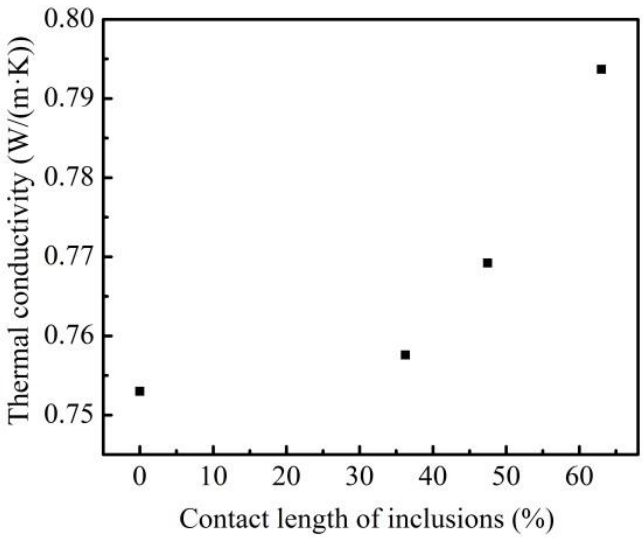

Figure 2.12. Effect of contact length among inclusions on effective thermal conductivity of porous material

2.5 CONCLUSIONS

Effective thermal conductivity of some porous materials with simple structure was investigated by analytical models and numerical simulation in this work. Significant conclusions drawn from the results were: (1) analytical models can provide accurate prediction in some cases, but it is not unrealistic to expect an analytical model to predict accurate results for all porous materials by only considering volume fraction; (2) numerical simulation can provide more accurate results than analytical models', and is more flexible for any structures; besides, numerical simulation could be a good way to evaluate effective thermal conductivity of textiles with complicated structures and experimental conditions due to the difficulties in experiment; (3) more important parameters need to be considered for improving analytical model, such as inclusion shapes, the length ratio of inclusions in cross section, and contact area.

3 STUDY ON THE THERMAL PROPERTY OF HIGH POROUS NONWOVEN FABRICS

3.1 INTRODUCTION

In nonwoven fabrics, pores of all geometrical shapes are possibly formed and the pore sizes could be in a large scope due to the randomly arrangement of fibers. Thereby, heat transfer through nonwoven fabrics may in general be represented by several mechanisms: conduction through solid fibers, conduction through air in the interfiber spaces, free convection, and radiation[69]. Despite the fact that there are several mechanisms operative in the transfer of heat through nonwovens, the phenomenon can be quantified by an effective thermal conductivity for the nonwoven.

In theoretical work, the most widely used model for predicting effective thermal conductivity was proposed by Bogaty[23], who took the textiles as a fiber-air mixture and assumed that the air is stagnant. In Bogaty's model, the volume fraction of each material and the orentations of fibers are needed. Due to the difficulty of determining fiber's orentation, Bogaty's model was simplified by Militky[21], who assumed the fibers were arranged in both series and parallel structures. He also proposed that the average value from these two kinds structures was the effective thermal conductivity of textiles. These two models had good agreements with the experimental results in some cases. Other concepts for describing the heat conduction through textiles were either based on thermal resistance network or differentiation[9, 64, 74, 75], which need to over simplify the structures of textiles. In addition, for some materials with complicated physical structures, these models are not appropriate.

The heat convection in textiles is often ignored due to its complexity. But the natural convection could exist when the temperature difference on both side of textiles and the pore size of textiles is big enough.

Two techniques were used for determining the heat radiation, one is called direct method, which is based on the study of the interaction between the fiber and radiation via the resolution of the Maxwell equations. The resolution was done with the Mie theory and made it possible to obtain radiative properties of a single fiber. The radiative properties of the medium were given by averaging the properties of a fiber over size and orientation distributions within the medium[85, 86]. The second method is an inverse method based on

the inversion of the radiative transfer equation starting from measurements of reflection and transmission [87, 88]. Methods of determining heat radiation were reported in literatures, but they require determination of the scattering parameter and emissivity of the hot and cold side boundaries. These parameters are beyond the scope of this paper, and we will address them, for the materials reported here in a future paper.

In this work, the thermal conductivity of nonwoven fabrics with various parameters including areal density, porosity and thickness was evaluated to investigate the effect of structure on the thermal property. Components of thermal conductivity, convection, and radiation were also estimated.

3.2 METHODOLOGY

3.2.1 MATERIALS AND MEASUREMENTS

The polyester hollow fiber, supplied by the Sinopec Yizheng Chemical Fibre Company Limited (Suzhou of China), was used to prepare nonwoven fabrics in a carding machine and a needle-punching machine. The nonwoven fabrics were conditioned in a constant temperature and constant humidity box for 24 hours before measurements.

The thermal conductivity of fiber was evaluated by measuring the thermal conductivity of composites including fibers and polymer [48]. In this work, a bundle of hollow fibers were put into PEO solution in which the air bubbles were removed by a vacuum pump. After drying, the thermal conductivity of composite were measured, and the thermal conductivity of fiber could be calculated.

The thermal conductivity of composites and nonwoven fabrics were measured by an Alambeta instrument, which enables quick measurements of both steady-state and transient-state thermal properties. The temperature difference between the upper and bottom heating plates which were directly contact with the both sides of nonwoven fabric was constant (10°C or 40°C), and then the instrument directly measured the stationary heat flow density and the sample thickness under a pressure of 200Pa or 1000Pa pressure[54]. At last, the values of thermal conductivity, and thermal resistance were determined accordingly. The average values of five repeated measurements were adopted.

3.2.2 DETERMINATION OF THE CHARACTERISTIC OF FIBER

3.2.2.1 Fiber geometric characteristic and density

The profile of hollow fiber was observed by scanning electron microscope and was taken as cylinder. Fiber diameter was around 45±5μm, hollow diameter was 22±3μm.

The air volume content in hollow fiber can be determined by using image processing analysis by matlab. Firstly, the SEM images of fibers were imported into matlab, converted the SEM images into binary images, and then extracted the hollow area and the fiber area (as shown in figure 3.2), at last, an in-house Matlab code was developed to calculate the area ratio of fiber material and the hollow part to the total area. The mathematical expressions are given by,

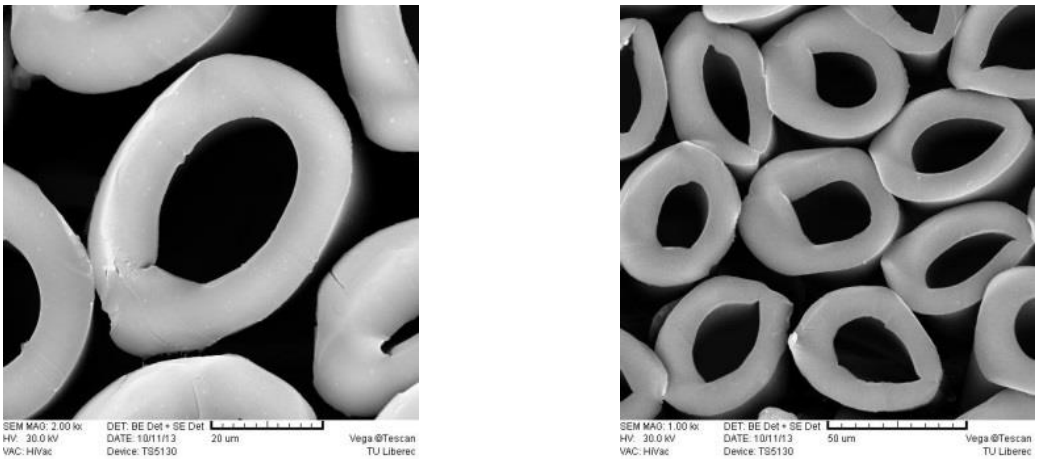

Figure 3.1. Images of hollow fibers

$$\varepsilon_f = A_f / A_t \tag{3.1a}$$

$$\varepsilon_h = A_h / A_t \tag{3.1b}$$

$$\varepsilon = \varepsilon_h / \varepsilon_f \tag{3.1c}$$

Where ε_f is ratio of fiber area to total area of figure 3.2, ε_h is ratio of hollow area to total area of figure 3.2, ε is porosity of hollow fiber, A_f, A_h, and A_t are the areas of fiber cross-section, hollow cross-section and the total area of figure 3.2, respectively. The air volume content in hollow fiber was 27±8% based on the above method.

Figure 3.2. (A) The cross-section area of fiber material (white); (B)The cross-section area of hollow (white)

And hollow fiber density was 1034kg/m^3 which was calculated from the following equation,

$$\rho_h = \frac{n \cdot m}{\pi r^2 l \cdot n} \tag{3.2}$$

Where ρ_h is hollow fiber density (kg/m^3), n represents the number of fibers, m represents mass of single fiber (kg), r is the diameter and hollow diameter (m), l represents length of single fiber (m). And the density of fiber material, ρ_f, can be easily obtained by equation,

$$\rho_f = \frac{\rho_h}{1-\varepsilon} \tag{3.3}$$

3.2.2.2 Fiber thermal conductivity

It is very difficult to measure the thermal conductivity of a single fiber due to its fine diameter. Therefore, one widely used method[48] for evaluating the thermal conductivity of fiber is to measure the thermal conductivity of the composite specimen including a bundle of the fibers, and then the thermal conductivity of the fiber can be calculated. On the other hand, numerous analytical models for predicting the effective thermal conductivity of composites were developed in recent years. The numerical results were in good agreements with experimental results[21, 70-73]. In this work, the thermal conductivity of PEO was 84.7×10^{-3} W/(m·K), the effective thermal conductivity of the composite, 3.12% fiber and 96.88% PEO in volume, was 86.6×10^{-3} W/(m·K). According to Equation (8), the thermal conductivity of fiber was 119.2×10^{-3} W/(m·K).

3.2.3 DETERMINATION OF THE CHARACTERISTIC OF NONWOVEN FABRICS

In nonwoven fabrics, pores of all geometrical shapes are possible due to the randomly arrangement of fibers (as shown in figure 3). And there is no doubt that the pore size and the pore shape have important influence in convective heat transfer. We assumed that the pores in nonwoven fabric are evenly distributed cylinders. And then, the mean effective pore diameter of nonwoven fabrics is given by Verschoor[89],

$$D = \frac{\pi d}{4\left(1-\phi_n\right)} \tag{3.4}$$

Where D is the mean effective pore diameter, d is the mean fiber diameter, ϕ_n is the mean porosity of the nonwoven fabric. The porosity of nonwoven fabric is given by,

$$\phi_n = \left(1-\frac{\rho_n}{\rho_h}\right)\times 100\% \tag{3.5}$$

Where ρ_n and ρ_h are the density of nonwoven fabric and hollow fiber, respectively.

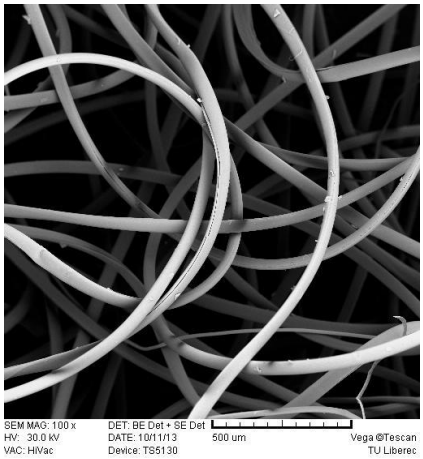

Figure 3.3. Image of nonwoven fabric

3.3 RESULTS AND DISCUSSIONS

3.3.1 THEORETICAL ANALYSIS OF CONDUCTION, CONVECTION, AND RADIATION

The effective thermal conductivity of nonwoven fabric k_e is given by

$$k_e = \frac{Q_{cond} + Q_{conv} + Q_{rad}}{A\Delta t} \tag{3.6}$$

Or

$$k_e = k_{cond} + k_{conv} + k_{rad} \tag{3.7}$$

where Q_{cond}, Q_{conv}, and Q_{rad} are heat flow through nonwoven fabrics by conduction, convection, and radiation, respectively, A is the area heat flow going through, Δt is the temperature gradient on the both sides of nonwoven fabric, k_{cond} is the conductivity of the nonwoven fabric due to conduction, k_{conv} is the conductivity of the nonwoven fabric due to convection, and k_{rad} is the conductivity of the nonwoven due to radiation.

Thermal conductivity k_{cond} in this work can be obtained by applying Militky's model, which is given by[21],

$$k_{cond} = \frac{k_f V_f + k_a V_a}{2} + \frac{k_f k_a}{2\left(k_f V_a + k_a V_f\right)} \tag{3.8}$$

Where k_f and k_a are thermal conductivities of fiber and air, V_f and V_a are volume fractions of fiber and air. The first term of the right side of this equation describes an ideal model of a textile construction whose fibers are totally parallel to the flow of heat, while the second term describes an ideal model of a textile construction whose fibers are totally in series to the flow of heat.

We assumed that the pores inside nonwoven fabric are cylinders, then the conductivity of the nonwoven fabric due to convection k_{conv} can be obtained by[34],

$$k_{conv} = \begin{cases} k_a & \dfrac{g\beta\Delta TL^3}{\upsilon^2}\Pr < 1700 \qquad (3.9a) \\ 0.059k_a\left[\dfrac{g\beta\Delta TL^3}{\upsilon^2}\Pr\right]^{2/5} & 1700 < \dfrac{g\beta\Delta TL^3}{\upsilon^2}\Pr < 7000 \qquad (3.9b) \\ 0.212k_a\left[\dfrac{g\beta\Delta TL^3}{\upsilon^2}\Pr\right]^{1/4} & 7000 < \dfrac{g\beta\Delta TL^3}{\upsilon^2}\Pr < 3.2\times10^5 \qquad (3.9c) \\ 0.061k_a\left[\dfrac{g\beta\Delta TL^3}{\upsilon^2}\Pr\right]^{1/3} & \dfrac{g\beta\Delta TL^3}{\upsilon^2}\Pr > 3.2\times10^5 \qquad (3.9d) \end{cases}$$

Where k_a is the thermal conductivity of air, g is gravitational acceleration, β is coefficient of volume expansion, ΔT is the temperature gradient of both sides of nonwoven fabric, L is the characteristic length of the pore in nonwoven fabric, υ is kinematic viscosity of air. $Pr=(\mu C_p/k_a)$ is Prandtl number, μ is dynamic viscosity of air, C_p is specific heat capacity of air ,and k is thermal conductivity of air. When equation (9.1) is applied, which means there is

no convective heat transfer. And the conductivity of the nonwoven due to radiation, k_{rad}, can be obtained by [33],

$$k_{rad} = \frac{16\sigma T_m^3}{3\beta_R} \tag{3.10}$$

Where σ is the Stefan-Boltzmann constant, σ=5.669×10^{-8}W/m^2·K^4, T_m is the mean temperature in the nonwoven fabric, and β_R is the Rosseland average extinction coefficient. In this work, the k_{rad} was estimated by equation (7) due to the parameter β_R is beyond the scope of this paper. And k_e can be obtained experimentally. The experimental results are shown in table 3.1.

Table 3.1. Sample parameters vs. thermal property of nonwoven fabrics

Thickness (mm)	Porosity (%)	Pore diameter(mm)	k_e (W/(m·K))	k_{cond} (W/(m·K))	k_{rad} (W/(m·K))
6.25±0.04	97.87±0.026	1.66±0.02	48.3±1.1	27.21	21.09
6.9±0.04	97.87±0.026	1.66±0.02	48.1±0.9	27.22	20.88
7.59±0.05	95.32±0.022	0.76±0.012	46.2±1.1	28.1	18.1
	96.12±0.021	0.91±0.013	47.5±0.8	27.87	19.63
	97.07±0.023	1.21±0.017	47.8±1.2	27.5	20.3
	97.87±0.026	1.66±0.02	49±1.3	27.21	21.79
	98.35±0.021	2.14±0.022	53.2±1.3	27.17	26.03
	98.83±0.025	3.01±0.028	54.4±1.1	27	27.4
8.01±0.05	97.87±0.026	1.66±0.02	48.7±0.8	27.21	21.49
8.53±0.07	96.99±0.023	1.17±0.016	47.9±1.2	27.71	20.19
	97.32±0.027	1.32±0.019	47.9±1.3	27.53	20.37
	97.64±0.028	1.5±0.018	48.3±1.4	27.34	20.96
	97.87±0.026	1.66±0.02	49.6±1.1	27.23	22.37
	98.07±0.027	1.83±0.023	50.2±1.3	27.1	23.1
	98.16±0.028	1.92±0.027	51.2±1.2	27.05	24.15
	98.30±0.027	2.08±0.029	52.4±1.4	26.96	25.44
	98.33±0.028	2.12±0.03	53.1±1.1	26.89	26.21
9±0.06	97.87±0.026	1.66±0.02	48.9±0.9	27.21	21.69

3.2 THE RELATIONSHIP BETWEEN DENSITY AND POROSITY

The density or the porosity of the nonwoven fabric is an important parameter to characterise thermal properties. Obviously, the density of the nonwoven fabric is inversely proportional to the porosity of nonwoven fabric according to equation (3.5), and the correlation between them was given in figure 3.4. Meanwhile, the densities of nonwoven fabrics were in a more wide range with respect to the porosities of nonwoven fabrics.

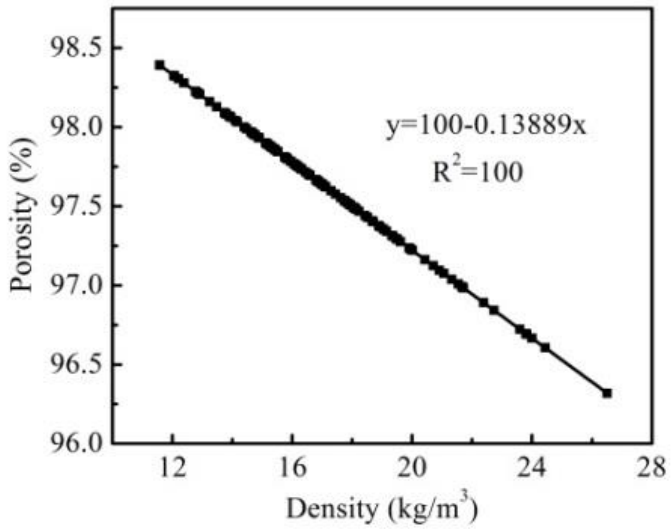

Figure 3.4. The relation of density and porosity

3.3 EFFECT OF POROSITY ON THERMAL PROPERTY

According to the theoretical analysis, the convective heat transfer can be ignored due to the critical value is much less than 1700 (equation 3.9a). Therefore, if only the conduction mechanism was considered, effective thermal conductivity of nonwoven fabric should decrease continually with the decreasing density or porosity. The effective thermal conductivity should finally be close the conductivity of the air. However, the experiment results showed big differences with the above speculation, which suggested that the heat radiation must contribute appreciably to the apparent thermal conductivity of nonwoven fabrics. Figure 3.5 showed the effective thermal conductivity of nonwoven fabrics and the contributions of conductive and radiative heat transfer to the total heat transfer. Conductivity heat transfer declined as the increase of porosity due to the very low thermal conductivity of air, but the radiative heat transfer got intensive when the void space inside nonwoven fabric became larger. At last, the effective thermal conductivity of nonwoven fabrics increased as

the increase of porosity since the increased contribution from radiation was larger than the loss from heat conduction. What's more, the contribution of radiative heat transfer was smaller than the conductive heat transfer to the effective heat transfer.

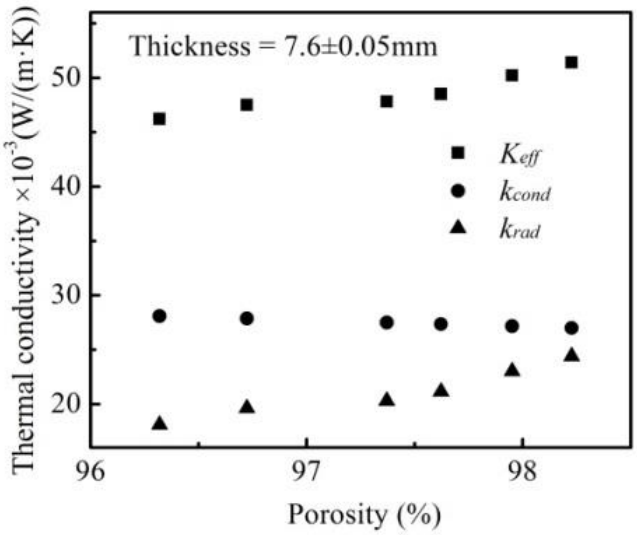

Figure 3.5. Effect of porosity on thermal property

3.4 EFFECT OF EFFECTIVE PORE DIAMETER ON THERMAL PROPERTY

It is well known that the heat radiation through air is much more intensive than through other materials. Therefore, the radiative heat transfer would be more and more tense as the increase of the pore size inside nonwoven fabric. When keeping the thickness of nonwoven fabrics as constant, the effective thermal conductivity increased as the increase of effective pore size. The increased effective thermal conductivity is due to the increased radiative heat transfer (as figure 3.6 shown). The heat transfer ratio by conduction and radiation were almost the same when the effective pore diameter was bigger than 2mm.

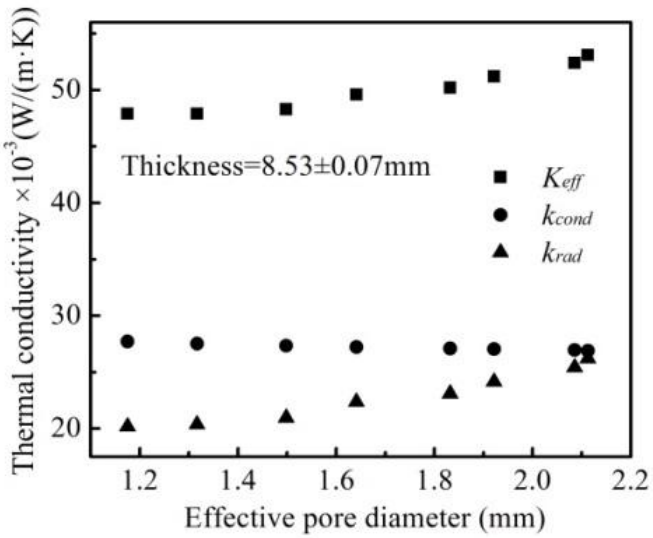

Figure 3.6. Effect of effective pore diameter on thermal property

3.5 EFFECT OF THICKNESS ON THERMAL PROPERTY

If the porosity of nonwoven fabrics were kept constant, the change of thickness had no significant impact on the conductive heat transfer and the radiative heat transfer. If the porosity was kept constant, the nonwoven fabrics could be taken as a homogenous porous material whose thermal conductivity would not be changed as the change of thickness.

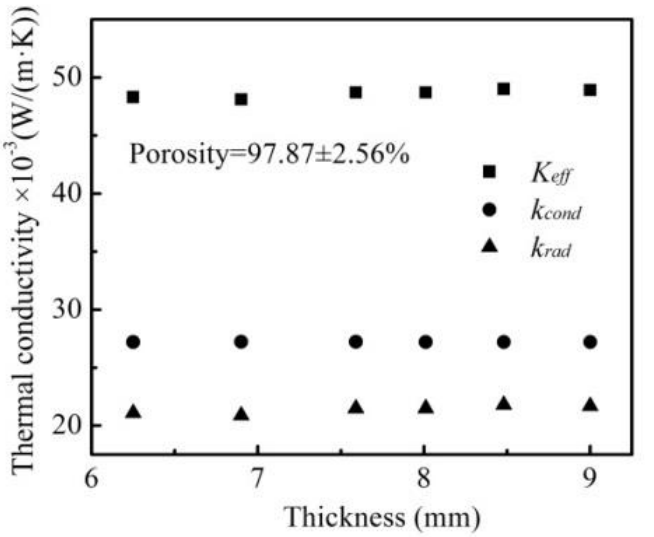

Figure 3.7. Effect of thickness on thermal property

3.4 CONCLUSION

The thermal property of the nonwoven fabric with various structure parameters was investigated in this study, some conclusions can be made based on the results, (1) both the conductive heat transfer and radiative heat transfer contributed to the thermal property of nonwoven fabrics; (2) the effective thermal conductivity of nonwoven fabric increased as the increase of the porosity and the pore size, however, the thickness did not have a significant influence on thermal conductivity of nonwoven fabric; (3) the ratio of radiative heat transfer to total heat transfer increased as the increase of pore size ; (4) the ratio of radiative heat transfer was smaller than the ratio of convective heat transfer when the pore size was smaller than 2mm. Owing to the importance of surrounding conditions and experimental conditions, more experiments with various conditions are still needed in order to understand the heat transfer mechanisms more comprehensively.

4 STUDY ON AIR PERMEABILITY AND THERMAL RESISTANCE OF TEXTILE UNDER HEAT CONVECTION

4.1 INTRODUCTION

Nowadays, the thermal conductivity/resistance of textiles can be measured by several methods and instruments, such as Alambeta[54], Tci analyzer[58], sweating guarded hot plate[90], and the laser flash technique[91], which only considered the heat conduction. But heat convection exists everywhere in real conditions when there is windy or when the object is moving. And there is still no commercial instrument for evaluating the thermal conductivity/resistance of textiles under convection conditions. On the other hand, the air permeability is always one parameter relating to convective heat transfer[92]. Therefore, in this chapter, one device for evaluating the thermal resistance of textiles under heat convection, and investigate the effect of structure and air permeability on the thermal resistance.

4.2 MATERIALS AND METHODS

4.2.1 MATERIALS

Plain woven fabrics from different materials with various pore sizes were applied since the aim of this work is to investigate the effect of structure (porosity, pore size, and pore area) on the air permeability and thermal resistance under heat convection. Besides, it is not easy to find the fabrics with various pore sizes from one kind of material. The specifications of samples are given in table 4.1.

Table 4.1 The specifications of samples

Samples	Areal density (g/m^2)	Thickness (mm)	Bulk density (kg/m^3)	Density of fiber (kg/m^3)	Porosity	Pore size (mm^2)	η %
PA	142.77±2.60	0.36±0.012	396.58±7.22	1150	0.66±0.006	0	0
PES	85.36±0.56	0.28±0.009	304.88±1.99	1370	0.78±0.001	0.0015±0.0008	0.82
Visc	85.38±1.16	0.19±0.007	449.37±6.11	1500	0.70±0.004	0.009±0.0003	1.57
Co45	198.17±5.03	0.80±0.01	247.71±6.29	1540	0.84±0.004	0.044±0.0166	13.16
PP	177.66±2.87	0.82±0.013	216.66±3.50	946	0.77±0.004	0.096±0.0078	12.79
Co20	82.11±2.51	0.56±0.01	146.64±4.48	1540	0.90±0.003	0.188±0.0554	35.88

Note: PA represents polyamide, PES represents polyester, Visc represents viscose, Co45 represents cotton fabric by using 45 Tex cotton yarn, PP represents polypropylene, Co20 represents cotton fabric by using 20 Tex cotton yarn , η represents the ratio of pore's area to sample's area.

4.2.2 METHODS

The schematic diagram of self-designed testing device for evaluating thermal resistance of textile under heat convection is shown in figure 4.1. This device consists of one heater which provides hot air flow going through the testing sample, an air flow channel, a sample holder which is in the air channel, two anemometers for recording the speed of air flow, three thermocouples for recording the temperature on the both sides of sample, one data acquisition module which connects the thermocouples with laptop and collect the data from thermocouples, and one laptop which is able to save and read data. The output of heater was 42.35°C, velocity was 4.86m/s, and the heating time duration was 5s.

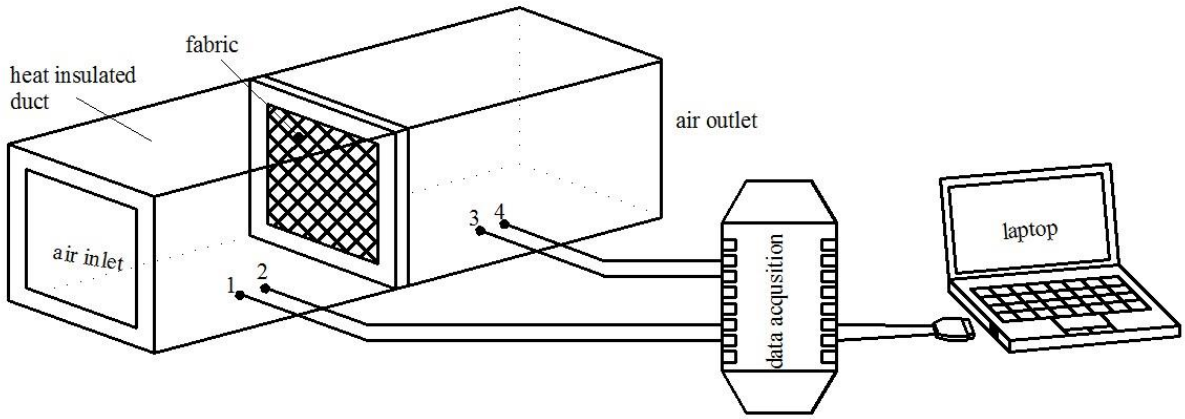

Figure 4.1. Schematic diagram of testing device. (1,4 are anemometers; 2,3 are thermocouples)

The air permeability of samples was measured by air permeability tester FX3300, which measures airflow rate under constant air pressure drop. The morphology of samples was

observed by Dino-elite digital microscope, which is able to measure the dimensions and areas of sample and pores. The porosity of sample can be calculated by equation $p = 1 - (\rho_{fabric}/\rho_{fiber})$, P is porosity, ρ_{fabric} and ρ_{fiber} are the densities of fabric and fiber, respectively. Five measurements for each sample were given, and an average value and standard deviation were determined.

4.3 RESULTS AND DISCUSSION

4.3.1 MORPHOLOGY OF SAMPLES

The images of samples were evaluated by Dino-elite digital microscope and given in figure 4.1. The magnitudes were 210 and 50 since the pore size of Co20 is too big. According to the images, the pore size and the ratio of pore's area to sample's area can be obtained, and the results are given in table 4.1. The pore size and the ratio of pore's area to sample's area of polyamide were defined to be zero since it is too density to identify the pore size in two dimensional image.

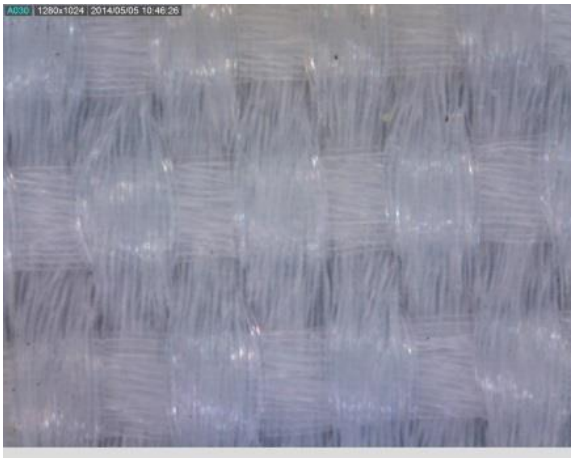

PA (210×)

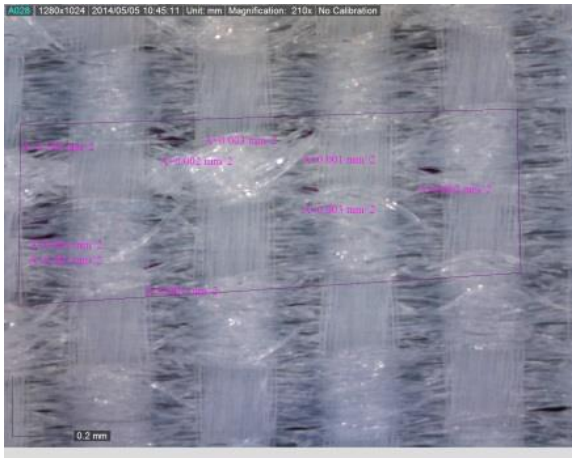

PES (210×)

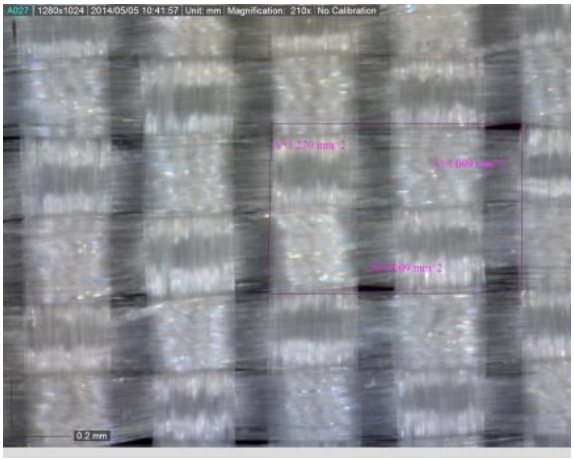

Visc (210×)

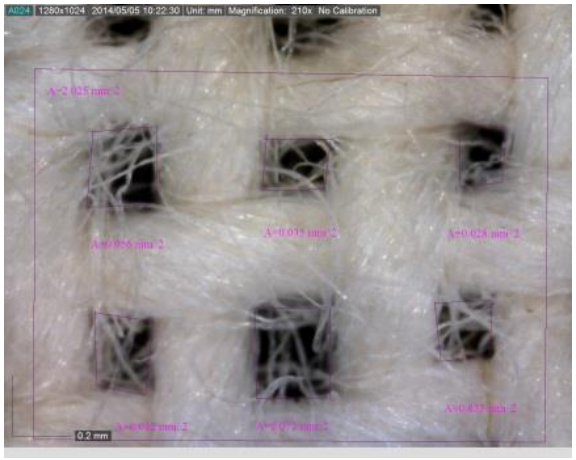

Co45 (210×)

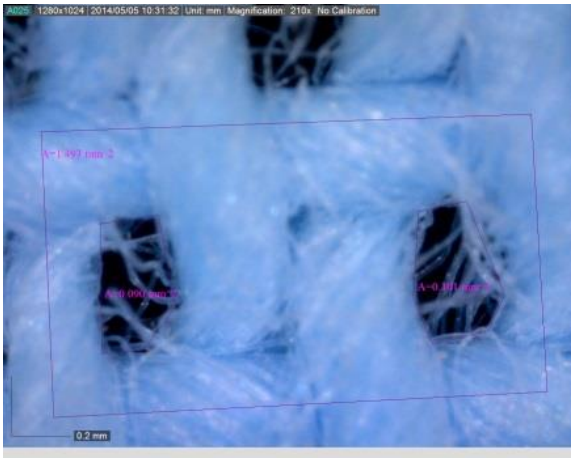

PP (210×)

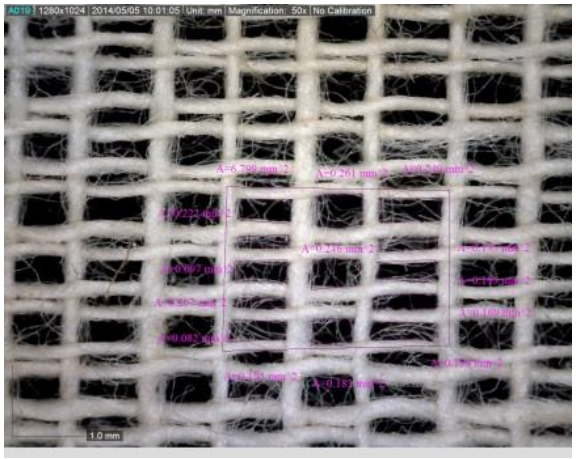

Co20 (50×)

Figure 4.2. Images of samples

4.3.2 AIR PERMEABILITY OF SAMPLES

Air permeability describes the rate of flow of a fluid through a porous material. And the mathematical expression is given by,

$$q = Q/At \tag{4.1}$$

And Darcy derived one equation for calculating the air permeability based on hydraulic radius theory, which states that rate of flow is directly proportional to the pressure gradient causing the flow[93]. The equation is as follows,

$$q = \frac{k_p \cdot \Delta p}{\mu \cdot L} \tag{4.2}$$

Or

$$Q = A \cdot t \cdot \frac{k_p \cdot \Delta p}{\mu \cdot L} \tag{4.3}$$

Where q is the rate of flow (m/s), k_p is the flow permeability coefficient (m^2), Δp is the pressure gradient (pa), μ is the dynamic viscosity of the flow (pa·s), L is the thickness of sample (m), Q is the volume flowing in time (m^3), A is the cross-section area (m^2) where flow goes through, t is time.

The results of air permeability of samples from FX3300 are given in table 4.2 and figure 4.3.

Table 4.2 Air permeability of samples under different pressure

Samples	10Pa (mm/s)	Slope	20Pa	Slope	30Pa	Slope
PA	5.74±0.103	0.574	12±0.187	0.6	17.02±0.22	5.67
PES	18.82±0.258	1.882	36.4±0.69	1.82	52.48±1.19	1.75
Visc	24.5±1.45	2.45	45.96±1.87	2.3	60.3±1.53	2.1
Co45	61.3±6.35	6.13	119±13.28	5.95	174.6±25.26	5.82
PP	133.2±12.29	13.32	214±8.746	10.7	316±24.36	10.53
Co20	740±22.34	74	1204±51.76	60.2	1592±31.14	53.07

Note: slope is the quotient of air permeability and pressure gradient, the smaller difference between slopes for the same fabric, the better direct proportional relation between pressure gradient and air permeability.

The air permeability showed one strong correlation with air pressure gradient according to equation (4.2) and (4.3) as well as from experimental results. The rate of flow is almost directly proportional to the pressure gradient based on the experimental results, but the slope had a slight decrease when the pressure gradient becomes higher, especially for the samples which have higher porosity, bigger pore size, or bigger pore's area ratio.

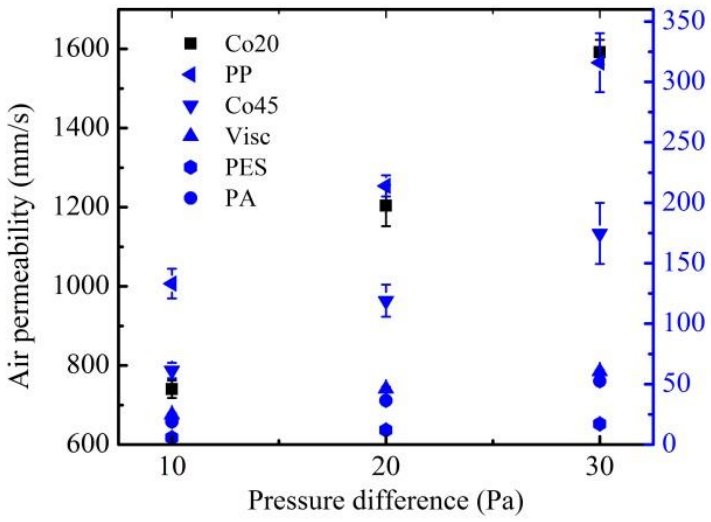

Figure 4.3. Effect of pressure gradient on air permeability

Owing to the different concepts in evaluating porosity, pore size, and the ratio of pore's area to total area of sample, there are no obvious relationships among them (table 4.1). Porosity defines as the ratio of total void volume to the total volume occupied by the solid and the void volumes[94], which is a general description of void part in materials, and it does not

give the information about the pore size and the pore shape. The pore size and the pore's area ratio in this work were evaluated by two dimensional images. They can be used to determine the size of air flow channel and the distribution of pores since the plain woven fabrics have regular structure (figure 4.2). When the pore as a channel in material, the pore size and pore's area ratio must have more significant correlations than porosity with air permeability as well as the thermal property under convective heat transfer since the speed and volume of air flow are highly depending on the cross section area of air channel[95].

Some researchers[93, 96, 97] stated that there has one correlation between porosity and air permeability coefficient/air permeability. Generally, the air permeability would increase as the increase of porosity. But the air permeability of polyester and polypropylene fabrics in this work has a big difference even they almost have the same porosity, and also the air permeability of Co45 fabric is lower than the air permeability of polypropylene fabric even the porosity of Co45 fabric is higher (figure 4.4). The reason of this phenomenon could be due to the different pore sizes. Polypropylene fabric has the biggest pore size, which is corresponding to the highest air permeability; polyester fabric has the smallest pore size, which is corresponding to the lowest air permeability (figure 4.4 and figure 4.5). And there is one significant relationship between pore size and air permeability, which increases as the increase of pore size (figure 4.5). Besides, the pore's area ratio has a directly proportional correlation with air permeability (figure 4.6).

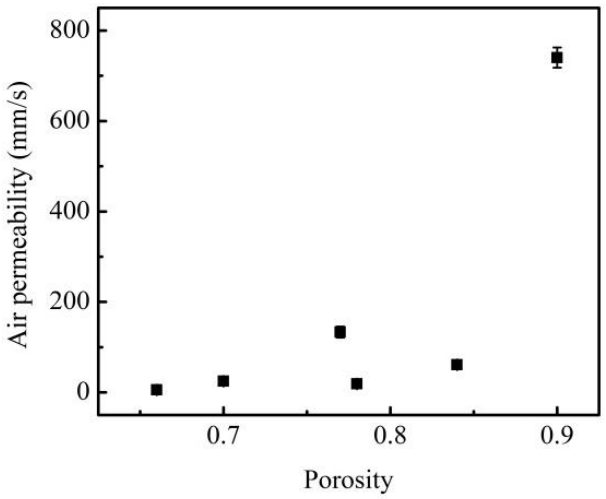

Figure 4.4 Effect of porosity on air permeability

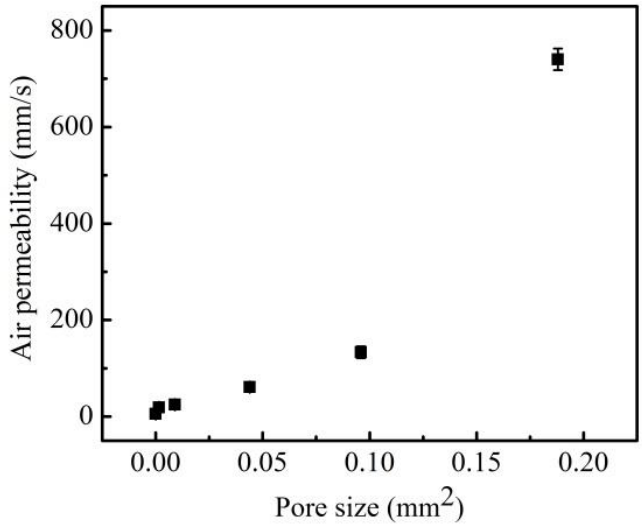

Figure 4.5 Effect of pore size on air permeability

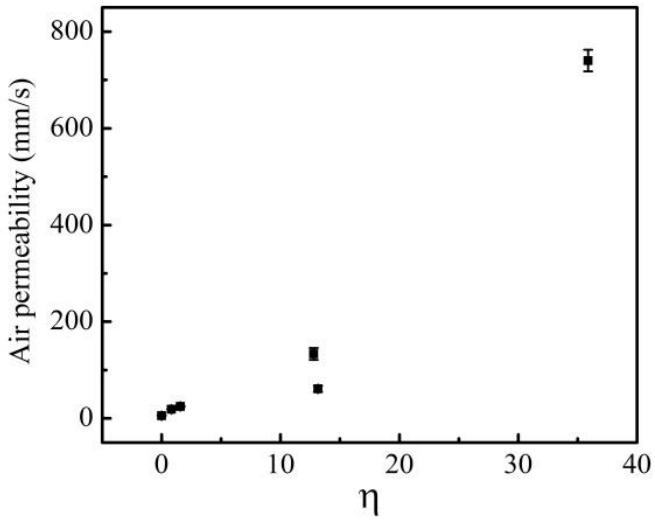

Figure 4.6 Effect of pore's area ratio on air permeability

4.3.3 THERMAL PROPERTY OF SAMPLES

4.3.3.1 Thermal conductivity of fiber

Since the aim of this work is to investigate the effect of structure (porosity, pore size and pore's area ratio) on the thermal property under heat convection, therefore, the results from difference material need to be normalized. It means that the materials and the thickness should be the same.

The thermal property of fabrics was measured by Alambeta, and the results are given in table 4.3. Based on the results from Alambeta and the knowledge about porosity, the thermal conductivity of fibers can be obtained by using equations (4.4) - (4.6)[21].

$$k_P = \phi k_a + (1-\phi)\, k_f \tag{4.4}$$

$$k_s = \frac{k_a k_f}{\phi k_f + (1-\phi)\, k_a} \tag{4.5}$$

$$k_e = \left(k_P + k_S\right)/2 \tag{4.6}$$

Where k_p and k_s are thermal conductivity of fabric when the fibers are parallel and series to the heat flow, k_e, k_a, and k_f are the thermal conductivity of fabric, air and fiber, respectively, ϕ is the porosity of fabric.

Table 4.3 Thermal property of samples

Samples	Thermal conductivity of fabric $\times 10^{-3}$ (W/(m·K))	Thermal resistance of fabric $\times 10^{-3}$ (K/W)	Thermal diffusivity of fabric $\times 10^{-6}$ (m^2/s)	Thermal conductivity of fiber $\times 10^{-3}$ (W/(m·K))
PA	40.18±1.46	8.99±0.829	0.0435±0.0024	95.16
PES	31.93±1.32	8.77±1.78	0.0843±0.02	76.67
Visco	31.25±0.61	6.08±0.933	0.0413±0.0095	55.83
Co45	41.19±1.45	19.42±2.01	0.1132±0.0125	214.03
PP	42.8±0.758	18.92±1.03	0.1081±0.019	162.05
Co20	34.56±0.647	16.4±1.19	0.1613±0.01282	211.85

4.3.3.2 Temperature difference on the both sides of samples

The temperatures on both sides of samples were monitored responding to time by one self-made device as described above, and the results are given in figure 4.7. According to Fourier's law and Newton's law of cooling, we can simply define that the bigger temperature difference on both sides of sample, the more heat energy blocked by the sample, which also means that the sample has better thermal resistance.

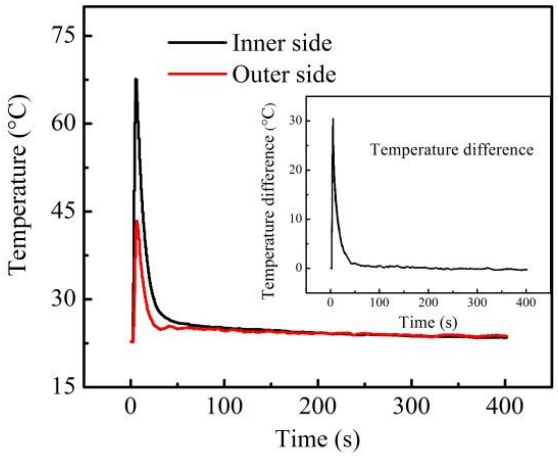
Inner side
Outer side
Temperature (°C)
Time (s)
Temperature difference
Temperature difference (°C)
Time (s)

A

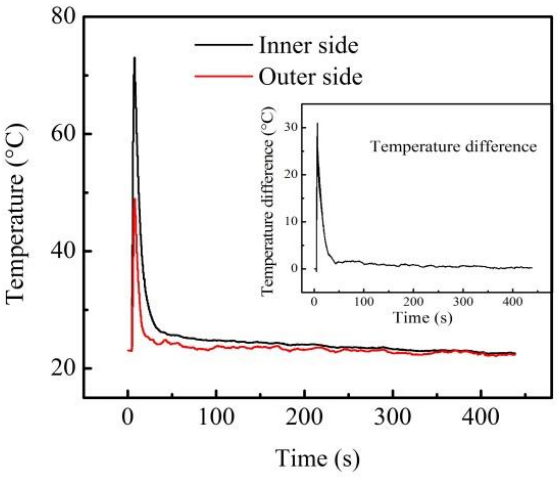
Inner side
Outer side
Temperature (°C)
Time (s)
Temperature difference
Temperature difference (°C)
Time (s)

B

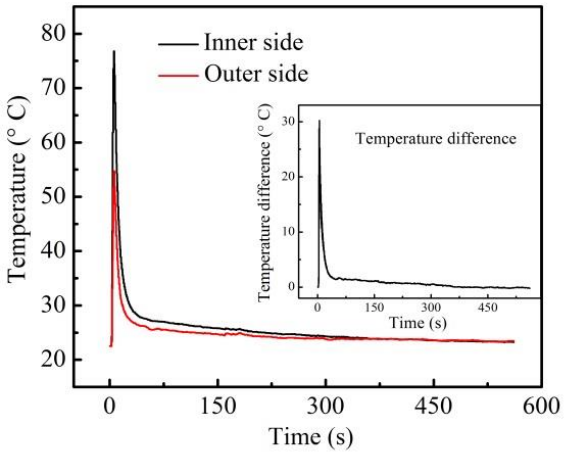
Inner side
Outer side
Temperature (° C)
Time (s)
Temperature difference
Temperature difference (° C)
Time (s)

C

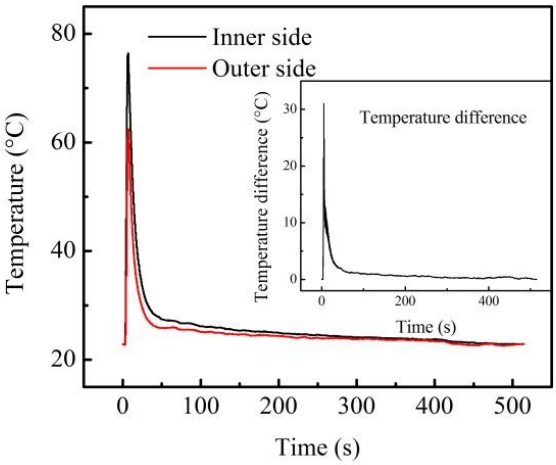

D

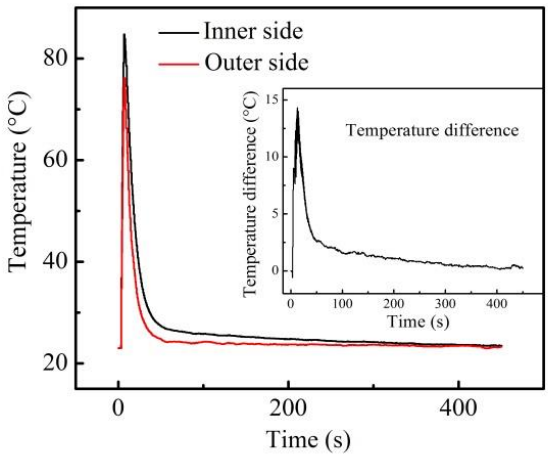

E

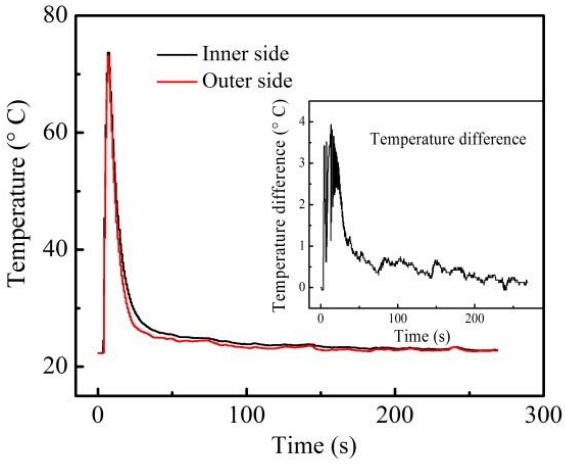

F

Figure 4.7. Temperature distributions on the both sides of samples (A: PA; B: PES; C: Visc; D: Co45; E: PP; F: Co20)

According to Fourier's law,

$$Q = -kA\frac{dT}{dx} \tag{4.7}$$

Then we can get,

$$\frac{dT}{dx} = \frac{1}{k} \cdot \frac{Q}{A} \tag{4.8}$$

$$\frac{dT_i}{dx_i} = \frac{1}{k_i}\frac{Q}{A} \tag{4.9}$$

Where Q is heat flow, k is thermal conductivity of material, A is the cross-sectional area which the heat flow going through, dT is the temperature difference on both sides of sample, dx is the thickness of sample, dT_i is the temperature difference on both sides of sample i (i=PA, PES, Visc, Co45, PP, Co20), dx_i is the thickness of sample i, k_i is thermal conductivity of fiber material i.

The maximum temperature difference (shown in figure 4.7) and the normalized maximum temperature difference (from equation 4.9) on both sides of samples are given in table 4.4.

Table 4.4 Maximum temperature difference on the both sides of samples

Samples	Max. temperature difference (°C)	Normalized Max. temperature difference dT/dx (°C/mm)	Velocity through fabrics(m/s)	h_e (W/(m2·K))
PA	30.98±0.49	86.05±1.47	0	--
PES	30.53±0.43	87.85±1.29	0.02	21.97
Viscose	29.66±0.50	85.41±1.5	0.03	32.95
Co45	30.29±0.81	85.16±2.43	0.06	65.91
PP	15.34±0.93	32.04±2.79	0.23	252.65
Co20	4.09±0.43	17.05±1.68	0.76	762.4

Note: '- -' means the value cannot be calculated in this work.

Owing to the penetrating of air flow through the textile, the heat energy went through the textile as well. The heat flow through textiles can be expressed by,

$$Q_t = cm\Delta T = c\rho V\Delta T = c\rho Av\Delta T \tag{4.10}$$

And also can be given by,

$$Q_t = Q_{cond} + Q_{conv} = h_e A \Delta T \tag{4.11}$$

Therefore, the effective heat transfer coefficient h_e can be calculated by solving equations (4.10) and (4.11)

$$h_e = c\rho v \tag{4.12}$$

The specific heat c and density ρ of air at 50°C is 1005 J/(kg·K) and 1.093kg/m^3, respectively[98], the velocity values are given in table 4.4 based on experiment.

4.3.4 EFFECTS OF STRUCTURE ON THE THERMAL PROPERTY OF SAMPLES

Generally, the textiles having higher porosity blocked less heat energy under convective condition (as shown in figure 4.8). However, the porosity is not the only factor which influences the convective heat transfer. The pore size showed a more significant relationship with the thermal property of textiles, the less heat energy blocked by textiles which have bigger pore size (figure 4.9). And also as the increase of pore's area ratio, the normalized maximum temperature difference on the both sides of samples decreased (figure 4.10). Since the heat energy was carried by air, therefore, the total heat energy amount which went through samples depends on the rate of flow and the temperature gradient of air. As discussed above, the structure of samples is a very important factor of air permeability as well as thermal property. Therefore, the air permeability could be better to describe the thermal property of textile under convective heat transfer, and figure 4.11 shows that the air permeability is directly proportional to the normalized maximum temperature difference.

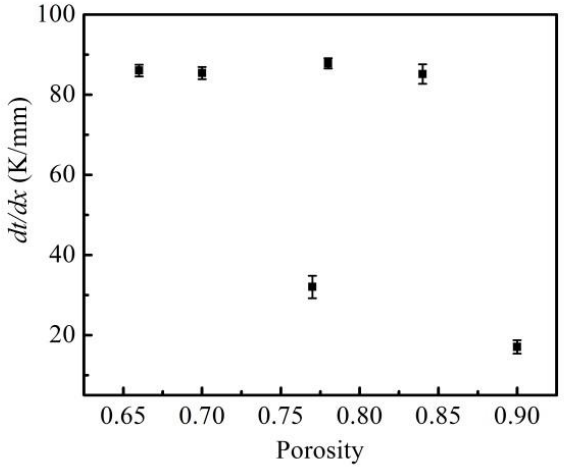

Figure 4.8. Effects of porosity on thermal property of samples

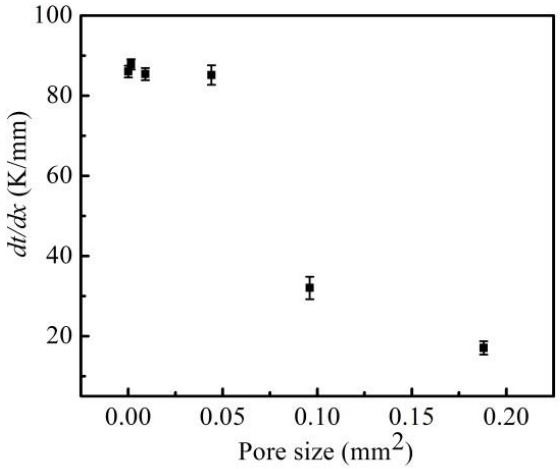

Figure 4.9. Effects of pore size on thermal property of samples

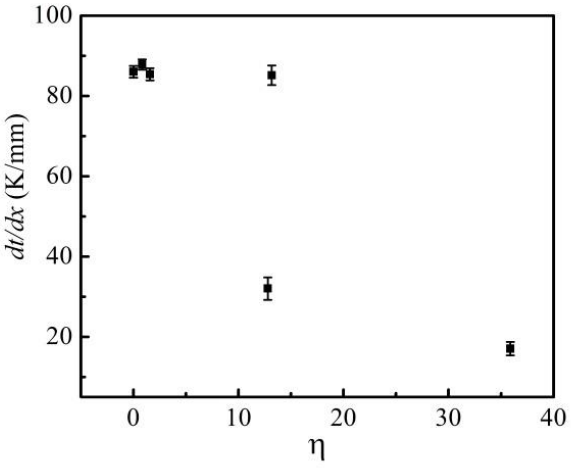

Figure 4.10. Effects of pore's area ratio on thermal property of samples

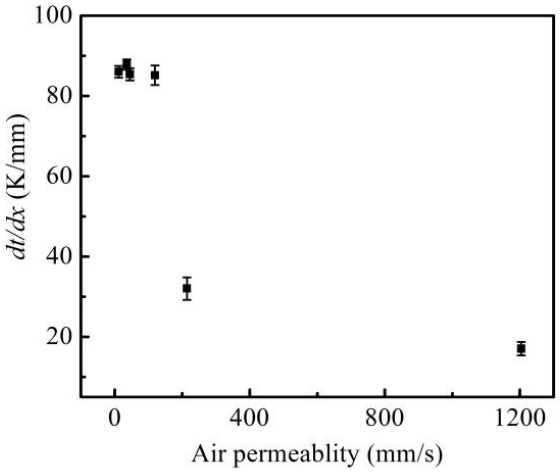

Figure 4.11. The relationship between air permeability and thermal property

4.4 CONCLUSIONS

In this work, the effects of structure on air permeability and thermal property of textiles are investigated, based on the experimental results, some conclusions can be draw: (1) the structure of samples has a big influence in air permeability and thermal property; (2) the pore size and pore's area ratio have more significant effect on air permeability and thermal property then porosity; (3) air permeability is directly proportional to thermal property under convective heat transfer.

5 3D NUMERICAL SIMULATION OF LAMINAR FLOW AND CONJUGATE HEAT TRANSFER THROUGH FABRIC

5.1 INTRODUCTION

Textile as clothing is an integral part of human beings with a primary role to protect the body against unsuitable environments by avoiding mechanical, thermal and chemical damages and maintaining thermal balance, which means the clothing needs to be sensitive enough to the environment and generates a reasonable thermal microenvironment around the body to help it deal with external weather conditions. The exchange of heat follows distinct phenomena of simultaneous conduction, convection, radiation. Heat transfer through conduction and radiation has been well understood and documented [15, 99-103]. However, convective heat transfer through fabric is difficult to model as there are no exact solutions for porous material under heat convection as well as the limited research work in this area[92, 104]. The main problem faced in heat convection is the calculation of heat transfer coefficients or Nusselt number.

The equation of heat transfer coefficient is given by,

$$h = \frac{q}{\Delta T} \tag{5.1}$$

Or

$$h = \frac{Nu \cdot \lambda}{x} \tag{5.2}$$

The general equation of Nusselt number is given by,

$$Nu = C\, Re^{m}\, Pr^{n} \tag{5.3}$$

Where h is heat transfer coefficient, q is heat flux, ΔT is temperature difference, λ is thermal conductivity, x is thickness of sample, Nu is Nusselt number, Re is Reynolds number, Pr is Prandtl number, C, m and n are constants. However, these solutions are valid only for a specific set of conditions, so for every new situation, a new set of empirical coefficients has to be designed[5].

Beithou [105] studied the effect of the porosity of the porous medium on the Nusselt number for natural convection and reported that with the increase in the porosity, there is a linear increase in the Nusselt number. Hatch[106] confirmed that fabric structural features, not

component fibers, are the most important controllers of thermal dissipation. Moreover heat transfer is highly related to fabric thickness, bulk density and the air volume fraction. On the other hand, numerical method has been widely used in every area due to its reliable accuracy, flexibility for both realistic conditions and ideal conditions, and more detailed information. Bhattacharjee [92] studied the heat transfer coefficient of fabric under natural and force heat convection by numerical simulation, they found that the values from numerical simulation had a good agreement with the values from experiment, however, the fabrics in their numerical simulation were taken as plate without pores.

Therefore, in this work numerical simulation is applied to investigate the local temperature distributions, local heat flux distributions, local/average heat transfer coefficients, and local Nusselt numbers of fabrics taken as plate and porous material under conductive and convective heat transfer.

5.2 PHYSICAL MODEL, BOUNDARY CONDITIONS, GOVERNING EQUATIONS AND NUMERICAL METHOD

The 3-D geometric model consists of polyester fabric and air flow, which is shown in figure 1. In order to save the computation time, the dimensions of polyester fabric were 30mm×4mm×0.8mm in length (x direction), width (y direction) and height (z direction), and the dimensions of air flow above fabric were 30mm×4mm×4mm in length, width and height, the dimensions of air flow below fabric were 30mm×4mm×2mm in length, width and height. Therefore, the coordinates of geometric domain were X (0, 30), Y (0, 4), and Z (-2, 4.8). The mesh quality of geometric models was evaluated by two parameters which were minimum orthogonal quality and maximum aspect ratio. The minimum orthogonal qualities of simulation 1 and 2 were over 0.99 and the maximum aspect ratios were around 7.56, which mean the mesh qualities were very high. The minimum orthogonal quality and maximum aspect ratio of simulation 3 were 0.28 and 15.6, which mean the mesh quality was also good enough.

In order to simulate different conditions of human-clothing-environment, three kinds of simulation were carried out.

Simulation 1: the fabric was taken as a plate and contact with human body;

Simulation 2: the fabric was taken as a plate having an air gap between human body and fabric, and the air flow below fabric cannot move;

Simulation 3: the fabric was taken as a porous plate having an air gap between human body and fabric, and the air flow below the fabric can freely move. The pore's diameter is 1mm, and the distance between two pores is 2mm.

According to the objective of simulation, the boundary conditions were given: the temperature contacting with human body was 310K, the temperature of air flow above fabric was 273K at a velocity (5m/s). From the above known information, the following useful information for simulation can be obtained:

The Mach number

$$M_a = u_0 \Big/ \sqrt{kRT_0} \tag{5.4}$$

The total pressure

$$\frac{p_t}{p_b} = \left[1 + \frac{k-1}{2} M_a^2\right]^{k/(k-1)} \tag{5.5}$$

The pressure drop

$$\Delta p = p_t - p_b \tag{5.6}$$

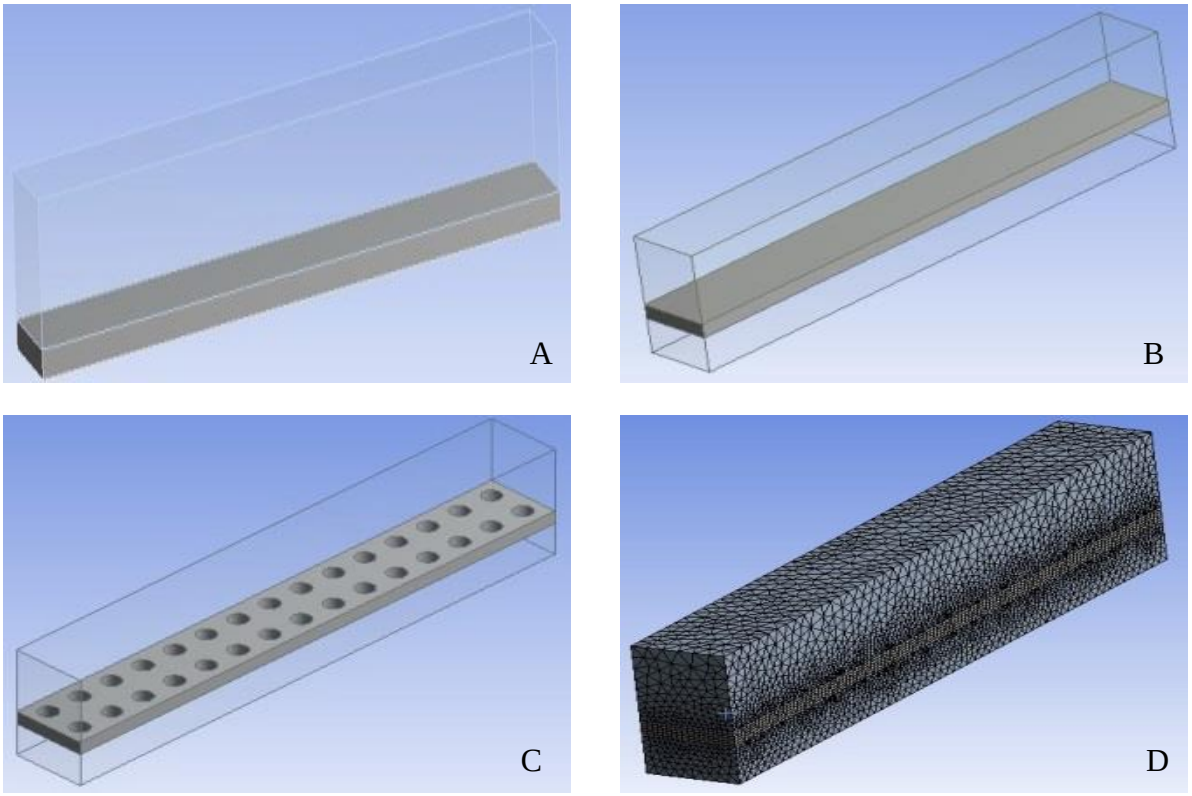

Figure 5.1. Geometric models and computational grid (A) geometric model of simulation 1; (B) geometric model of simulation 2; (C) geometric model of simulation 3; (D) computational grid of simulation 3.

The governing equations for calculation are given as follows. The heat conduction equation for the solid part is:

$$\nabla \cdot \left(\lambda_s \nabla T_s \right) = 0 \tag{5.7}$$

The mass, momentum and energy equations as well as the ideal gas equation of state are given by:

$$\nabla \cdot \left(\rho U \right) = 0 \tag{5.8}$$

$$\nabla \cdot \left(\rho UU \right) = -\nabla p + \nabla \cdot \left(\mu \left(\nabla U - \frac{2}{3} \nabla \cdot UI \right) \right) \tag{5.9}$$

$$\nabla \cdot \left(\rho UH \right) = \nabla \cdot \left(\lambda_f \nabla T_f \right) \tag{5.10}$$

$$p = \rho RT \tag{5.11}$$

Where λ_s is thermal conductivity of solid ($W \cdot m^{-1} \cdot K^{-1}$), λ_f is Thermal conductivity of fluid ($W \cdot m^{-1} \cdot K^{-1}$), I is the unit tensor.

The partial differential equations governing the problem are reduced to a system of algebraic equations using finite volume procedure. The discretization of the convective and diffusive fluxes across the control surfaces is modeled using the QUICK scheme and the pressure-velocity coupling is handled with the SIMPLE method. The convergence criterion is that the residual variations of the mass, momentum and energy conservation equations become less than 10^{-7}.

5.3 RESULTS AND DISCUSSIONS

5.3.1 TEMPERATURE DISTRIBUTION IN XZ-PLANE

The temperature distributions (TD) and heat flux distributions (HFD) in xz-plane at y=2mm are given in figure 5.2. The temperature gradually decreased from the bottom of geometric model (human skin) to the top of air flow, and the temperature decrease on the fabric surface and the air temperature increase in the near region of fabric surface, which indicated that the heat conduction and heat convection were coupled numerically. In addition, the temperatures of fabric and air close to the air flow inlet (left side of figures) were lower than the temperatures close to the air flow outlet due to the cooling effect of cold air flow. And the temperature distribution of simulation 3 is quite different with the other simulations due to the existence of pores where the cold air flow can go through.

And the temperature distributions in xz-plane at y=2 were compared in figure 2D. For simulation 1 and 2, the temperatures were decreasing gradually in the near region of bottom (skin), but for simulation 3, the temperature was decreasing dramatically at the beginning which is due to the air flow move much faster than the heat transfer rate by conduction. In the region of air flow above fabric, the temperature distributions were almost the same.

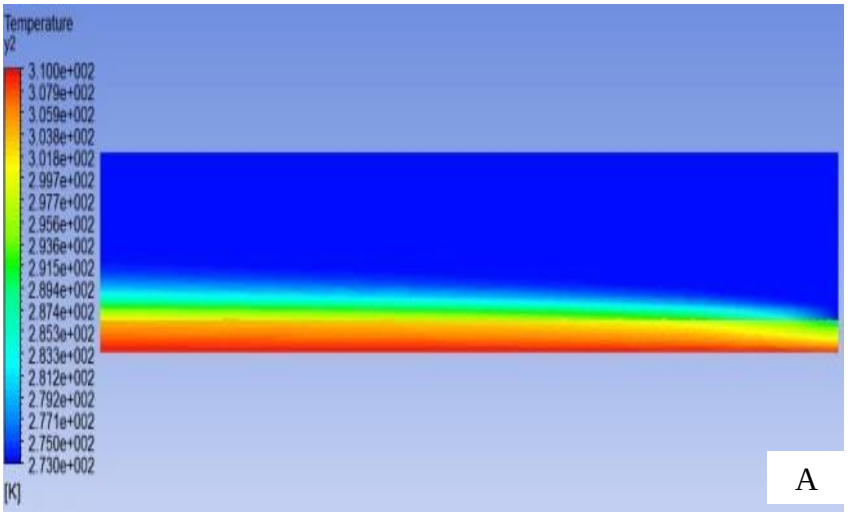
Temperature
y2
3.100e+002
3.079e+002
3.059e+002
3.038e+002
3.018e+002
2.997e+002
2.977e+002
2.956e+002
2.936e+002
2.915e+002
2.894e+002
2.874e+002
2.853e+002
2.833e+002
2.812e+002
2.792e+002
2.771e+002
2.750e+002
2.730e+002
[K]
A

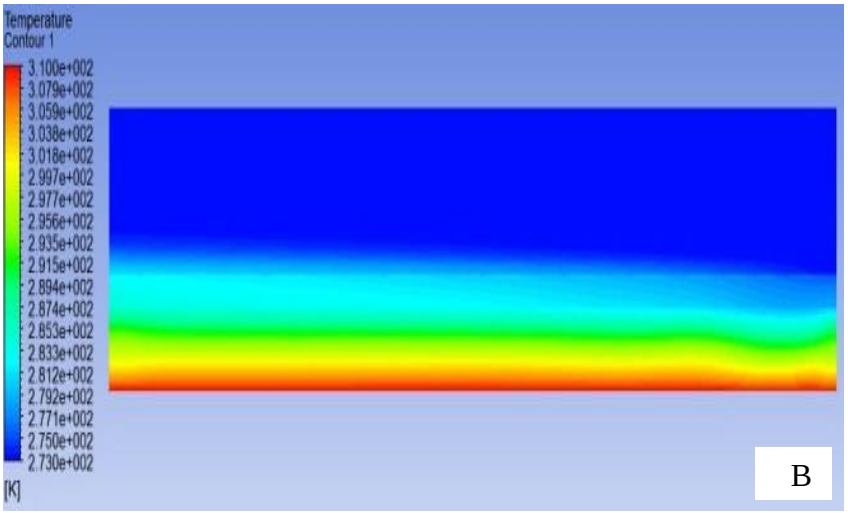
Temperature
Contour 1
3.100e+002
3.079e+002
3.059e+002
3.038e+002
3.018e+002
2.997e+002
2.977e+002
2.956e+002
2.935e+002
2.915e+002
2.894e+002
2.874e+002
2.853e+002
2.833e+002
2.812e+002
2.792e+002
2.771e+002
2.750e+002
2.730e+002
[K]
B

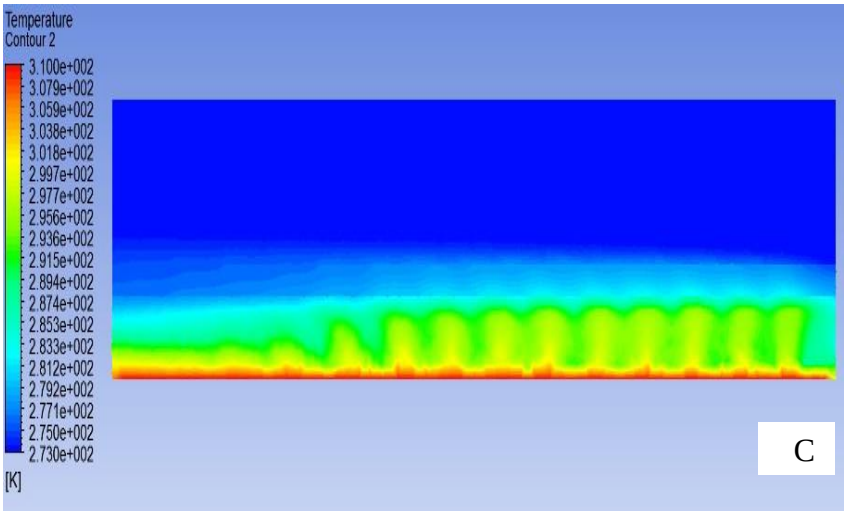
Temperature
Contour 2
3.100e+002
3.079e+002
3.059e+002
3.038e+002
3.018e+002
2.997e+002
2.977e+002
2.956e+002
2.936e+002
2.915e+002
2.894e+002
2.874e+002
2.853e+002
2.833e+002
2.812e+002
2.792e+002
2.771e+002
2.750e+002
2.730e+002
[K]
C

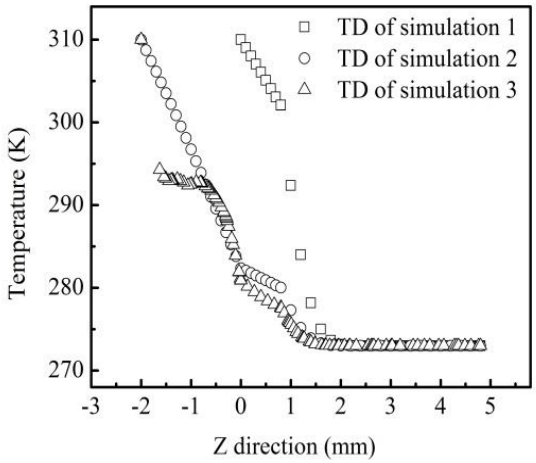

D

Figure 5.2. Temperature distribution in xz-plane (A) Temperature distribution of simulation 1 in xz-plane at y=2mm; (B) Temperature distribution of simulation 2 in xz-plane at y=2mm; (C) Temperature distribution of simulation 3 in xz-plane at y=2; (D) Temperature distributions of simulations in xz-plane at x=15mm and y=2mm.

5.3.2 TEMPERATURE DISTRIBUTION AND HEAT FLUX DISTRIBUTION ON FABRIC SURFACE

The temperature distributions and heat flux distributions on the fabric surface are given in figure 5.3. The temperatures of fabric surface were higher and higher when it was further and further to the inlet of cold air flow. In contrast, the heat fluxes were less and less. For simulation 3, the temperature distribution and heat flux distribution had the same trend with simulation 1 and 2, but the local temperature and heat flux were quite different due to the difference of fabric structure and the air flow motion. And the air flow motion of simulation 3 is given in figure 5.4.

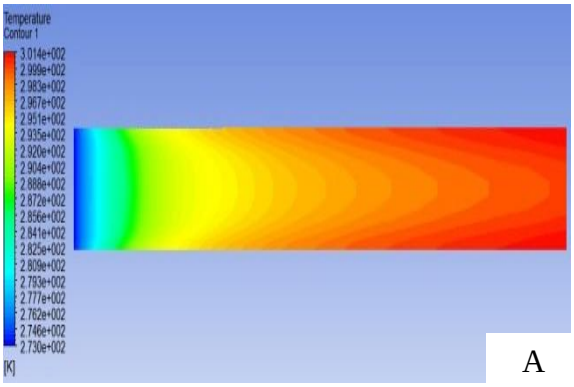

A

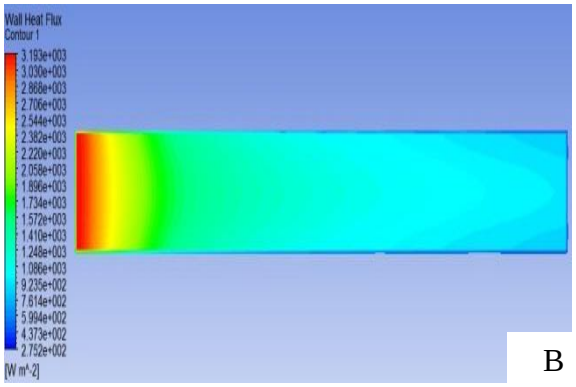

B

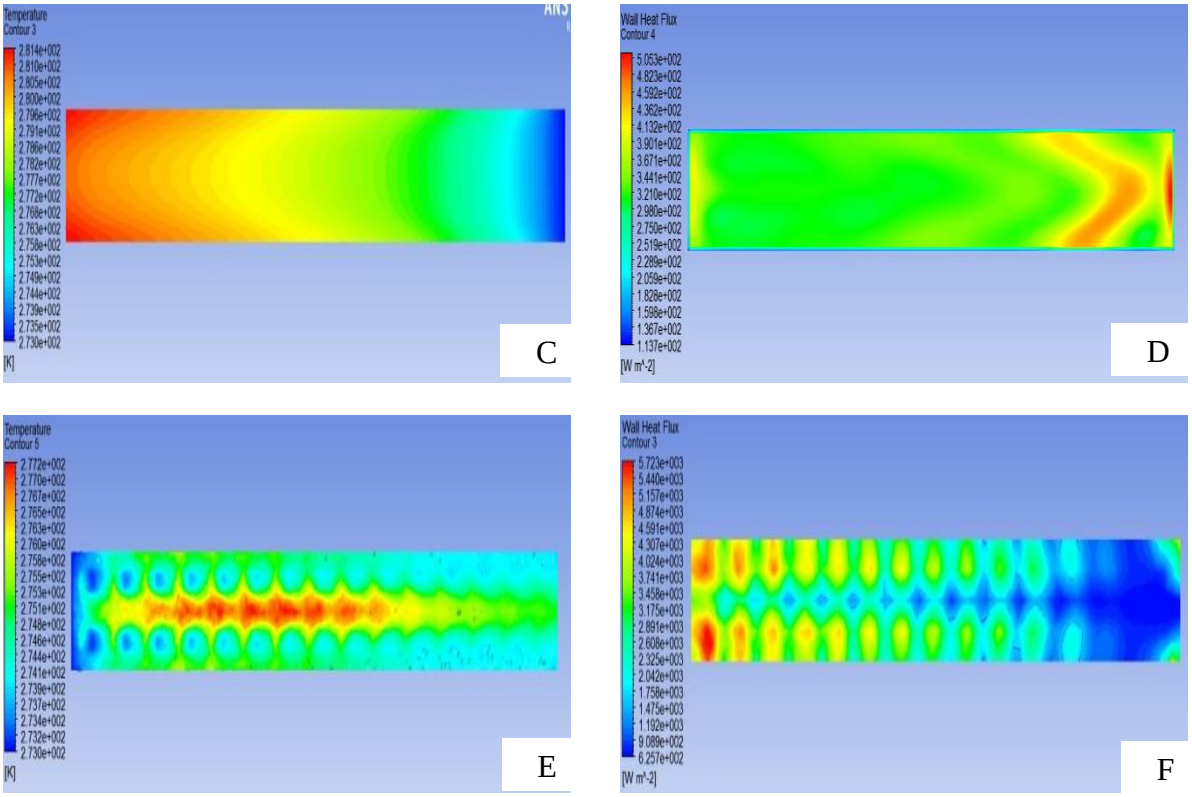

Figure 5.3. Temperature and heat flux distributions on the fabric surface (A) Temperature distribution of simulation 1 on the upper surface of fabric; (B) Heat flux distribution of simulation 1 through fabric; (C) Temperature distribution of simulation 2 on the upper surface of fabric; (D) Heat flux distribution of simulation 2 through fabric; (E) Temperature distribution of simulation 3 on the upper surface of fabric; (F) Heat flux distribution of simulation 3 through fabric.

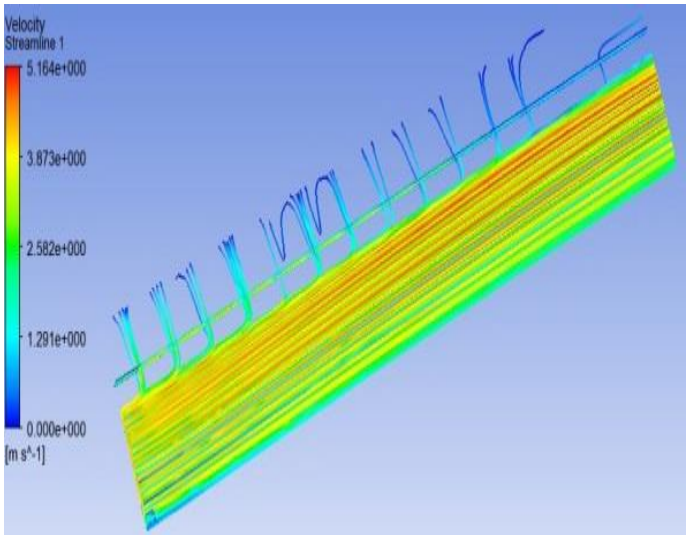

Figure 5.4. Velocity profile of simulation 3

The more clear comparison of temperature and heat flux distributions on fabric surface is given in figure 5.5. The temperatures of simulation 1 and 2 were going higher as the distance

increases since the cold air flow was cooling the fabric surface as well as heated by the fabric surface at the same time. Therefore, the cooling effect of air flow was reduced as the increase of distance, and then the temperature was higher as the increase of distance. For simulation 3, the temperature and heat flux distribution were different at y=2 (the middle line of fabric surface) and y=3 (the middle line of pores on the fabric surface) due to the air flow motion. The temperature increased first, and then decreased at y=2 since the air flow below fabric had more tense cooling at the outlet (figure 5.4). The temperature had a cyclical fluctuations at y=3 since the cold air flow went through the regular solid-pore structure of fabric. With respect to the heat flux distribution, the higher temperature was corresponding to the lower heat flux.

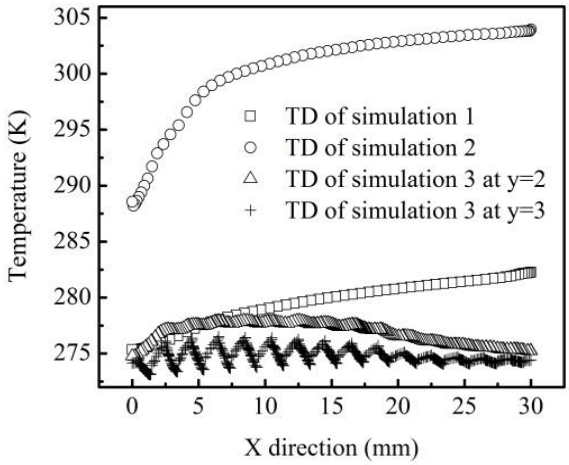

A

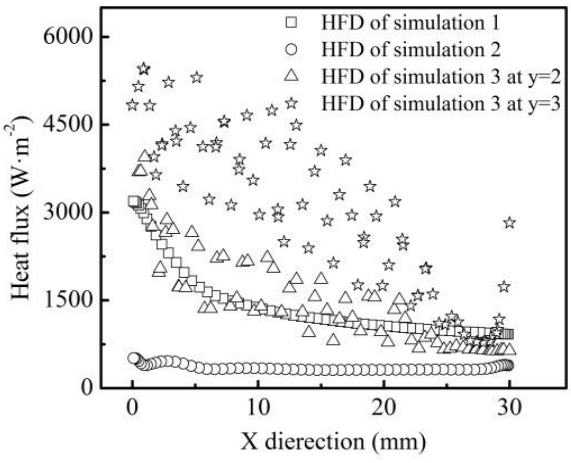

B

Figure 5.5. Comparison of temperature and heat flux distributions (A) Temperature distributions of simulations in xy-plane at y=2mm and z=0 (upper surface of fabric); (B) Heat flux distributions of simulations through fabric

5.3.3 COMPARISON OF HEAT TRANSFER COEFFICIENT AND NUSSELT NUMBER

In order to obtain the heat transfer coefficient of fabric under heat convection, the temperature gradient and heat flux are needed according to equation (5.2), and the local heat transfer coefficient is given by,

$$h_x = \frac{q_x}{(T_{air} - T_{skin})} \tag{5.12}$$

The local Nusselt number is given by,

$$Nu_x = h_x x / \lambda_a \tag{5.13}$$

Substituting equation (5.12) into equation (5.13), then the local Nusselt number is given,

$$Nu_x = \frac{h_x x}{\lambda_a} = \frac{q_x}{T_{skin} - T_{air}} \frac{x}{\lambda_a} \tag{5.14}$$

On the other hand, the Nusselt number is one function of Reynolds number (the ratio of inertial force to viscous force) and Prandtl number (the ratio of molecular diffusivity of momentum to molecular diffusivity of heat), which can be expressed generally by equation (5.1). But for particular situations, the constants of *C*, *m*, and *n* are always different. And for flat plate in laminar flow, the Nusselt number can be obtained by[5],

$$Nu_x = 0.332\, Re_x^{0.5}\, Pr^{1/3} \tag{5.15}$$

Where $Re_x = \rho u x / \mu$, and $Pr_x = \nu / \alpha$.

The heat transfer coefficient and Nusselt number are given in figure 5.6. Normally, the relationship between Reynolds number and Nusselt number should be given, but in this paper, the distance is given instead of Reynolds number since the Reynolds number is one function of distance and the aim of this paper is to investigate the distribution of Nusselt number on the fabric surface. The heat transfer coefficients and Nusselt numbers from simulation 1 had a very good agreement with the results from equation (5.15) (as shown in figure 5.6) since this model was derived from the geometry model of simulation 1. It also indicated that the simulation process and results were correct and reliable. But the heat transfer coefficients and Nusselt numbers from simulation 2 were much smaller than the results from model due to the very low thermal conductivity of air gap, which slowed down the heat transfer rate. The heat transfer coefficients of simulation 3 at y=2 had a general

decrease trend and had a small fluctuations around the values from model. The fluctuation of results is due to the different heat transfer rates of heat conduction through fabric and the heat convection by air flow. The heat transfer coefficients of simulation 3 at y=3 had a similar trend with simulation 3 at y=2, but the values were much higher than the values from model, which indicates that the existence of pores increases the heat transfer rate. The Nusselt numbers of simulation 3 at y=2 were fluctuant around the values from model, but the Nusselt numbers of simulation 3 at y=3 were fluctuant and much higher than the results from model, which means the heat transfer by convection is much higher than the heat transfer by conduction.

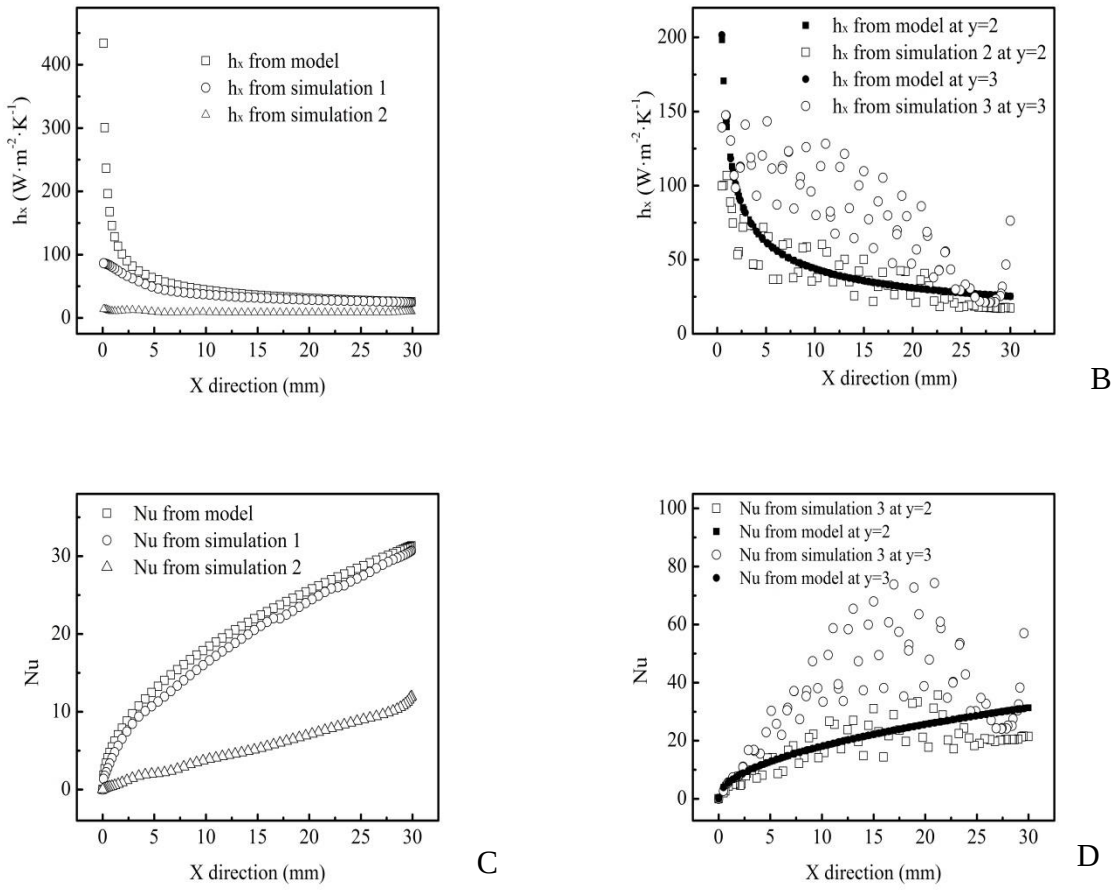

Figure 5.6. comparison of local heat transfer coefficients and Nusselt numbers (A) comparison of local heat transfer coefficient of model and simulation 1 and 2; (B) comparison of local heat transfer coefficient of model and simulation 3 at y=2 and y=3; (C) comparison of local Nusselt number of model and simulation 1 and 2; (D) comparison of local Nusselt number of model and simulation 3 at y=2 and y=3.

In addition, the average heat fluxes through fabrics were obtained by area-weight average method. There were 1346.9 $W \cdot m^{-2}$, 342.3 $W \cdot m^{-2}$, and 2520.4 $W \cdot m^{-2}$ for simulation 1,

simulation 2, and simulation 3, respectively. Then, the average heat transfer coefficients of simulations were 36.4 $W \cdot m^{-2} \cdot K^{-1}$, 9.25 $W \cdot m^{-2} \cdot K^{-1}$, and 68.12 $W \cdot m^{-2} \cdot K^{-1}$, respectively. Therefore, the thermal insulation of fabric will be much better when there has air gap between fabric and skin. And the porosity will have a negative effect on thermal insulation when there has air flow motion and the air flow penetrates the fabric.

5.4 CONCLUSIONS

The heat transfer coefficient and Nusselt number of fabrics in different conditions under heat convection was investigated numerically in this work, and some conclusions can be draw based on the results,

(1) The numerical simulation of flow and conjugate heat transfer through fabric can be an accurate and reliable method according to the good agreement between the simulation results and a well-known analytical model; (2) the stagnate air gap between fabric and skin plays a positive role in increasing the thermal insulation, and the porosity of fabric has an negative impact on increasing thermal insulation; (3) the local heat transfer coefficients and Nusselt numbers of porous fabrics have big difference, and the skin would have difference thermal feeling at different local area. In addition, more work is needed to be studied in order to investigate the effect of pore size, pore's distribution, the angle between air flow and fabric, and the air flow velocity on the thermal insulation of fabric.

6 CONCLUSIONS

The main contribution of this work is to investigate the thermal property of textiles, which consists of four parts,

(1) Comparison of some widely used analytical models for predicting the thermal conductivity of textiles under conductive heat transfer, and investigation of the factors influencing the thermal conductivity of textiles by numerical method, and some conclusions can be obtained,

Analytical models can provide accurate prediction when the structure of samples is simple; the numerical simulation can provide more accurate results than analytical models', and is more flexible for any complicated structures; the effective thermal conductivity of textile will be lower as the increase of porosity, pore size, and major-axis length, as the decrease of contact area; and also the distribution of pores will influence the thermal conductivity of textiles; therefore, a more delicate model is needed for predicting the thermal conductivity of textile.

(2) Investigation of structure influencing the thermal property of textiles under conductive, convective and radiative heat transfer, and some conclusions are as follows,

Both porosity and pore size influenced the thermal conductivity of textile having very high porosity (>95%) under heat conduction; the effective thermal conductivity of textile was contributed by conductivity heat transfer and radiative heat transfer, and the ratio of radiative heat transfer reached up to 50% to the total heat transfer in some cases.

(3) Investigation of the effect of structure (porosity, pore size, and pore's area ratio) on the air permeability and thermal property of textile under convective heat transfer,

The structure of samples has a big influence in air permeability and thermal property; the pore size and pore's area ratio have more significant effect on air permeability and thermal property then porosity; air permeability is directly proportional to thermal property under convective heat transfer.

(4) Investigation of the impact of structure on the thermal resistance of textile under heat convection numerically,

The numerical simulation of flow and conjugate heat transfer through fabric can be an accurate and reliable method according to the good agreement between the simulation results and a well-known analytical model; the stagnate air gap between fabric and skin plays a

positive role in increasing the thermal insulation, and the porosity of fabric has an negative impact on increasing thermal insulation; the local heat transfer coefficients and Nusselt numbers of porous fabrics have big difference, and the skin would have difference thermal feeling at different local area. In addition, more work is needed to be studied in order to investigate the effect of pore size, pore's distribution, the angle between air flow and fabric, and the air flow velocity on the thermal insulation of fabric.

7 FUTURE WORK

In order to more comprehensively and deeply understand the thermal property of textile under convection and moisture conditions, the future work should include,

(1) Improve the testing device for evaluating thermal property of textile under convective heat transfer. This device should be able to measure the air velocity, air temperature, temperature of sample on both sides, and heat flow or heat flux. And the samples should have variables in porosity, pore size, pore's area ratio to total cross-sectional area of sample, and thickness.

(2) Investigate the thermal property/temperature changes of textiles during the process of liquid absorption, and investigate the energy absorption during the dry process of wet textiles.

(3) Analyze the impact of structure of textile on heat and mass transfer by numerical method.

PUBLICATIONS

1. **Guocheng Zhu**, Dana Kremenakova, Yan Wang, Jiri Militky, Study on air permeability and thermal resistance of textile under heat convection, Textile research journal. (accepted)

2. **Guocheng Zhu**, Dana Kremenakova, Yan Wang, Jiri Militky, Study on the thermal property of high porous nonwoven fabrics, industria textila. (accepted)

3. **Guocheng Zhu**, Dana Kremenakova, Yan Wang, Jiri Militky, Temperature change of cotton fabric during liquid adsorption process, International Journal of Clothing Science and Technology. (accepted)

4. **Guocheng Zhu**, Dana Kremenakova, Yan Wang, Jiri Militky, Air permeability of polyester nonwoven fabrics, Autex Research Journal. (accepted)

5. **Guocheng Zhu**, Dana Kremenakova, Yan Wang, Jiri Militky, Buyuk Mazari Funda, An anslysis of effective thermal conductivity of heterogeneous materials, Autex Research Journal, vol 14(1), (2014), pp.14-21.

6. **Guocheng Zhu**, Jiri Militky, Yan Wang, Juan Huang, Dana Kremenakova, Comparison of Effective Thermal Conductivity of Hollow Fibers by Prediction Models and FE Method, *Applied Mechanics and Materials*, Vol 440, (2014), pp.3-8.

7. **Guocheng Zhu**, Sayed Ibrahim, Dana Kremenakova, Yan Wang, Simulation of airflow motion in jet nozzle with different geometric parameters, *Advanced Materials Research*, Vol 683 (2013), pp.869-876.

8. Jiri Militky, **Guocheng zhu**, Dana Kremenakova, selected properties of functional materials (charpter 16), 1st ed, ops, czech republic, (2013), pp.207-215.

9. Yan Wang, Jacob Wiener, **Guocheng Zhu**, Langmuir isotherm models applied to the sorption of dyes from effluent onto polyamide nanofibers, AUTEX RJ, vol 13(6), (2013), pp.95-98.

10. **Guocheng Zhu**, Sayed Ibrahim, Dana Kremenakova, The optimization of experimental parameters for Jet-ring spinning, *Vlakna a Textil*, Vol 19 (2012), pp.60-67.

11. **Guocheng Zhu**, Sayed Ibrahim, Dana Kremenakova, Optimization application of air-jet nozzle in ring spinning system, *world journal of engineering*, Vol 9 (2012), pp.455-461.

12. **Guocheng Zhu**, Jiri. Militky, Sayed Ibrahim, Yan Wang, Dana Kremenakova, Simulation of airflow motion in jet nozzle with different tangentially injected orifice

parameters, STRUTEX 19, December 2012, Liberec, Czech Republic. (ISBN 978-80-7372-913-4).

13. **Guocheng Zhu**, Sayed Ibrahim, Jiri. Militky, Yan Wang, Mishra Rajesh, Dana Kremenakova The effect of the pore size and pores distribution on the thermal insulation of fibers and fiber bundles, STRUTEX 19, December 2012, Liberec, Czech Republic. (ISBN 978-80-7372-913-4).

14. **Guocheng Zhu**, Jiri. Militky, Yan Wang, Lukasova V., Dana Kremenakova, Prediction of hollow fibers effective thermal conductivity, STRUTEX 19, December 2012, Liberec, Czech Republic. (ISBN 978-80-7372-913-4).

15. **Guocheng Zhu**, Dana Kremenakova, Yan Wang, Huang Juan, Mohanapriya Venkataraman, Jiri Militky, Evaluation of thermal conductivity of hollow fiber padding by experiment, TexSci 2013, Sept. 23-25, Liberec, Czech Republic. (ISBN 978-80-7372-989-9)

REFERENCES

1. Gibson, P.W., et al., *Application of Nanofiber Technology to Nonwoven Thermal Insulation.* Journal of Engineered Fibers and Fabrics, 2007. **2**(2): p. 32-40.
2. Lubos, H., *The effective thermal resistance of fibrous layers in sleeping bags.* Res J Textile Apparel, 2004. **8**(1): p. 27-32.
3. Song, G., ed. *Improving comfort in clothing* Woodhead Publishing Series in Textiles. 2011, Woodhead Publishing Limited, Cambridge.
4. S.L. Kakani and A. Kakani, eds. *Material science*. 1st ed. 2004, New age international limited, New Delhi.
5. Cengel, Y.A., ed. *Heat transfer: A practical approach*. 2nd ed. 2003, McGraw-Hill, New York.
6. Yamanaka, A. and T. Takao, *Thermal Conductivity of High Strength Polyethylene Fiber and its Application for Cryogenic Use.* Sen-I Gakkaishi, 2012. **68**(4): p. P111-P117.
7. Tian, T. and K.D. Cole, *Anisotropic thermal conductivity measurement of carbon-fiber/epoxy composite materials.* International Journal of Heat and Mass Transfer, 2012. **55**(23-24): p. 6530-6537.
8. Lu, G., et al., *Effects of non-ideal structures and high temperatures on the insulation properties of aerogel-based composite materials.* Journal of Non-Crystalline Solids, 2011. **357**(22-23): p. 3822-3829.
9. Das, A., R. Alagirusamy, and P. Kumar, *Study of heat transfer through multilayer clothing assemblies: A theoretical prediction.* AUTEX Research Journal, 2011. **11**(2): p. 54-60.
10. Zhu, F. and K. Li, *Determining Effective Thermal Conductivity of Fabrics by Using Fractal Method.* International Journal of Thermophysics, 2010. **31**(3): p. 612-619.
11. Bhattacharjee, D. and V.K. Kothari, *Heat transfer through woven textiles.* International Journal of Heat and Mass Transfer, 2009. **52**(7–8): p. 2155-2160.
12. Gallego, N.C., et al., *The thermal conductivity of ribbon-shaped carbon fibers.* Carbon, 2000. **38**(7): p. 1003-1010.
13. Nield, D.A., *Convection in a Porous-Medium with Inclined Temperature-Gradient.* International Journal of Heat and Mass Transfer, 1991. **34**(1): p. 87-92.

14. Jiang, P.X. and X.C. Lu, *Numerical simulation and theoretical analysis of thermal boundary characteristics of convection heat transfer in porous media.* International Journal of Heat and Fluid Flow, 2007. **28**(5): p. 1144-1156.
15. Lee, S.C. and G.R. Cunnington, *Conduction and radiation heat transfer in high-porosity fiber thermal insulation.* Journal of Thermophysics and Heat Transfer, 2000. **14**(2): p. 121-136.
16. Yamanaka, A., et al., *The radiation effect on thermal conductivity of high strength ultra-high-molecular-weight polyethylene fiber by gamma-rays.* Journal of Applied Polymer Science, 2006. **101**(4): p. 2619-2626.
17. *ISO 11092/Amd1:2012. Textiles – Physiological effects – Measurement of thermal and water-vapour resistance under steady-state conditions (sweating guarded-hotplate test) – Amendment 1.*
18. Dias, T. and G.B. Delkumburewatte, *The influence of moisture content on the thermal conductivity of a knitted structure.* Measurement Science & Technology, 2007. **18**(5): p. 1304-1314.
19. Kavlany, M., ed. *Priciples of heat transfer in porous materials* Mechanical engineering series. 1995, Spinger, New York.
20. Kothari, V.K. and D. Bhattacharjee, *Prediction of thermal resistance of woven fabrics. Part I: Mathematical model.* Journal of the Textile Institute, 2008. **99**(5): p. 421-432.
21. Jiri Militky and D. Kremenakova. *Prediction of fabrics thermal conductivity*. in *5th International textile, clothing & design conference – Magic World of Textiles*. 2010. Dubrovnik, Croatia.
22. *Neckář, B.: Yarns - Creation, structure, properties, SNTL, ISBN 80-03-00213-3, Praha (1990) in Czech*.
23. Bogaty, H., N.R.S. Hollies, and M. Harris, *Some Thermal Properties of Fabrics: Part I: The Effect of Fiber Arrangement.* Textile Research Journal, 1957. **27**(6): p. 445-449.
24. Jakob, M., ed. *Heat Transfer*. 1st ed. Vol. 1. 1949, John Wiley & Sons, New York.
25. Zukauskas, A., J.P. Hartnett, and T.F. Irvine, eds. *"Heat Transfer from Tubes in Cross Flow" In Advances in Heat Transfer*. Vol. 8. 1972, Academic Press, New York.
26. Churchil.Sw and H. Ozoe, *Correlations for Laminar Forced Convection in Flow over an Isothermal Flat Plate and in Developing and Fully Developed Flow in an Isothermal Tube.* Journal of Heat Transfer-Transactions of the Asme, 1973. **95**(3): p. 416-419.

27. Churchill, S.W. and M. Bernstein, *Correlating Equation for Forced-Convection from Gases and Liquids to a Circular-Cylinder in Cross-Flow.* Journal of Heat Transfer-Transactions of the Asme, 1977. **99**(2): p. 300-306.
28. Whitaker, S., *Forced Convection Heat-Transfer Correlations for Flow in Pipes, Past Flat Plates, Single Cylinders, Single Spheres, and for Flow in Packed-Beds and Tube Bundles.* Aiche Journal, 1972. **18**(2): p. 361-371.
29. Farnworth, B., *Mechanisms of Heat-Flow through Clothing Insulation.* Textile Research Journal, 1983. **53**(12): p. 717-725.
30. EM, S., ed. *Radiation heat transfer*. 1978, McGraw-Hill, New York.
31. Monika Bogusławska Baczek and L. Hes, *Determination of heat transfer by radiation in textile fabrics by means of method with known emissivity of plates.* Journal of Industrial Textiles, 2013. **0**(00): p. 1-15.
32. Hes lubos and s. J. *Theoretical and experimental analysis of heat conductivity for nonwoven fabrics*. in *PA: INDA-TEC Transactions*. 1989. Philadephia.
33. Kaemmerlen, A., et al., *Transient modeling of combined conduction and radiation in wood fibre insulation and comparison with experimental data.* International Journal of Thermal Sciences, 2010. **49**(11): p. 2169-2176.
34. J.P.Holman, ed. *Heat Transfer*. 10th ed. 2010, McGraw-Hill, New York.
35. Issi, J.P., J. Heremans, and M.S. Dresselhaus, *Electronic and Lattice Contributions to the Thermal-Conductivity of Graphite-Intercalation Compounds.* Physical Review B, 1983. **27**(2): p. 1333-1347.
36. Piraux, L., et al., *The Temperature-Variation of the Thermal-Conductivity of Benzene-Derived Carbon-Fibers.* Solid State Communications, 1984. **50**(8): p. 697-700.
37. L. Piraux, J-P. Issi, and P. Coopmans, *Apparatus for thermal conductivity measurements on thin fibres.* Measurement, 1987. **5**(1): p. 2-5.
38. Poulaert, B., et al., *Thermal-Conductivity of Highly Oriented Polyethylene Fibers.* Polymer Communications, 1990. **31**(4): p. 148-151.
39. Lavin, J.G., et al., *The Correlation of Thermal-Conductivity with Electrical-Resistivity in Mesophase Pitch-Based Carbon-Fiber.* Carbon, 1993. **31**(6): p. 1001-1002.
40. Zhang, X., S. Fujiwara, and M. Fujii, *Measurements of thermal conductivity and electrical conductivity of a single carbon fiber.* International Journal of Thermophysics, 2000. **21**(4): p. 965-980.

41. Zhang, X., S. Fujiwara, and M. Fujii, *Short-hot-wire method for the measurement of the thermal conductivity of a fine fibre.* High Temperatures-High Pressures, 2000. **32**(4): p. 493-500.
42. Fujiwara, S., X. Zhang, and M. Fujii, *Short-hot-wire method for the measurement of total hemispherical emissivity of a fine fibre.* High Temperatures-High Pressures, 2001. **33**(3): p. 271-278.
43. Parrot JE and S. AD., eds. *thermal conductivity of solids*. 1975, london, pion. 23-31.
44. Wang, C.Y., *Thermal conductivity of a material containing a layer of thin strips or a staggered array of thin strips.* Journal of Heat Transfer-Transactions of the Asme, 1999. **121**(1): p. 174-177.
45. Schuster, J., et al., *Measuring and modeling the thermal conductivities of three-dimensionally woven fabric composites.* Mechanics of Composite Materials, 2009. **45**(2): p. 165-174.
46. Dasgupta, A. and R.K. Agarwal, *Orthotropic Thermal-Conductivity of Plain-Weave Fabric Composites Using a Homogenization Technique.* Journal of Composite Materials, 1992. **26**(18): p. 2736-2758.
47. Hind, S., D. Raizenne, and F. Robitaille, *Prediction of the effective transverse thermal conductivity of carbon based textile composites with varying constituent properties and reinforcement geometry.* Design, Manufacturing and Applications of Composites, 2006: p. 432-441.
48. Al-Sulaiman, F.A., Y.N. Al-Nassar, and E.M.A. Mokheimer, *Numerical prediction of the thermal conductivity of fibers.* Heat and Mass Transfer, 2006. **42**(5): p. 449-461.
49. Krach, A. and S.G. Advani, *Influence of void shape, void volume and matrix anisotropy on effective thermal conductivity of a three-phase composite.* Journal of Composite Materials, 1996. **30**(8): p. 933-946.
50. Jones, F.W. and F. Pascal, *Numerical-Model Calculations of the Effects of Grain Sizes and Orientations on the Thermal-Conductivities of Composites (Vol 23, Pg 365, 1994).* Geothermics, 1995. **24**(1): p. 131-131.
51. Jones, F.W. and F. Pascal, *Numerical-Calculations of the Thermal-Conductivities of Composites - a 3-D Model.* Geophysics, 1995. **60**(4): p. 1038-1050.
52. Jones, F.W. and F. Pascal, *Numerical-Model Calculations of the Effects of Grain Sizes and Orientations on the Thermal-Conductivities of Composites.* Geothermics, 1994. **23**(4): p. 365-371.

53. Taylor, R.E., J. Jortner, and H. Groot, *Thermal-Diffusivity of Fiber-Reinforced Composites Using the Laser Flash Technique.* Carbon, 1985. **23**(2): p. 215-222.
54. Lubos Hes and I. Dolezal, *New method and equipment for measuring thermal properties of textiles.* Journal of the textile machinery society of japan, 1989. **42**: p. 71-75.
55. *ASTM D1518-03. Standard test method for thermal transmittance of textile materials. Annual Book of ASTM Standards West Conshohocken, USA.* 2003.
56. Fournier, M., et al., *Measurement of textile materials thermal properties.* European Physical Journal-Special Topics, 2008. **153**: p. 143-145.
57. Fuente, R., et al., *Simultaneous Measurement of Thermal Diffusivity and Optical Absorption Coefficient of Solids Using PTR and PPE: A Comparison.* International Journal of Thermophysics, 2012. **33**(10-11): p. 1876-1886.
58. *http://www.ctherm.com/products/tci_thermal_conductivity/*.
59. Karaca, E., et al., *Effects of Fiber Cross Sectional Shape and Weave Pattern on Thermal Comfort Properties of Polyester Woven Fabrics.* Fibres & Textiles in Eastern Europe, 2012. **20**(3): p. 67-72.
60. Lizak, P., A. Murarova, and S.C. Mojumdar, *Heat transfer through a textile layer composed of hollow fibres.* Journal of Thermal Analysis and Calorimetry, 2012. **108**(3): p. 851-857.
61. Lizak, P., et al., *Thermal transport characteristics of polypropylene fiber-based knitted fabrics.* Journal of Thermal Analysis and Calorimetry, 2012. **108**(3): p. 837-841.
62. Kothari, V.K. and K. Bal, *Development of an instrument to study thermal resistance of fabrics.* Indian Journal of Fibre & Textile Research, 2005. **30**(4): p. 357-362.
63. Paul, H.L. and K.R. Diller, *Comparison of thermal insulation performance of fibrous materials for the advanced space suit.* Journal of Biomechanical Engineering-Transactions of the Asme, 2003. **125**(5): p. 639-647.
64. Ymashita Yoshihiro, Yamda Hiroakia, and M. Hajimeb, *Effective Thermal Conductivity of Plain Weave Fabric and its Composite Material Made from High Strength Fibers* Journal of Textile Engineering, 2008. **54**(4): p. 111-119.
65. Stuart, I.M. and B.V. Holcombe, *Heat-Transfer through Fiber Beds by Radiation with Shading and Conduction.* Textile Research Journal, 1984. **54**(3): p. 149-157.

66. L.Paul, H. and K.R. Diller, *comparison of thermal insulation performance of fibrous materials for the advanced space suit.* journal of biomechanical engineering, 2003. **125**: p. 639-647.
67. Hager, N.E. and R.C. Steere, *Radiant Heat Transfer in Fibrous Thermal Insulation.* Journal of Applied Physics, 1967. **38**(12): p. 4663-4668.
68. Strong, H.M., F.P. Bundy, and H.P. Bovenkerk, *Flat Panel Vacuum Thermal Insulation.* Journal of Applied Physics, 1960. **31**(1): p. 39-50.
69. Martin, J.R. and G.E.R. Lamb, *Measurement of Thermal-Conductivity of Nonwovens Using a Dynamic Method.* Textile Research Journal, 1987. **57**(12): p. 721-727.
70. Eucken, A., *Allgemeine Gesetzmabigkeiten fur das Warmeleitvermogen verschiedener Stoffarten und Aggregatzustande.* Forschung Gabiete Ingenieur, 1940. **11**(1): p. 6-20.
71. Maxwell, J.C., ed. *A Treatise on Electricity and Magnetism*. 3rd ed. Vol. Chapter 9. 1954, Dover Publications Inc, New York.
72. Wang, J., et al., *A new structural model of effective thermal conductivity for heterogeneous materials with co-continuous phases.* International Journal of Heat and Mass Transfer, 2008. **51**(9-10): p. 2389-2397.
73. Levy, F.L., *A modified Maxwell-Eucken equation for calculating the thermal conductivity of two-component solutions or mixtures.* Int. J. Refrigeration 1981. **4**(4): p. 223-225.
74. Ismail, M.I., A.S.A. Ammar, and M. Elokeily, *Heat Transfer through Textile Fabrics: Mathematical Model.* Applied Mathematical Modelling, 1988. **12**(4): p. 434-440.
75. Matusiak, M., *Modelling the thermal resistance of woven fabrics.* Journal of the Textile Institute, 2012. **104**(4): p. 426-437.
76. Weidong Yu and C. Chu, eds. *Textile physics*. 2009, Donghua university press, Shanghai.
77. King G and A. Cassie, *propagation of temperature changes through textiles in humid atmospheres. part 1: rate of absorption of water vapor by wool fibers.* Trans Faraday Soc, 1940. **36**: p. 445-453.
78. Akinc, M. and D.M. Martin, *Heat of Adsorption of Water on E-Glass Fiber Surfaces.* Physics and Chemistry of Glasses, 1983. **24**(5): p. 117-121.
79. Nordon, P., et al., *sorption kinetics of water vapour in wool fibres: evaluation of diffusion coefficients and analysis of integral sorption.* Textile Research Journal, 1960(10): p. 761-770.

80. Li, Y. and B.V. Holcombe, *A 2-Stage Sorption Model of the Coupled Diffusion of Moisture and Heat in Wool Fabrics.* Textile Research Journal, 1992. **62**(4): p. 211-217.
81. Li, Y. and Z.X. Luo, *Physical mechanisms of moisture diffusion into hygroscopic fabrics during humidity transients.* Journal of the Textile Institute, 2000. **91**(2): p. 302-316.
82. Carson, J.K., et al., *An analysis of the influence of material structure on the effective thermal conductivity of theoretical porous materials using finite element simulations.* International Journal of Refrigeration-Revue Internationale Du Froid, 2003. **26**(8): p. 873-880.
83. Dasgupta, A., R.K. Agarwal, and S.M. Bhandarkar, *Three-dimensional modeling of woven-fabric composites for effective thermo-mechanical and thermal properties.* Composites Science and Technology, 1996. **56**(3): p. 209-223.
84. Francl, J. and W.D. Kingery, *Thermal Conductivity:IX, Experimental Investigation of Effect of Porosity on Thermal Conductivity.* Journal of the American Ceramic Society, 1954. **37**(2): p. 99-107.
85. Cunnington, G.R. and S.C. Lee, *Radiative properties of fibrous insulations: Theory versus experiment.* Journal of Thermophysics and Heat Transfer, 1996. **10**(3): p. 460-466.
86. Marschall, J. and F.S. Milos, *The calculation of anisotropic extinction coefficients for radiation diffusion in rigid fibrous ceramic insulations.* International Journal of Heat and Mass Transfer, 1997. **40**(3): p. 627-634.
87. Nicolau, V.P., M. Raynaud, and J.F. Sacadura, *Spectral Radiative Properties Identification of Fiber Insulating Materials.* International Journal of Heat and Mass Transfer, 1994. **37**: p. 311-324.
88. Milandri, A., F. Asllanaj, and G. Jeandel, *Determination of radiative properties of fibrous media by an inverse method-comparison with the Mie theory.* Journal of Quantitative Spectroscopy & Radiative Transfer, 2002. **74**(5): p. 637-653.
89. Verschoor, D.J. and Greebler, *Heat Transfer by Gas Conduction and Radiation in Fibrous Insulation.* Trans. ASME, 1952. **74**: p. 961.
90. *http://thermal.mtnw-usa.com/products/guarded-hotplates/sweating*.
91. *http://www.netzsch-thermal-analysis.com/en/products-solutions/thermal-diffusivity-conductivity.html*.

92. Bhattacharjee, D. and V.K. Kothari, *Prediction of thermal resistance of woven fabrics. Part II: Heat transfer in natural and forced convective environments.* Journal of the Textile Institute, 2008. **99**(5): p. 433-449.
93. Carman, P.G., ed. *Flow of Gases Through Porous Media*. 1956, Butterworth Scientific Pubications, London.
94. Kavlany, M., ed. *principles of heat transfer in porous media*. 2nd ed. mechanical engineering series. 1999, Springer, New York.
95. John D. Anderson, J., ed. *Fundamentals of Aerodynamics*. Third ed. 2001, McGraw-Hill Higher Education, New York.
96. Davies, N.C. *The separation of airborne dust and particles*. 1952. London: Proceedings of institute of mechanical engineers.
97. Mohammadi, M. and P. Banks-Lee, *Air permeability of multilayered nonwoven fabrics: Comparison of experimental and theoretical results.* Textile Research Journal, 2002. **72**(7): p. 613-617.
98. Shiming Yang and W. Tao, eds. *Heat transfer*. 4th ed. 2006, Higher education press, Beijing.
99. Mohammadi, M., P. Banks-Lee, and P. Ghadimi, *Determining effective thermal conductivity of multilayered nonwoven fabrics.* Textile Research Journal, 2003. **73**(9): p. 802-808.
100. Guocheng Zhu, et al., *An analysis of effective thermal conductivity of heterogeneous materials.* Autex Research Journal, 2014. **14**(1): p. 14-21.
101. Etemoglu, A.B., et al., *Mathematical modelling of combined diffusion of heat and mass transfer through fabrics.* Fibers and Polymers, 2009. **10**(2): p. 252-259.
102. Darvishzadeh, M., et al., *Improvement Modelling of Heat Transfer by Using Complex Neural Net in Fibrous Structures.* Fibers and Polymers, 2012. **13**(4): p. 542-548.
103. Raeisian, L., et al., *An Investigation in Structural Parameters of Needle-Punched Nonwoven Fabrics on Their Thermal Insulation Property.* Fibers and Polymers, 2013. **14**(10): p. 1748-1753.
104. Bhattacharjee, D. and V.K. Kothari, *Measurement of Thermal Resistance of Woven Fabrics in Natural and Forced Convections.* Research Journal of Textile and Apparel, 2008. **12**(2): p. 39-49.
105. Beithou, N., K. Albayrak, and A. Abdulmajeed, *Effects of porosity on the free convection flow of non-Newtonian fluids along a vertical plate embedded in a porous medium.* Tr. J. Eng. Environ. Sci., 1998. **22**: p. 203-209.

106. Hatch, K.L., et al., *In Vivo Cutaneous and Perceived Comfort Response to Fabric. Part 1: Thermophysiological Comfort Determinations for Three Experimental Knit Fabrics.* Textil. Res. J., 1990. **60**(7): p. 405-412.